Modality-specific circuits for skylight orientation in the fly visual system

Inaugural-Dissertation

to obtain the academic degree

Doctor rerum naturalium (Dr. rer. nat.)

submitted to the Department of Biology, Chemistry, Pharmacy

of Freie Universität Berlin

by

Gizem Sancer

Born in Izmir, Turkey

2020

1st Reviewer:

Prof Dr. Mathias F. Wernet

2nd Reviewer:

Prof Dr. Peter Robin Hiesinger

Date of defense: 02.10.2020

I hereby declare that this thesis has been written by myself and the experimental work is entirely my own work, the contributions have been indicated clearly and acknowledged.

1. ACKNOWLEDGMENT

I would like to thank my supervisor, Prof Dr. Mathias Wernet, for his support and guidance through each stage of my doctoral work. He gave me the best opportunities to elevate my work and from beginning to end, he encouraged me to work harder, to do my best, and helped me achieve my goals.

Special thanks to Prof. Dr. Robin Hiesinger for all the invaluable feedback and support during my doctoral work, but especially for his encouragement for me to start my doctoral studies in Berlin.

Some parts of this work would not be possible without Juliane Uhlhorn, Emil Kind, Julika Volkman, and Johannes Hammacher. I would like to thank them for believing my skills, working with me in synchrony, and for their continuous support. We learned how valuable the teamwork is and had fun together in those sleepless nights before the deadline.

I would like to express my appreciation to former and current lab members of Wernet & Hiesinger and Hassan Lab, who gave me their time and share their ideas. I am grateful for their continuous support, constructive feedback and friendship which elevated me when I feel exhausted and uneasy.

Thanks should also go to my biggest supporter on this journey, Ferdi Rıdvan Kıral. He always supported and nurtured me to continue no matter what and lifted me up when I struggled.

Last but not the least, I would like to thank my family, İdil, Yaşar and Güler Sancer for their continuous support even from far away and Lalehan Eymirlioğlu for encouraging me to start this journey.

TABLE OF CONTENTS

2. INTRODUCTION

Understanding how sensory information is processed by the brain is one of the major goals of neuroscience. How does the brain extract the pieces of relevant information from the complex environment that are necessary for the animals to survive? How does it then translate this collected information into behavior? These questions have been addressed in many neuroethological studies that investigated the link between the environment and behavior. Importantly, different sensory systems from various organisms are being used as models to understand which computations in the brain translate specific stimuli into appropriate behavioral responses (Clark et al., 2013).

Both in mammals and invertebrates, the visual system has long served as a powerful model to investigate the interplay between synaptic connectivity neuronal computations, and visual perception (Klapoetke et al., 2017; Longden, 2018; Maisak et al., 2013; Mauss et al., 2017; Salay et al., 2018; Song and Lee, 2018; Temizer et al., 2015). Its rather compact brain in combination with the availability of various molecular genetic tools have made *Drosophila* one of the most popular organisms for investigating the neuronal circuit responsible for visual sensory processing (Dewar et al., 2017; Paulk et al., 2013; Zhu, 2013). Despite its small brain, this little fly species manifests very sophisticated behaviors in response to both simple and complex visual stimuli and can perceive several different modalities of light, such as color and motion (Borst, 2014; Heath et al., 2020; Klapoetke et al., 2017; Lin et al., 2016; Longden, 2016; Ribeiro et al., 2018; Wu et al., 2016).

For improving their navigational skills, flies can extract different forms of valuable information from their environment, simply by using receptors tuned to different modalities of the incident light. For example, they can detect both immobile and moving landmarks (including celestial bodies like the sun), which can be used as a reference when setting a specific heading. Furthermore, flies can distinguish between different wavelengths, hence equipping them with trichromatic color vision (Heath et al., 2020; Longden, 2018; Schnaitmann et al., 2013). In addition, flies can also sense polarized skylight as a separate modality, which in nature results from atmospheric scattering of sunlight. The directional information encoded in the polarized light pattern in the sky can be used by flies (as well as other insects) to inform

their navigational decisions (Mathejczyk and Wernet, 2019; Warren et al., 2018; Weir et al., 2016; Wernet et al., 2012). How are these different modalities of the light encoded in the brain? In order to address this question, the work summarized in this thesis focuses on describing the morphology and synaptic interconnections of specific neural circuit elements responsible for computing one specific visual modality.

2.1. The retinal basis for detecting different modalities

The adult fly eye is composed of ~750-unit eyes (ommatidia) that each harbor eight light-sensing photoreceptor neurons called R1-R8 (Kind et al., 2020; Wolff and Ready, 1993). These photoreceptors can be classified according to differences in morphology and Rhodopsin expression, as well as based on which neuropil layer in the brain they project their axons to or based on which behavioral response they inform. In each ommatidium, so-called outer photoreceptors (R1-R6) express the same broadband Rhodopsin (Rh1/ninaE) expressed in optically isolated light-gathering membranes (rhabdomeres) and project axons to the first neuropil (lamina), where they synapse onto post-synaptic targets by forming a complex wiring pattern known as 'neural superposition'(Langen et al., 2015). Outer photoreceptors have been shown to mediate motion vision and image formation (Heisenberg and Buchner, 1977). In the middle of each ommatidium, the rhabdomeres of so-called inner photoreceptors R7 and R8 are stacked on top of each other, R7 always being located distally from R8. Since they can express four different rhodopsin molecules, inner photoreceptors generate at least three different ommatidial subtypes: In the main part of the eye, 'pale' and 'yellow' ommatidial subtype are distributed stochastically and create a retinal mosaic (Perry et al., 2016). In pale ommatidia, expression of the UV-sensitive opsin Rh3 in R7 is coupled with expression of blue sensitive Rh5 in the underlying R8 (Chou et al., 1996; Papatsenko et al., 1997). In yellow ommatidia, expression of UV-sensitive Rh4 in R7 is coupled with expression of green-sensitive Rh6 in the underlying R8 photoreceptor (Chou et al., 1996; Huber et al., 1997; Salcedo et al., 1999). Due to the differences in wavelength sensitivity, the pale/yellow mosaic of R7 and R8 photoreceptor subtypes is suitable for detecting color (Salcedo et al., 1999). Indeed, it has been shown that this retinal mosaic is required for fly color vision

(Heisenberg and Buchner, 1977; Melnattur et al., 2014; Schnaitmann et al., 2013, 2018; Yamaguchi et al., 2010).

A third ommatidial subtype is always found at the dorsal rim of the eye, hence called ‘dorsal rim area’ (DRA), where one or two rows of ommatidia manifest both molecular and morphological specializations (Labhart and Meyer, 1999; Tomlinson, 2003; Wada, 1974; Wernet et al., 2003). Only in DRA ommatidia, both R7 and R8 express the same UV-sensitive molecule (Rh3), therefore they appear not suitable for color vision (Fortini and Rubin, 1990). Instead, R7 and R8 in the DRA manifest a very specific morphology by forming untwisted rhabdomeric membranes, thereby rendering them sensitive to polarized skylight (Smola and Tscharntke, 1979; Wernet et al., 2012; Wunderer and Smola, 1982). In agreement with this morphology, it was shown that *Drosophila* DRA ommatidia are both necessary and sufficient for mediating orientation behavior in response to polarized light which serves as a navigational guidance cue in both walking and flying flies (von Philipsborn and Labhart, 1990; Weir and Dickinson, 2012; Wernet et al., 2012).

2.2. Processing of color in the optic lobes

Photoreceptors R7 and R8 from all ommatidial subtype send their axons directly to the second neuropil of the optic lobe (medulla), which is the most complex neuropil of the optic lobe with more than 80 different cell types and ~40,000 neurons (Fischbach and Dittrich, 1989; Takemura et al., 2008). The medulla contains ~750 repetitive columnar units that are organized retinotopically, thus each point in space within the visual field is represented in separate medulla columns (Takemura et al., 2008). So-called columnar cell types occur once per medulla column and therefore repeated ~750 times across one medulla, whereas multicolumnar neurons innervate several columns and may provide communication between them (Fischbach and Dittrich, 1989; Millard and Pecot, 2018). Both columnar and multicolumnar cell types show specific arborization patterns within specific medulla layers (termed M1-M10, from distal to proximal) (Fischbach and Dittrich, 1989). Importantly, both pale and yellow R7 and R8 project their axons to specific layers within the medulla (R7 terminating in M6 and R8 terminating in M3), suggesting that the processing of different forms of spectral information (UV versus longer wavelengths) begins in different medulla layers (Fischbach and Dittrich, 1989; Jagadish et al., 2014).

In most cases, color vision requires color-opponent neurons that compare different wavelengths in an antagonistic manner (Hurvich and Jameson, 1957). Together, pale and yellow R7 and R8 generate the hardware suitable for detecting different wavelengths so they can be further processed. Indeed, behavioral studies indicate that *Drosophila* is capable of wavelength discrimination and true color vision while also revealing a strong intrinsic preference for UV over green light (Gao et al., 2008; Heath et al., 2020; Melnattur et al., 2014; Otsuna et al., 2014; Schnaitmann et al., 2013, 2018). The latter behavior is mediated by UV-sensing (pale and yellow) R7 cells and their main post-synaptic partner, a multicolumnar cell type in distal medulla called Dm8 (Fischbach and Dittrich, 1989; Gao et al., 2008; Karuppudurai et al., 2014; Nern et al., 2015). In the absence of functional Dm8 cells, UV preference behavior is lost, and rescue experiments further revealed that Dm8 is also sufficient for mediating UV preference behavior (Gao et al., 2008). Interestingly, Dm8 receives synaptic input from ~13 adjacent UV-sensitive R7 cells and pools this multicolumnar information (Gao et al., 2008; Karuppudurai et al., 2014). On the output site, Dm8 relays this pooled information to a columnar trans-medullary cell type named Tm5c that also receives direct synaptic input from a single R8 cell from this column. In addition to Dm8 input, Tm5c gets direct information from blue/green sensitive R8 and completes minimal architecture of the circuit mediating spectral preference and color vision In addition to Dm8 input, Tm5c receives direct information from blue/green sensitive R8 and complete the essential architecture of the circuit mediating spectral preference and color vision (Karuppudurai et al., 2014).

It was recently shown that color-opponency already arises within the terminals of inner photoreceptors themselves: R7 and R8 from the same column are synaptically connected via reciprocal inhibitory chemical synapses which produce color opponent responses within photoreceptor terminals via histamine-gated chloride channels and provide crucial insight into how UV signals are compared with blue or green light (Schnaitmann et al., 2018). Another study revealed that presynaptic signals of R7 and R8 are further sculpted via intercolumnar wavelength comparisons, an effect mediated by another multicolumnar distal medulla cell type called Dm9 (Heath et al., 2020). While Dm9 cells receive major synaptic input from both R7 and R8 cells, they also provide strong synaptic feedback onto these photoreceptors. Activity imaging from R7 and R8 axon terminals in the absence of

functional Dm9 cells revealed that this cell is indeed sufficient for mediating interommatidial antagonism. (Heath et al., 2020; Uhlhorn and Wernet, 2020).

2.3. The detection of polarized light

Like in many other insects, photoreceptors (R7 and R8 for *Drosophila*) residing in the DRA of *Drosophila*, form a pair of cells with untwisted rhabdomeres arranged orthogonally, thereby acting as an opponent analyzer pair for the detection of the polarized skylight pattern. Taken together, all DRA ommatidia form a 'fan-shaped' array of analyzers whose preferred e-vector orientations change gradually across the DRA (Weir et al., 2016). So far, it remains unknown how neural circuits integrate over the DRA fan-shaped array, in order to extract a directional signal for informing an unambiguous behavioral response. When compared to non-DRA counterparts, R7 and R8 in the DRA not only differ in terms of their rhabdomeric morphology and rhodopsin expression, but also in layer targeting of their axons in the medulla (Labhart and Meyer, 1999; Wernet et al., 2012; Wunderer and Smola, 1982). Only in DRA columns, both R7 and R8 terminate in medulla layer M6, usually known to be the R7 target layer in the rest of the medulla (Chin et al., 2014). Since correct layer targeting is crucial for correct synaptic partner choice (Kulkarni et al., 2016), this difference in layer targeting points towards specific differences in circuitry within DRA columns. Differences in synaptic partner choice between polarization-sensitive DRA inner photoreceptors and color-sensitive pale/yellow R7 and R8 cells is particularly interesting since these two circuits process different modalities of the light. However, when work on this thesis began, virtually nothing was known about the differences between circuits processing color and polarization vision. More importantly, nothing was known about the identity of circuit elements directly post-synaptic to DRA photoreceptors, in any insect species. Although polarization-sensitive neurons have been reported from the medulla of locusts (el Jundi et al., 2011), as well as from crickets (Labhart, 1988) , it remains unknown whether they are directly connected to photoreceptors, and whether they are modality-specific, i.e. specifically avoiding contacts with non-DRA photoreceptors.

Over the years, several models have been put forth, aimed at modeling the computations executed by cell types downstream of the insect DRA (Gkanias et al., 2019; Wehner and Labhart, 2006). In some cases, these models were even

implemented for guiding the navigation bio-inspired robots (Lambrinos et al., 2000). In all cases, these studies have suffered from the fact that the cell types involved were dramatically under-studied. The results of this thesis therefore also serve to fill this gap in knowledge, thereby enabling the formulation of improved computational models in the near future.

2.4. Beyond the optic lobes: visual processing in central brain

The optic lobes are the major site for processing visual information. For instance, direction-selective responses arise via multiple synaptic steps from outer photoreceptors towards the lobula plate and probably represent the best understood computation in the fly brain (Borst, 2014). Before connecting to descending neurons (and thereby inducing specific motor programs), further processing and integration of visual information can occur in the central brain, for instance in several optic glomeruli and the central complex. The central complex of the fly (consisting of ellipsoid body, fan-shaped body and noduli) is an evolutionarily highly conserved brain region involved in different visually-guided behaviors such as feature detection, spatial memory, or navigation (Heinze and Homberg, 2007; el Jundi et al., 2014; Liu et al., 2006; Ofstad et al., 2011; Seelig and Jayaraman, 2013; Turner-Evans and Jayaraman, 2016). The neural pathways that carry different forms of visual information from the optic lobes to the central complex have been characterized in different insect species, including *Drosophila*. The so-called 'anterior visual pathway' (AVP), or 'compass pathway' is a particularly prominent circuit that connects the eye to the central brain (Homberg, 2004). The AVP has been proposed to carry information about different skylight cues such as the position of the sun, pattern of the polarized skylight, or the spectral gradients that are all necessary for navigation. The AVP consists of multiple relay stations: First, multicolumnar projection neurons, called MeTu cells (medulla to tubercle neurons), directly connect the medulla to a specific visual glomerulus called the anterior optic tubercle (AOTU) (Ito et al., 2014; Omoto et al., 2017; Otsuna et al., 2014). From there, information is transmitted via TuBu cells (tubercle to bulb neurons) to the bulb neuropil where central complex ring neurons of the ellipsoid body form dendritic branches. Therefore, visual information reaches the central complex via this Metu→TuBu→R-neuron pathway (Omoto et al., 2017).

Several behavioral and physiological studies focusing on different insect species revealed that the AOTU plays an important role for orientation behavior in response to skylight polarization (Mappes and Homberg, 2004, 2007; Pfeiffer et al., 2005), as well as color processing (Paulk et al., 2008; Ryglewski et al., 2017). Like in other insects, cellular components of the *Drosophila* AVP also respond to skylight cues, such as bright objects (Mota et al., 2013; Omoto et al., 2017; Shiozaki and Kazama, 2017; Sun et al., 2017). However, our knowledge about *Drosophila* is limited since it remains unknown whether other skylight cues like polarization and color are also transmitted to the central brain via this pathway. Prior to this work, there existed only one study describing the connections within this pathway (Medulla to bulb and to ellipsoid body connections) and transmitted detailed description of MeTu connections from the medulla to AOTu was missing.

The information that is transmitted via anterior visual pathway enters the central complex via ring neurons that are selective for specific visual features (Omoto et al., 2017; Seelig and Jayaraman, 2013; Shiozaki and Kazama, 2017; Sun et al., 2017). So-called ‘compass neurons’ that receive input from ring neurons process both visual and self-motion cues and encode the heading of the fly (Green et al., 2017; Kim et al., 2019; Seelig and Jayaraman, 2013, 2015; Sun et al., 2017). For example, a particular class of compass neurons (E-PG neurons) that track the internal heading of the animal also encodes the position of the sun in the central complex (Giraldo et al., 2018; Green et al., 2017; Seelig and Jayaraman, 2015). When these cells are silenced, flies lose the ability to perform menotaxis, i.e. to set a course using the sun as a reference (Giraldo et al., 2018). Interestingly E-PG neurons are the homologs of CL1 neurons in other insect species that are responsive to different skylight cues including skylight polarization (Heinze and Homberg, 2009; Homberg et al., 2011; Immonen et al., 2017; el Jundi et al., 2015; Stone et al., 2017). However, it remains unknown right now how skylight polarization is represented in the central brain of *Drosophila* or whether similar compass neurons are involved in the processing of skylight polarization.

3. AIM

One of the greatest challenges of neuroscience is to understand the neuronal computations underlying one specific behavior. The anatomical characterization of sensory systems can provide valuable insight into how the brain extracts the relevant pieces of information from a complex visual scene, leading to new hypotheses on how these inputs are then translated into appropriate behavioral responses. Hence, the characterization of circuit elements that transmit information from peripheral sensory organs to the brain is essential for understanding the brain's computational logic. Due to its relatively small size and reduced complexity, the *Drosophila* visual system has long served as a powerful model system for understanding the cellular implementation of those neural circuits encoding the relationship between stimuli (input) and behavior (output).

In this study, I investigated the visual circuits underlying orientation behaviors in response to the polarized skylight, an important navigational cue for many insects. Various studies demonstrated that *Drosophila* melanogaster exhibits orientation behavior in response to polarized light, when walking or flying. The specialized ommatidia for the detection of polarized light mediating these behavioral responses have been characterized, yet the underlying neural circuitry remains virtually unknown. This study focused on the cellular characterization of elements downstream of polarization-sensitive DRA photoreceptors and the pathways that transfer skylight polarization information to the central brain. This study therefore aimed at elucidating the cellular units and their synaptic interconnections, together forming the neural circuits for polarization vision The detailed description of modality-specific differences in circuit architecture (connectivity, synaptic distribution) when comparing circuits for polarization vision and color vision in the *Drosophila* brain serves as a model system for better understanding dedicated visual circuits across animal species.

4. MANUSCRIPTS

4.1. Manuscript I

Modality-Specific Circuits for Skylight Orientation in the Fly Visual System

Gizem Sancer, Emil Kind, Haritz Plazaola-Sasieta, Jana Balke, Tuyen Pham, Amr Hasan, Lucas O. Münch, Maximilien Courgeon, Thomas F. Mathejczyk, Mathias F. Wernet

Current Biology Volume 29, Issue 17, 9 September 2019, Pages 2812-2825.e4

Contribution:

I designed and conducted most of the experiments (except Fig 1 and 7) under the supervision of Prof. Dr. Mathias Wernet and performed the data analysis that is presented in this manuscript. The manuscript was written by me, Emil Kind and Prof. Dr. Mathias Wernet.

The original article including the supplemental information is included on the flowing pages and available online at:

DOI: https://doi.org/10.1016/j.cub.2019.07.020

4.2. Manuscript II

Cellular and synaptic adaptations of neural circuits processing skylight polarization in the fly

Gizem Sancer, Emil Kind, Juliane Uhlhorn, Julia Volkmann, Johannes Hammacher, Tuyen Pham, Haritz Plazaola-Sasieta, Mathias F. Wernet

Journal of Comparative Physiology A volume 206, pages233–246(2020)

Contribution:

I designed and conducted most of the experiments (except Figure 5 and 6) under the supervision of Prof. Dr. Mathias Wernet and performed the data analysis that is presented in this manuscript. The manuscript was written by me, Emil Kind, Juliane Uhlhorn, and Prof. Dr. Mathias Wernet.

The original article including the supplemental information is included on the flowing pages and available online at:

DOI: https://doi.org/10.1007/s00359-019-01389-3

4.3. Manuscript III

Parallel visual pathways with topographic versus non topographic organization connect the *Drosophila* eyes to the central brain

Lorin Timaeus, Laura Geid, Gizem Sancer, Mathias F. Wernet, Thomas Hummel

Contribution:

I contributed the experiments presented in Figure 3 C-J, generated this data as well as Supplemental Figure 2 and analyzed the data under supervision of Prof. Dr. Mathias Wernet. Together with Prof. Dr. Mathias Wernet I contributed to writing the manuscript.

This manuscript has been accepted for publication in iScience (Cell Press), to be published in 2020.

Highlights

- A visual circuit conveys visual information from the periphery to the central brain of *Drosophila*
- Several synaptic pathways form parallel channels using to the anterior optic tubercle (AOTU)
- Some pathways appear to maintain topographic relationships whereas at least one does not
- Different target neurons in the central brain are identified

Parallel visual pathways with topographic versus non-topographic organization connect the *Drosophila* eyes to the central brain

Lorin Timaeus [1], Laura Geid [1, 2], Gizem Sancer [3], Mathias F. Wernet [3], Thomas Hummel [1*]

[1] Department of Neurobiology, University of Vienna, Vienna, Austria.

[2] Center for Brain Research, Medical University of Vienna, Austria.

[3] Department of Biology, Freie Universität Berlin, Germany.

*Corresponding Author: thomas.hummel@univie.ac.at

Summary

One hallmark of the visual system is a strict retinotopic organization from the periphery towards the central brain, where functional imaging in *Drosophila* revealed a spatially accurate representation of visual cues in the central complex. This raised the question how this is implemented on a circuit level, as the majority of visual neurons entering the central brain converge in optic glomeruli. We discovered a spatial segregation of topographic versus non-topographic projections of distinct classes of medullo-tubercular (MeTu) neurons into a specific visual glomerulus, the AOTU. These parallel channels are synapse onto different tubercular-bulbar (TuBu) neurons which in turn relay visual information onto specific central complex ring neurons in the bulb neuropil. Hence, our results provide the circuit basis for spatially accurate representation of visual information and highlight the AOTU's role as a prominent relay station for spatial information from the retina to the central brain.

Abbreviations

AOTU	Anterior Optic Tubercle	**MeTu**	Medullo-tubercular neuron
CX	Central Complex	**PLP**	Posterior Lateral Protocerebrum
EB	Ellipsoid Body	**PVLP**	Posterior Ventro-lateral Protocerebrum
LC	Lobula Columnar neuron	**SU**	Small Unit (of AOTU)
LU	Large Unit (of AOTU)	**TuBu**	Tubercular-bulbar neuron

Introduction

Most insects rely on visual cues for accurate maneuvering, which requires appropriate processing and fast integration of various visual stimuli (Egelhaaf and Kern, 2002, Heinze, 2017, Mauss et al., 2017). Fast decisions on whether to veer away from or approach an immobile or moving object while remaining able to quickly orientate within a complex, three-dimensional environment are key tasks for their survival (Mauss et al., 2017). Research focused on dissecting neural circuits in the periphery of the visual system as well as in the central brain of a large variety of insect species, including the genetic model organism *Drosophila melanogaster*, has provided considerable insights into how information is processed beyond photoreceptor cells (Borst, 2014, Silies et al., 2014, Behnia and Desplan, 2015). Although the resolution of an insect compound eye does not rival that of a vertebrate retina (Kirschfeld, 1976), neuronal elements for the internal representation of certain features of the visual world have been successfully identified: Functional studies, more recently using genetically encoded effectors in *Drosophila*, have linked distinct structures of the visual system to processing discrete aspects of visual perception (Fisher et al., 2015, Schnell et al., 2010, Bahl et al., 2015, Ribeiro et al., 2018). Of special interest is the central complex (CX), a structure of interconnecting neuropils (named the protocerebral bridge, ellipsoid body, fan-shaped body, and noduli) located at the midline of the protocerebrum. Across insect orders, the CX's various functions comprise higher locomotor control, integration of multisensory input, representation of navigational cues, and different forms of memory formation (Strauss,

2002, Heinze and Homberg, 2007, el Jundi et al., 2014, Turner-Evans and Jayaraman, 2016, Varga et al., 2017, Liu et al., 2006, Ofstad et al., 2011).

The CX plays an important role in processing visual information in various insect orders, where neural pathways connecting the CX with the optic lobes have been characterized in hemi- and holometabolous insects (Homberg, 2015, Turner-Evans and Jayaraman, 2016, Honkanen et al., 2019, El Jundi et al., 2018, Franconville et al., 2018). In *Drosophila*, numerous studies using a variety of genetic tools described roles of the CX in visual pattern memory (Liu et al., 2006), encoding of visual experience and self-motion (Shiozaki and Kazama, 2017), flight-dependent visual responses (Weir and Dickinson, 2015), sun-guided navigation (Giraldo et al., 2018), and visual landmark recognition (Seelig and Jayaraman, 2015, Green et al., 2017), including sensorimotor remapping of visual information (Fisher et al., 2019), suggesting a substantial role of the CX in guiding object recognition for orientating in space. While the neuroarchitecture of the *Drosophila* CX shows clear signs of a topographic organization (Lin et al., 2013, Franconville et al., 2018), the cellular composition and synaptic wiring diagram of neural circuits that relay spatial information from the optic lobes into the CX remain incompletely understood.

One prominent CX input pathway for visual information, with the ellipsoid body (EB) on the receiving end, has been identified as distinct classes of Ring neurons (R neurons), which form a stack of several ring-shaped layers in *Drosophila* (Hanesch et al., 1989, Wolff et al., 2015, Franconville et al., 2018). Afferent neurons are synaptically connected with R neurons via distinct microglomerular structures in the bulb neuropil adjacent to the EB (formerly referred to as the lateral triangle) (Ito et al., 2014). These connections are distributed retinotopically, since their positions correlate to small receptive fields on the ipsilateral side (Seelig and Jayaraman, 2013, Omoto et al., 2017). The transmission of spatial information from the optic lobes to the EB likely involves two synaptic neuropils: First, the R neuron dendrites in the bulb neuropil receive direct synaptic input from tubercular-bulbar neurons (or TuBu neurons), originating from the anterior optic tubercle (AOTU), one of several conserved optic glomeruli (Ito et al., 2014, Otsuna and Ito, 2006, Panser et al., 2016). Functional studies

already described how R neurons inherit their receptive field properties from TuBu neurons (Sun et al., 2017, Shiozaki and Kazama, 2017). Secondly, distinct classes of medulla projection neurons (medullar-tubercular neurons, or MeTu neurons) directly connect the medulla with the AOTU (Omoto et al., 2017, Otsuna et al., 2014). In contrast, the majority of remaining optic glomeruli are exclusively innervated by lobula columnar (LC) neurons (Otsuna and Ito, 2006, Wu et al., 2016). The AOTU is unusual among optic glomeruli in that it can be further subdivided - into a medially located large unit (LU; also named AOTUm (Omoto et al., 2017), receiving input from the lobula via LC neurons), and a more lateral, small unit (SU, receiving input from the medulla via MeTu neurons). While functional studies revealed that upon visual stimulation some optic glomeruli can be linked to specific behavioral responses, e.g. the detection of and response to small objects, escape, or reaching behavior (Keles and Frye, 2017, Wu et al., 2016), spatial information should be lost in the majority of optic glomeruli, due to convergence of intermingling LC inputs (Wu et al., 2016, Panser et al., 2016). However, other studies revealed that some LC afferents display some rough spatial restriction along the dorso-ventral axis of the AOTU, indicating that a topographic pathway into the central brain may exist here (Wu et al., 2016). Hence, it remains unclear whether there is only a rough topographic representation of visual information along one spatial axis in the central brain, or whether additional pathways with higher resolution also exist.

Here, we show that stereotyped topographic maps are built by distinct MeTu neuron subtypes within the SU of the AOTU, which is spatially separated from LC representation in the LU. Interestingly, the overlapping dendritic fields of different MeTu subtypes in the medulla diverge into multiple parallel visual channels that are subsequently maintained via parallel synaptic pathways from the AOTU to the bulb neuropil. Within the bulb, topographic channels connect with distinct receptive fields of CX ring neurons, whereas non-topographic channels have different R-neuron targets. Based on these data we propose a model in which specific domains of the AOTU form a central relay station for both topographic and non-topographic visual information, organized in multiple parallel channels, ideally suited for conveying distinct visual features to the central brain.

Results

Distinct types of afferent arborizations within optic glomeruli

Optic glomeruli and olfactory glomeruli are prominent neuropil structures located in different regions of the adult brain, with olfactory glomeruli concentrated within the antennal lobes of the deutocerebrum, whereas optic glomeruli form the AOTU, the posterior ventrolateral protocerebrum (PVLP), and the posterior lateral protocerebrum (PLP)(Fig. 1A). To determine whether a common connectivity logic could be shared by olfactory and optic glomeruli, we investigated the arborization patterns of afferent fibers projecting into optic glomeruli. Olfactory glomeruli are characterized by a sensory class-specific convergence of afferent axons, each glomerulus thereby representing a unique odorant receptor identity (Laissue and Vosshall, 2008) (Fig. 1B). Within each olfactory glomerulus, single sensory axon terminals arborize throughout the glomerular volume with all converging axon branches broadly overlapping and tightly intermingling (Hummel et al., 2003) (Fig. 1C).

Inputs from LC neurons to optic glomeruli in the PLP/PVLP region are restricted to the ventrolateral brain region (Otsuna and Ito, 2006, Wu et al., 2016) (Fig. 1D). In contrast, the more dorsally located AOTU receives afferent input via the anterior optic tract, containing both LC and MeTu fibers (Otsuna and Ito, 2006, Fischbach and Lyly-Hunerberg, 1983, Panser et al., 2016, Omoto et al., 2017) (Fig. 1J). Using specific driver lines from the FlyLight and Vienna Tiles collection (Jenett et al., 2012, Kvon et al., 2014), a variety of LC neuron types could be identified and their class-specific segregation into single optic glomeruli visualized (Costa et al., 2016, Panser et al., 2016) (Fig. 1F-L). In analogy to work on olfactory glomeruli in the antennal lobe (Hong et al., 2012, Hong et al., 2009), we found that specific cell surface molecules are differentially expressed between different optic glomeruli. (Fig. 1E shows an example of the expression for Connectin and Capricious in different subsets of optic glomeruli).

To characterize afferent arborizations within optic glomeruli, we first generated single cell clones (see Transparent Methods for details) for different LC neuron types (LC06, LC10,

LC12; Fig. 1G, H). Similar to olfactory sensory neurons axon terminals, we found that each LC axon ramified throughout a single optic glomerulus and all neurons of the same LC class converged onto a common glomerular space (Fig. 1G, H), thereby confirming the rather homogeneous arborization pattern within synaptic glomeruli in the PVP/PLVP neuropil (Wu et al., 2016). In contrast, a more diverse pattern of afferent innervation was observed in the AOTU large and small units (Fig. 1D, K): Our systematic characterization of a large collection of AOTU-specific expression lines confirmed that the LU is the target field of LC neurons whereas the SU is innervated by MeTu neurons (Fig. K-M, and see below)(Panser et al., 2016, Omoto et al., 2017, Otsuna et al., 2014). Single LC afferent terminals in the LU arborized throughout large areas of the glomerular subunit's volume, with some enrichment in the dorsal versus ventral regions of the LU (Fig. 1J")(Wu et al., 2016). In contrast, single MeTu afferents in the SU were more variable, ranging from broad (in close proximity to the LU) to spatially restricted in more lateral regions (Fig. 1N, O, Figs. S1 and S3-S4), indicating that different MeTu classes for distinct spatial representation might exist within the AOTU. This structural feature of spatially restricted afferent terminals makes the SU of the AOTU a candidate for a neuropil that could maintain topographic representation of visual information within the central brain.

Morphological and molecular domain organization of the AOTU

To determine how the architecture of the AOTU correlated with patterns of afferent innervation, we first co-labeled glial membranes with the neuropil epitope N-Cadherin (Fig. 2A, B). As previously reported (Omoto et al., 2017), a subdivision of the SU neuropil into multiple domains along the medial-lateral axis became visible, whereas the LU appears like a homogeneous neuropil without any obvious morphological substructures (Fig. 2A, B). This organization of the SU neuropil into several subdomains was further supported by the combinatorial expression pattern of various cell adhesion molecules. For example, we found the synaptic cell adhesion molecule Teneurin-m to be broadly expressed throughout the AOTU neuropil with the exception of the central subdomain of the SU (SU-c) and the anterior part of

the lateral SU (SU-l) (Fig. 2C). On the other hand, the adhesion molecules Connectin and Capricious were specifically expressed in the SU-c and medial SU (SU-m) domains, respectively (Fig. 2D, E, F, G). We then tested whether the SU subdomains matched different classes of MeTu afferents (Fig. 2H-K). Based on the terminal arborization patterns from 13 independent expression lines (see Transparent Methods) we could distinguish at least three distinct, non-overlapping populations of MeTu neurons. Based on the segregation of their axons within the AOTU, these neurons were classified as MeTu-lateral (-l), MeTu-central (-c) and MeTu-medial (-m) (compare Fig. 2N-P) [see discussion for a related description by (Omoto et al., 2017)]. A more detailed analysis of molecular markers in combination with MeTu expression lines revealed a further subdivision of the lateral SU domain (SU-l) into distinct anterior and posterior subdomains (SU-l_a versus SU-l_p, Fig. 2C', F'), which was not apparent for the LU (Fig. 2C', D', E', G'). Furthermore, by combining independent Gal4 and LexA expression lines, a similar anterior-posterior division of the central SU domain (SU-c) into SU-c_a and SU-c_p subdomains was found (Fig. 2H). Importantly, the terminals of specific MeTu driver lines co-labeled specifically with neuropil markers defining these specific subdomains of the SU, indicating that specific subdomains are indeed targeted by specific MeTu classes (Fig. 2J, H'). In contrast, other expression lines labeled a broader set of neurons innervating more than one subdomain (Fig. 2K).

To get further insights into the neuronal identity of the different MeTu populations, we visualized their dendritic arborizations in the medulla neuropil (Fig. 2L-P'). Interestingly, all three MeTu classes formed dendrites in medulla layer M6, where the UV-sensitive R7 photoreceptor cells target their main synaptic partner, the distal medulla cell type Dm8 (Karuppudurai et al., 2014, Ting et al., 2014, Gao et al., 2008, Nern et al., 2015). However, MeTu dendrites were located below the terminals of R7 cells and therefore separated from the R7/Dm8 synaptic area (Fig. 2L, M). For the majority of MeTu-l and MeTu-c neurons, the M6 layer appeared to be the only layer with dendritic signal (Fig. 2L, P'). In contrast, MeTu-m neurons formed dendritic arborizations in two additional medulla layers located both proximal and distal to layer M6, most likely layer M2 and layer M8 (Fig. 2M, M', N', O'). Interestingly, in

M6, MeTu-m dendrites segregated from MeTu-l/-c dendrites (Fig. 2N',O'), thereby revealing three distinct sub-layers within this medulla layer (R7/Dm8, MeTu-m, MeTu-l/-c) (Fig. 2Q). In summary, the AOTU receives direct input from distinct types of MeTu neurons, which differ in their dendritic layering, target subdomain, and molecular identity (summarized in Fig. 2Q).

Photoreceptor connectivity of MeTu subtypes

To investigate whether direct synaptic contacts between MeTu-l/-c dendrites in layer M6 and inner photoreceptors R7 (and less likely R8) might exist, the trans-synaptic tracer 'transTango' (Talay et al., 2017) was expressed under the control of either R7- or R8-specific rhodopsin-Gal4 driver combinations, respectively (Fig. 3A, B; see Transparent Methods for details). Significant labeling of the SU was detected following the transTango expression in R7 (A'), whereas no signal was detected in the AOTU in the case of R8 > transTango (B'). In the former case, the obtained patchy signal indicated that only UV-sensitive R7 cells are indeed synaptically connected to some, but probably not all MeTu-l/-c neurons. Although dendrites of MeTu-l and MeTu-c cells were mostly restricted to medulla layer M6, we noticed that some MeTu cell clones formed vertical processes reaching beyond medulla layer M6 (almost reaching M3), thereby making R7 photoreceptor → MeTu synapses a possibility (see MeTu-l clone in Fig. 3C). In order to systematically test which MeTu subtypes could be post-synaptic to R7 photoreceptors, we generated a transcriptional fusion of a ~3.5 kb fragment containing the promoter sequences of the histamine receptor Ort, driving expression of membrane tagged mCD8:GFP (see Transparent Methods for details). Since histamine is the neurotransmitter expressed by all insect photoreceptors (Stuart, 1999), many of their synaptic targets should be marked by Ort expression (Gao et al., 2008). As expected, this ort-mCD8:GFP transgene labeled many cell types throughout the optic lobes as putative photoreceptor targets (Fig. S2), including MeTu axon projections into discrete domains of the AOTU (Fig. 3D). Out of the five domains of the SU, only three were clearly positive for ort-mCD8:GFP, namely SU-l_a, SU-c_a and SU-c_p. We therefore proceeded to confirm that processes from MeTu subtypes terminating in these domains indeed co-labeled with GFP,

using a combination of different subdomain-specific drivers. Out of both MeTu-l subtypes, only axons of MeTu-l_a neurons co-labeled with GFP, whereas MeTu-l_p did not (Fig. 3E, F). In contrast, axons from both MeTu-c subtypes (c_a and c_p; both individually labeled using different driver lines), co-labeled with GFP (Fig. 3G-I). Finally, axons of MeTu-m cells never co-labeled with GFP (Fig. 3J). In summary, of all MeTu cells innervating the SU of the AOTU, only MeTu-l_a, MeTu-c_a, and MeTu-c_p were identified as potential synaptic targets of R7 photoreceptors (Fig 3K).

Topographic organization of AOTU afferents

Next, we proceeded to a more systematic characterization of how AOTU subdomains correlate with MeTu neuron identity at a single cell level. Clonal analysis revealed a stereotypical, subtype-specific pattern of MeTu innervation, where any given MeTu axon terminates in only one of the five SU subdomains (Fig. 4A-C). For MeTu-l and MeTu-c neurons, a spatially restricted termination pattern was observed in their respective SU subdomains (Fig. 4A, B). In contrast, afferent arborizations of MeTu-m cells extended throughout a large portion of their compartment (Fig. 4C, Fig. S1), resembling the previously published projection pattern of LC10 neurons in the LU (see Fig. 1J). The differences between MeTu-m neurons (with dendritic arborizations in multiple medulla layers and axonal convergence throughout their SU subdomain) versus MeTu-l + MeTu-c neurons (with dendrites restricted to medulla layer M6 and spatially restricted axon terminals in the AOTU) therefore support the existence of morphologically and functionally distinct visual channels into the central brain.

Dendritic fields of single MeTu-neurons always covered multiple medulla columns, yet the specific field size of individual MeTu-neuron clones varied considerably: at the anterior and posterior medulla border, neurons can be found that stretch across a major part of the dorsal medulla, either covering a large dendritic area in both axes (Fig. 4J), or spreading along the medulla border with limited a-p dimension (compare first two images in Fig. S5). In the central part of the medulla, dendrites of MeTu neurons are more circularly shaped, ranging

from ~20 medulla columns covered (lower cell in Fig. 4L) to >50 columns (Fig. S4; marked with an asterisk). Importantly, the differential labeling of randomly induced two-cell clones for either MeTu-l and MeTu-c neurons (using FLYBOW (Hadjieconomou et al., 2011), see Transparent Methods) manifested two crucial features with regard to the spatial organization of their terminals in the AOTU: First, MeTu-neurons of the same type (l/l or c/c) with neighboring dendritic fields in the medulla always projected to adjacent positions in the corresponding SU domain (Fig. 4K). Secondly, MeTu-neurons of different types (l/c) with overlapping dendritic fields in the medulla always projected to the same position along the d-v axis, yet in in adjacent SU domains (Fig. 4E). To determine whether MeTu-l and MeTu-c cells innervated their corresponding SU domain in a topographic fashion, we correlated their relative position of dendrites in the medulla with their axon terminals and AOTU, respectively (Fig. 4G-J). For both cell types we could observe a strict correlation between the dendritic position along the anterior-posterior (a-p) axis in the medulla and the axonal termination point along dorso-ventral (d-v) axis in the AOTU (Fig. 4N, n=35) (Figs. S3-S5). According to this wiring scheme, MeTu-l and MeTu-c neurons with dendrites at the anterior rim of the medulla neuropil target the most ventral position in their corresponding SU domain whereas neurons with dendrites at the posterior rim of the medulla connect to a dorsal edge of the SU (Fig. 4H, J). Furthermore, MeTu-(l/c) clones with dendrites in more medial medulla regions also targeted to medial position in the AOTU (Fig. 4K). The spatial arrangement of MeTu dendrites along the d-v axis of the medulla was not converted into a topographic targeting pattern along the a-p axis in their SU domains (Fig. 4F). The much more broad innervation pattern of many MeTu-m terminals in their respective domain is very different from the other MeTu classes, yet we cannot exclude that some MeTu-m neurons with more restricted terminals also form a topological arrangement (Fig. S1). In summary, these data revealed the structural organization of a topographic representation in the AOTU in which different MeTu cell types form multiple parallel channels from the medulla to a central brain.

AOTU efferents maintain domain identity and visual topography

If the AOTU served as a relay station of spatial information from the optic lobes to central integration centers of the brain, one would expect a matching pattern of connections between MeTu subtypes and corresponding AOTU output neurons along the d-v axis, at least for the lateral and central SU domains. We identified a large set of expression lines for AOTU projection neurons targeting the bulb region (TuBu neurons) (Omoto et al., 2017, Sun et al., 2017, Shiozaki and Kazama, 2017). These TuBu expression lines show domain-specific restriction of their dendritic fields, corresponding to the SU-l, -c and -m domains and were therefore classified as TuBu-l, -c & -m neurons, respectively (Fig. 5B, G; compare also (Omoto et al., 2017)). The dendritic field size of TuBu single cell clones matched the extent of axonal arborizations from corresponding MeTu cells. In agreement with subdomain-specific connectivity, TuBu-l and -c domains manifested the most restricted dendritic arbors whereas TuBu-m formed broad dendritic fields (Fig. 5H, J). We counted an average number of 8-12 TuBu neurons for different classes, covering a given SU domain along the d-v axis. To test if the spatial overlap of MeTu axon terminals and TuBu dendrites was indicative of synaptic connections we used the activity dependent GRASP technique (Karuppudurai et al., 2014, Macpherson et al., 2015). Indeed, GRASP between presynaptic MeTu neuron subtypes and various sets of TuBu neurons revealed a strict matching of synaptic partners within, but not across SU domains (Fig. 5C-D).

Non-stereotypic organization of AOTU efferents in the bulb region

TuBu axons form a single fascicle which extends from the AOTU towards the bulb, where they then segregate towards distinct domains according to their SU domain identity (Fig. 5K; compare also (Omoto et al., 2017): We found that TuBu-l and -c neurons terminated in adjacent regions of the superior bulb (BU_s), whereas axons of TuBu-m neurons targeted into the inferior bulb (BU_i) (Fig. 5F, G). Hence topographic and non-topographic visual pathways remain spatially segregated within the bulb (we did not analyze innervations of the SU_a, described in Omoto, Keles et al. 2017). We next analyzed the spatial organization of dendritic and axonal arborization of single cell and small size TuBu clones. To determine if the

retinotopic representation from the AOTU is translated into the terminals of TuBu cells within the bulb region, we compared the relative positions of TuBu dendrites in the SU with the location of their axon terminals in the bulb region by generating two-cell clones within a population of TuBu-l and TuBu-c neurons, respectively (Fig. 6A-C). This analysis revealed that adjacent dendritic positions in the AOTU are indeed maintained within neighboring domains of the bulb, although their relative position to each other within the bulb area is variable (Fig. 6A, B). To further characterize the spatial patterning of TuBu neurons we generated a series of single cell clones and compared the relative position of TuBu dendrites in the SU with their axon termination areas in the bulb, this time for individual TuBu clones (Fig. 6D). In contrast to the strict spatial correlation between MeTu neuron dendrite position along the a-p axis and its axon termination along the d-v axis, the position of TuBu dendritic fields within the SU domain did not predict their site of axon termination within the bulb area (Fig. 6E, F). For example, single TuBu-l clones with dendritic fields in the dorsal SU domain manifested projections either to the dorsal, ventro-lateral, or ventral-medial bulb domains (Fig. 6F, left column). Similarly, the dorsal bulb region could receive TuBu afferents from neurons with either dorsal, medial, or ventral SU positions (Fig. 6F, right column). Given the fixed spatial proximity of TuBu axon terminals with adjacent dendritic fields described above, these data suggest that the topographic map of the AOTU is maintained in the bulb were it translates into a more variable organization regarding the a-p and d-v axes of TuBu terminals within a sector of the bulb.

Projections of AOTU domain identity onto ring neurons of the EB

Efferent neurons from the bulb region have been shown to target specific ring layers within the EB (R neurons) (Wolff et al., 2015, Franconville et al., 2018). To characterize the matching between TuBu cells and the spatial positioning of R neuron subtype dendrites, we performed a series of co-labeling studies (Fig. 7A-F), which, for technical reasons, focused on two TuBu-classes: TuBu-l_p & TuBu-c_a in combination with different candidate R neuron types of the BU_s: R2, R4d, and R5. As previously shown, the BU_i is innervated by R3 neurons (Fig.

7G), but not targeted by TuBu-l or TuBu-c neurons (data not shown, compare (Omoto et al., 2017). In the BU_s we could identify matching projection patterns, in which all TuBu axons of one class appeared to contact only one specific R neuron type. This was particularly clear in the case of TuBu-l cells, which clearly overlap with R4d (Fig. 7A), but not with R2 or R5 (Fig. 7B, C). For TuBu-c neurons, a partial overlap with the dendritic fields of R2 was detected (Fig. 7E), while avoiding contacts with R4d and R5 (Fig. 7D, F). Furthermore, co-labeling revealed that dendrites of different R neuron types segregate into coherent, non-overlapping domains within the bulb neuropil (Fig. 7G-J). In summary, in our analysis of two representative TuBu classes and three candidate R neuron classes innervating the superior bulb (BU_s), we could dissect one fully matching pair of TuBu → R neuron circuit, as well as another pair with a partial overlap. Thus, yet another synaptic level is added to the parallel visual pathways described here, as distinct AOTU efferents remain separated and contact different EB rings (Fig. 7K).

Discussion

Like various other sensory modalities for which spatial information is critical, neural circuits in the visual system of many animals are organized in a topographic fashion to maintain the neighboring relationship of adjacent pixels detected by photoreceptors in the periphery, along the visual pathways into the central brain (Livingstone and Hubel, 1988). The topographic representation of different kinds of sensory information within the central brain of *Drosophila* is currently being investigated using molecular genetic tools in combination with cell-type specific driver lines (Tsubouchi et al., 2017, Patella and Wilson, 2018). Although it is well known that spatially-patterned visual stimuli induce coherent activity bumps in the Drosophila CX (Seelig and Jayaraman, 2013, Seelig and Jayaraman, 2015, Kim et al., 2017, Green et al., 2017), the pathway translating peripheral visual information into central activity patterns remains poorly understood.

Parallel topographic pathways into the central brain

Here we have shown that medulla inputs to the AOTU fall into two morphological types regarding their arborization patterns: broad innervation vs. spatially-restricted axon terminals. In both cases, only a single domain within the AOTU is targeted. While the topographic representation from the lobula neuropil is mostly lost in the broad innervation pattern of converging and intermingling LC projection neurons onto the majority of optic glomeruli (Panser et al., 2016, Wu et al., 2016, Keles and Frye, 2017), we could identify a unique spatial organization for the output channel from the medulla (Fig. 8). Topographic representation of the medulla (at least its dorsal half, where most driver lines used here are expressed) is maintained in the SU of the AOTU, which is spatially separated from lobula representation within the AOTU (the LU). Interestingly, a strict topographic correlation only exists between the a-p position of the dendritic fields of MeTu projection neurons in the medulla and their restricted axon termination along the d-v axis within distinct domains of the SU in the AOTU. No such topography exists along the d-v axis in the medulla. These neurons are therefore well suited for filtering out specific visual information (such as landmarks or celestial bodies) for guiding heading decisions during visually guided navigation (Giraldo et al., 2018).

Based on their morphology, as well as their molecular identity, three principle types of MeTu neurons provide input into the AOTU, with overlapping dendritic fields within the medulla but segregated axon terminals to distinct AOTU (sub-)domains. MeTu-l and -c classes have a similar neuronal morphology with dendrite arborization restricted to a single medulla layer (M6) and spatially narrow axon termination areas in four separate AOTU subdomains (SU-l_a, -l_p, -c_a, and -c_p), thereby building several pathways arranged in parallel (Fig. 8). Our nomenclature of the SU subdomain organization differs slightly from previous studies (Omoto et al., 2017), since it is now based on the expression patterns of different cell surface molecules, which might reflect the functional organization of these structures. Because of this new classification, both lateral and central domains (but not the medial domain) of the SU become further subdivided into anterior (SU-l_a and SU-c_p) and posterior halves (SU-l_p and SU-c_p). Nevertheless, it should be noted that the total number of subdomains remains the same in both nomenclatures, with the major difference being the posterior-lateral subdomain ('lp') has

been attributed to the central domain (SU-c_p) in our study, as part of the Connectin-positive central neuropil. Based on the connectome reconstruction of the hemibrain dataset (Scheffer et al., 2020), which reports in a total number of 347 MeTu neurons ('MC61-type'), we estimate ~60 MeTu neurons per topographic class (and twice that for MeTu-m cells), assuming an equal innervation of SU subdomains of similar volume. Since we counted 8-12 TuBu neurons from three independent expression lines, we estimate a convergence ratio from MeTu to TuBu neurons of about 8:1 to 5:1. Only the organization of the MeTu-l and MeTu-c neurons clearly enables a spatial projection of visual information from the columnar organization in the medulla to the corresponding AOTU domains, which seems well suited to relay topographic information along one spatial axis towards the central brain.

The transformation of topographic information in the central brain

The borders of the SU compartments are respected by molecularly defined populations of TuBu neurons, thereby defining the next synaptic elements in the parallel pathways towards the bulb neuropil. While this neuropil with its afferent (TuBu) and efferent (R neurons) channels has been intensively studied in recent years (Seelig and Jayaraman, 2015, Seelig and Jayaraman, 2013, Omoto et al., 2017, Sun et al., 2017, Shiozaki and Kazama, 2017, Franconville et al., 2018, Green et al., 2017), there still remains a gap in knowledge concerning how precise synaptic connections convey topographic information to the central complex. Four major findings of the TuBu→EB circuit are revealed by our study: First, the topographic position of TuBu dendrites in the SU is not translated into a defined position within the bulb, but instead exhibits a targeting plasticity within a restricted bulb area. Secondly, while the recent dissection of the AOTU→EB pathways described the bulb as a tripartite structure (Omoto et al., 2017) including both afferent and efferent neurons, we can now refine this picture by highlighting that, although our analysis of TuBu-neurons is mainly restricted to only two representative TuBu classes (one in the SU-l_p and the other in the SU-c_a domain), both these classes target to areas within the superior bulb (BU_s). More broadly expressed driver lines revealed exclusive TuBu neuron innervation of the BU_s, indicating that additional TuBu

classes target to this bulb area (data not shown). Thus, we expect at least four different classes of TuBu neurons to exclusively innervate the BU_s (TuBu-l_a, TuBu-l_p, TuBu-c_a, and TuBu-c_p), each of them connecting to a different set of output neurons, indicating an even more complex organization of the bulb, in particular the BU_s. Thirdly, TuBu classes project onto dendritic areas of R neuron classes (so called 'sectors') within the bulb, and specific connections are formed between TuBu neurons and R neuron classes. Although we could identify three R neuron classes within the BU_s, there probably exists a much higher diversity of connections within this small area of the bulb, reaching beyond the scope of this study. For instance, the postsynaptic partners of one subset of TuBu-c_a neurons as well as neurons contacted by R2 and R5 dendrites remain to be identified. Additional post-synaptic partners other than R neurons are contacted by TuBu neurons, like contralaterally projecting neurons described in the locust (el Jundi and Homberg, 2012) and the bumblebee (Pfeiffer and Kinoshita, 2012), which connect the AOTU units of both hemispheres (TuTu neurons).

It appears therefore that topography is conserved within the AOTU output neuron projections towards the bulb and ring neurons, which is in good agreement with their physiological responses to visual stimuli, like bright objects (Omoto et al., 2017, Sun et al., 2017, Shiozaki and Kazama, 2017). All ring neurons of the same type occupy the same ring layer within the ellipsoid body, raising the question of how topographic information is integrated within central complex neuropils. Interestingly, different MeTu neuron types with similar receptive fields may innervate different AOTU domains and thereby connect to different TuBu neuron populations forming parallel channels that then diverge within the bulb regions, where we found SU-l_p and SU-c_a efferents mapping onto separate ring neurons (R4d versus R2). Hence we could define at least two distinct topographic MeTu channels into the central brain. While functional differences between the BU_i and BU_s have been described (Omoto et al., 2017), functional studies (Seelig and Jayaraman, 2013, Sun et al., 2017) have not yet compared the physiological responses of different TuBu classes, or the responses of R neurons within the BU_s. Based on the data presented here, we would expect that retinotopic

information in the BU_s remains represented in the respective sector that is associated with their TuBu class.

An additional, non-topographic pathway into the central brain

A morphologically distinct class of MeTu cells is formed by MeTu-m cells. One distinguishing feature in respect to other MeTu cell types is that many cells arborize broadly in their respective AOTU domain. We found axon terminals of single MeTu-m neurons invariably spread across the a-p axis of their SU-domain, while in the d-v axis they either covered their domain completely or partially – the former case being reminiscent of the afferent organization of LC neurons from the lobula within optic glomeruli in the PVLP regions, while the latter case is similarly described for lobula neurons innervating the AOTU's large unit (LU) (Wu et al., 2016), where the topography of LC10 neurons in the LU has been analyzed, resulting in the distinction of four different LC10-classes. It remains to be seen whether MeTu-m neurons also could be divided into such classes. Those cells innervating the complete SU-m are well suited to form a non-topographic channel to the central brain. Interestingly, while topographic MeTu-l and -c neurons form dendritic fields within a single medulla layer, MeTu-m neurons integrate from three different medulla layers, reminiscent and in fact similar to some lobular LC neuron types, the main afferents of the AOTU large unit, for which a comparable rough topography along the dorso-ventral axis has previously been found (Wu et al., 2016). Furthermore, only MeTu-m neurons form a collateral arborization in the lobula, indicating that this pathway could directly integrate visual information from both the medulla and lobula. Our observation that MeTu-m neurons contact a population of TuBu neurons which projects into the inferior bulb area (Bu_i) separated from other TuBu neurons further suggests a different role for this pathway: Sun, Nern et al (2017) describe a contralateral inhibition mediated by the Bu_i, supporting a model in which the SU-m pathway is involved in suppressing ipsilateral stimuli with the expense of reduced spatial resolution.

Taken together, topographic and non-topographic afferents generate an interesting assembly of adjacent domains within the AOTU, from exclusively topographic medulla input

in SU-l and SU-c domains, non-topographic medullar (and potentially also lobular) input in SU-m, and another large area of non-topographic input exclusively from the lobula in the LU (Fig. 8). Thus, we have identified multiple parallel topographic pathways separated from a parallel non-topographic channel.

Evolutionary conservation of the anterior visual pathway

This principle visual pathway involving the AOTU as a central relay station between medullar/ lobular inputs and the central brain is widely shared among different insect taxa, where homologous structures can be found, e.g. orthopterans (Homberg et al., 2003), hymenopterans (Mota et al., 2011) and beetles (Immonen et al., 2017). The stimuli conveyed by this 'anterior visual pathway' have been addressed in only a few insect species so far. Most prominently, the AOTU has been associated with celestial orientation using polarized skylight in several species (Pfeiffer et al., 2005) or in chromatic processing (Paulk et al., 2008, Mota et al., 2013). Dorsal rim ommatidia harboring polarization-sensitive photoreceptors for polarized light vision are crucial for the sky-compass orientation and exist in most insects analyzed, like locusts (Pfeiffer et al., 2005, Homberg and Paech, 2002), butterflies (Heinze and Reppert, 2011, Labhart et al., 2009) and honeybees (Held et al., 2016), as well as flies (Wada, 1974, Wada, 1971, Wernet et al., 2003). However, it remains unknown whether MeTu neurons receive direct or indirect input from modality-specific cell types located in the DRA (Sancer et al., 2020, Sancer et al., 2019). In addition, processing of chromatic information was also shown to be accomplished via the AOTU in several insects (Otsuna et al., 2014, Mota et al., 2013). We have now identified inputs to this pathway, by identifying direct connections between MeTu cells and UV-sensitive R7 photoreceptor cells in medulla layer M6.

Furthermore, the molecular markers used here can serve as future tools to reveal the molecular mechanisms that underlie the formation of the LC-optic glomeruli network across species. Since *Drosophila* is among the smallest species for which the AOTU has been characterized, and is believed to be a behavioral generalist, even more sophisticated architectures of the SU-homologue could exist in other insect taxa. On the anatomical and

functional level, optic glomeruli share many features with the synaptic neuropil within the antennal lobe, which led to the postulation that the glomerular organization in the protocerebrum (optic glomeruli) and the deutocerebrum (olfactory glomeruli) are in fact homologous structures (Strausfeld, 1989, Mu et al., 2012). Indeed, we found molecular characteristics in the PVLP and AOTU that resemble the combinatorial code of cell-surface proteins in the olfactory system (e.g. expression patterns of Ten-m, Con, Caps and Sema1a in both systems). However, future developmental studies of mutant LC and MeTu neurons are needed to test to what extent common mechanisms of glomerular circuit assembly exist in both sensory systems. Although the idea of a serial homology of glomerular organized neural system is far from being resolved, it will be intriguing for further studies to analyze the developmental mechanisms that underlie the circuit formation of these parallel AOTU pathways and optic glomeruli circuits as well as to compare them with known molecular functions during olfactory system maturation.

Limitations of the study

We cannot exclude that the SU of the AOTU might consist of additional functional units that so far have not been identified and that we missed neurons in our analysis due to the lack of expression lines to visualize them. Populations of neurons that we classified as a single type might turn out to be different enough (by morphology and/or synapse partners) to justify the establishment of further pathways and we might have missed these cell types in our single cell labeling experiment, as this method involves random events where scarcer neurons can easily remain unnoticed. In vivo experiments measuring neuronal activity and responses to visual stimuli were beyond the scope of our study but will be an essential part for understanding the functional features of the circuit. The wealth of genetic tools and their manifold combinations in Drosophila certainly provide capabilities of detailed analyses. As the driver lines we used for our study to unravel the components of the visual pathway are publicly available and could be used to measure and manipulate neuronal activity we hope to have paved the way for future studies of components of this visual circuit.

Resource Availability

Lead Contact

Further information and requests for resources and reagents should be directed to and will be fulfilled by the Lead Contact, Thomas Hummel (thomashummel@univie.ac.at).

Materials Availability

The ort-mCD8::GFP construct is available on request without restriction.

Data and Code Availability

The datasets supporting the current study are available from the corresponding author on request.

Methods

All methods can be found in the accompanying Transparent methods supplemental file.

Acknowledgements

The authors would like to thank Chi-Hon Lee, Andrew Straw, Bassem Hassan, Iris Salecker, Tom Clandinin, Stefan Baumgartner, Robert AH White and Claude Desplan for fly stocks and reagents. This work was supported by the Deutsche Forschungsgemeinschaft (DFG) through Heisenberg Fellowship HU 992/1-1 and HU 992/2-1 (T.H.), through grants WE 5761/2-1 (M.F.W.), SFB958 (Teilprojekt A23), through the Schram Foundation (T.H.), AFOSR grant FA9550-19-1-7005 (M.F.W), through the Berlin Excellency Cluster NeuroCure (M.F.W.), with support from the Fachbereich Biologie, Chemie & Pharmazie of the Freie Universität Berlin (M.F.W.), as well as the Faculty of Life Sciences at the University of Vienna (T.H.) and the Division of Neurobiology at Freie Universität Berlin (support of FU Berlin and the National Institute of Health to Robin Hiesinger)(M.F.W.).

Author Contributions

Conzeptualization, T.H. and L.T.; Methodology, T.H., L.T., and M.F.W.; Investigation, L.T., L.G., and G.S.; Resources, T.H. and M.F.W.; Writing – Original Draft, L.T.; Writing – Review & Editing, L.T., T.H. and M.F.W.; Supervision, T.H.; Funding Acquisition, T.H. and M.F.W.

Declaration of Interests

The authors declare no competing interests.

References

BAHL, A., SERBE, E., MEIER, M., AMMER, G. & BORST, A. 2015. Neural Mechanisms for Drosophila Contrast Vision. *Neuron,* 88, 1240-1252.

BEHNIA, R. & DESPLAN, C. 2015. Visual circuits in flies: beginning to see the whole picture. *Curr Opin Neurobiol,* 34, 125-32.

BORST, A. 2014. Fly visual course control: behaviour, algorithms and circuits. *Nat Rev Neurosci,* 15, 590-9.

COSTA, M., MANTON, J. D., OSTROVSKY, A. D., PROHASKA, S. & JEFFERIS, G. S. 2016. NBLAST: Rapid, Sensitive Comparison of Neuronal Structure and Construction of Neuron Family Databases. *Neuron,* 91, 293-311.

EGELHAAF, M. & KERN, R. 2002. Vision in flying insects. *Curr Opin Neurobiol,* 12, 699-706.

EL JUNDI, B. & HOMBERG, U. 2012. Receptive field properties and intensity-response functions of polarization-sensitive neurons of the optic tubercle in gregarious and solitarious locusts. *J Neurophysiol,* 108, 1695-710.

EL JUNDI, B., PFEIFFER, K., HEINZE, S. & HOMBERG, U. 2014. Integration of polarization and chromatic cues in the insect sky compass. *J Comp Physiol A Neuroethol Sens Neural Behav Physiol,* 200, 575-89.

EL JUNDI, B., WARRANT, E. J., PFEIFFER, K. & DACKE, M. 2018. Neuroarchitecture of the dung beetle central complex. *J Comp Neurol,* 526, 2612-2630.

FISCHBACH, K. F. & LYLY-HUNERBERG, I. 1983. Genetic dissection of the anterior optic tract of Drosophila melanogaster. *Cell Tissue Res,* 231, 551-63.

FISHER, Y. E., LEONG, J. C., SPORAR, K., KETKAR, M. D., GOHL, D. M., CLANDININ, T. R. & SILIES, M. 2015. A Class of Visual Neurons with Wide-Field Properties Is Required for Local Motion Detection. *Curr Biol,* 25, 3178-89.

FISHER, Y. E., LU, J., D'ALESSANDRO, I. & WILSON, R. I. 2019. Sensorimotor experience remaps visual input to a heading-direction network. *Nature,* 576, 121-125.

FRANCONVILLE, R., BERON, C. & JAYARAMAN, V. 2018. Building a functional connectome of the Drosophila central complex. *Elife,* 7.

GAO, S., TAKEMURA, S. Y., TING, C. Y., HUANG, S., LU, Z., LUAN, H., RISTER, J., THUM, A. S., YANG, M., HONG, S. T., WANG, J. W., ODENWALD, W. F., WHITE, B. H., MEINERTZHAGEN, I. A. & LEE, C. H. 2008. The neural substrate of spectral preference in Drosophila. *Neuron,* 60, 328-42.

GIRALDO, Y. M., LEITCH, K. J., ROS, I. G., WARREN, T. L., WEIR, P. T. & DICKINSON, M. H. 2018. Sun Navigation Requires Compass Neurons in Drosophila. *Curr Biol,* 28, 2845-2852 e4.

GREEN, J., ADACHI, A., SHAH, K. K., HIROKAWA, J. D., MAGANI, P. S. & MAIMON, G. 2017. A neural circuit architecture for angular integration in Drosophila. *Nature,* 546, 101-106.

HADJIECONOMOU, D., ROTKOPF, S., ALEXANDRE, C., BELL, D. M., DICKSON, B. J. & SALECKER, I. 2011. Flybow: genetic multicolor cell labeling for neural circuit analysis in Drosophila melanogaster. *Nat Methods,* 8, 260-6.

HANESCH, U., FISCHBACH, K. F. & HEISENBERG, M. 1989. Neuronal Architecture of the Central Complex in Drosophila-Melanogaster. *Cell and Tissue Research,* 257, 343-366.

HEINZE, S. 2017. Unraveling the neural basis of insect navigation. *Curr Opin Insect Sci,* 24, 58-67.

HEINZE, S. & HOMBERG, U. 2007. Maplike representation of celestial E-vector orientations in the brain of an insect. *Science,* 315, 995-7.

HEINZE, S. & REPPERT, S. M. 2011. Sun Compass Integration of Skylight Cues in Migratory Monarch Butterflies. *Neuron,* 69, 345-358.

HELD, M., BERZ, A., HENSGEN, R., MUENZ, T. S., SCHOLL, C., ROSSLER, W., HOMBERG, U. & PFEIFFER, K. 2016. Microglomerular Synaptic Complexes in the Sky-Compass Network of the Honeybee Connect Parallel Pathways from the Anterior Optic Tubercle to the Central Complex. *Front Behav Neurosci,* 10, 186.

HOMBERG, U. 2015. Sky Compass Orientation in Desert Locusts-Evidence from Field and Laboratory Studies. *Front Behav Neurosci,* 9, 346.

HOMBERG, U., HOFER, S., PFEIFFER, K. & GEBHARDT, S. 2003. Organization and neural connections of the anterior optic tubercle in the brain of the locust, Schistocerca gregaria. *J Comp Neurol,* 462, 415-30.

HOMBERG, U. & PAECH, A. 2002. Ultrastructure and orientation of ommatidia in the dorsal rim area of the locust compound eye. *Arthropod Struct Dev,* 30, 271-80.

HONG, W., MOSCA, T. J. & LUO, L. 2012. Teneurins instruct synaptic partner matching in an olfactory map. *Nature,* 484, 201-7.

HONG, W., ZHU, H., POTTER, C. J., BARSH, G., KURUSU, M., ZINN, K. & LUO, L. 2009. Leucine-rich repeat transmembrane proteins instruct discrete dendrite targeting in an olfactory map. *Nat Neurosci,* 12, 1542-50.

HONKANEN, A., ADDEN, A., DA SILVA FREITAS, J. & HEINZE, S. 2019. The insect central complex and the neural basis of navigational strategies. *J Exp Biol,* 222.

HUMMEL, T., VASCONCELOS, M. L., CLEMENS, J. C., FISHILEVICH, Y., VOSSHALL, L. B. & ZIPURSKY, S. L. 2003. Axonal targeting of olfactory receptor neurons in Drosophila is controlled by Dscam. *Neuron,* 37, 221-31.

IMMONEN, E. V., DACKE, M., HEINZE, S. & EL JUNDI, B. 2017. Anatomical organization of the brain of a diurnal and a nocturnal dung beetle. *J Comp Neurol,* 525, 1879-1908.

ITO, K., SHINOMIYA, K., ITO, M., ARMSTRONG, J. D., BOYAN, G., HARTENSTEIN, V., HARZSCH, S., HEISENBERG, M., HOMBERG, U., JENETT, A., KESHISHIAN, H., RESTIFO, L. L., ROSSLER, W., SIMPSON, J. H., STRAUSFELD, N. J., STRAUSS, R., VOSSHALL, L. B. & INSECT BRAIN NAME WORKING, G. 2014. A systematic nomenclature for the insect brain. *Neuron,* 81, 755-65.

JENETT, A., RUBIN, G. M., NGO, T. T., SHEPHERD, D., MURPHY, C., DIONNE, H., PFEIFFER, B. D., CAVALLARO, A., HALL, D., JETER, J., IYER, N., FETTER, D., HAUSENFLUCK, J. H., PENG, H., TRAUTMAN, E. T., SVIRSKAS, R. R., MYERS, E. W., IWINSKI, Z. R., ASO, Y., DEPASQUALE, G. M., ENOS, A., HULAMM, P., LAM, S. C., LI, H. H., LAVERTY, T. R., LONG, F., QU, L., MURPHY, S. D., ROKICKI, K., SAFFORD, T., SHAW, K., SIMPSON, J. H., SOWELL, A., TAE, S., YU, Y. & ZUGATES, C. T. 2012. A GAL4-driver line resource for Drosophila neurobiology. *Cell Rep,* 2, 991-1001.

KARUPPUDURAI, T., LIN, T. Y., TING, C. Y., PURSLEY, R., MELNATTUR, K. V., DIAO, F., WHITE, B. H., MACPHERSON, L. J., GALLIO, M., POHIDA, T. & LEE, C. H. 2014. A hard-wired glutamatergic circuit pools and relays UV signals to mediate spectral preference in Drosophila. *Neuron,* 81, 603-615.

KELES, M. F. & FRYE, M. A. 2017. Object-Detecting Neurons in Drosophila. *Curr Biol,* 27, 680-687.

KIM, S. S., ROUAULT, H., DRUCKMANN, S. & JAYARAMAN, V. 2017. Ring attractor dynamics in the Drosophila central brain. *Science,* 356, 849-853.

KIRSCHFELD, K. 1976. Neural Principles in Vision. *In:* ZETTLER, F. A. W., R. (ed.) *Neural Principles in Vision. Proceedings in Life Sciences.* Berlin, Heidelberg: Springer.

KVON, E. Z., KAZMAR, T., STAMPFEL, G., YANEZ-CUNA, J. O., PAGANI, M., SCHERNHUBER, K., DICKSON, B. J. & STARK, A. 2014. Genome-scale functional characterization of Drosophila developmental enhancers in vivo. *Nature,* 512, 91-5.

LABHART, T., BAUMANN, F. & BERNARD, G. D. 2009. Specialized ommatidia of the polarization-sensitive dorsal rim area in the eye of monarch butterflies have non-functional reflecting tapeta. *Cell Tissue Res,* 338, 391-400.

LAISSUE, P. P. & VOSSHALL, L. B. 2008. The olfactory sensory map in Drosophila. *Adv Exp Med Biol,* 628, 102-14.

LEE, T. & LUO, L. 1999. Mosaic analysis with a repressible cell marker for studies of gene function in neuronal morphogenesis. *Neuron,* 22, 451-61.

LIN, C. Y., CHUANG, C. C., HUA, T. E., CHEN, C. C., DICKSON, B. J., GREENSPAN, R. J. & CHIANG, A. S. 2013. A comprehensive wiring diagram of the protocerebral bridge for visual information processing in the Drosophila brain. *Cell Rep,* 3, 1739-53.

LIU, G., SEILER, H., WEN, A., ZARS, T., ITO, K., WOLF, R., HEISENBERG, M. & LIU, L. 2006. Distinct memory traces for two visual features in the Drosophila brain. *Nature,* 439, 551-6.

LIVINGSTONE, M. & HUBEL, D. 1988. Segregation of form, color, movement, and depth: anatomy, physiology, and perception. *Science,* 240, 740-9.

MACPHERSON, L. J., ZAHARIEVA, E. E., KEARNEY, P. J., ALPERT, M. H., LIN, T. Y., TURAN, Z., LEE, C. H. & GALLIO, M. 2015. Dynamic labelling of neural connections in multiple colours by trans-synaptic fluorescence complementation. *Nat Commun,* 6, 10024.

MAUSS, A. S., VLASITS, A., BORST, A. & FELLER, M. 2017. Visual Circuits for Direction Selectivity. *Annu Rev Neurosci,* 40, 211-230.

MOTA, T., GRONENBERG, W., GIURFA, M. & SANDOZ, J. C. 2013. Chromatic processing in the anterior optic tubercle of the honey bee brain. *J Neurosci,* 33, 4-16.

MOTA, T., YAMAGATA, N., GIURFA, M., GRONENBERG, W. & SANDOZ, J. C. 2011. Neural organization and visual processing in the anterior optic tubercle of the honeybee brain. *J Neurosci,* 31, 11443-56.

MU, L., ITO, K., BACON, J. P. & STRAUSFELD, N. J. 2012. Optic glomeruli and their inputs in Drosophila share an organizational ground pattern with the antennal lobes. *J Neurosci,* 32, 6061-71.

NERN, A., PFEIFFER, B. D. & RUBIN, G. M. 2015. Optimized tools for multicolor stochastic labeling reveal diverse stereotyped cell arrangements in the fly visual system. *Proc Natl Acad Sci U S A,* 112, E2967-76.

NEWSOME, T. P., ASLING, B. & DICKSON, B. J. 2000. Analysis of Drosophila photoreceptor axon guidance in eye-specific mosaics. *Development,* 127, 851-60.

OFSTAD, T. A., ZUKER, C. S. & REISER, M. B. 2011. Visual place learning in Drosophila melanogaster. *Nature,* 474, 204-7.

OMOTO, J. J., KELES, M. F., NGUYEN, B. M., BOLANOS, C., LOVICK, J. K., FRYE, M. A. & HARTENSTEIN, V. 2017. Visual Input to the Drosophila Central Complex by Developmentally and Functionally Distinct Neuronal Populations. *Curr Biol,* 27, 1098-1110.

OTSUNA, H. & ITO, K. 2006. Systematic analysis of the visual projection neurons of Drosophila melanogaster. I. Lobula-specific pathways. *J Comp Neurol,* 497, 928-58.

OTSUNA, H., SHINOMIYA, K. & ITO, K. 2014. Parallel neural pathways in higher visual centers of the Drosophila brain that mediate wavelength-specific behavior. *Front Neural Circuits,* 8, 8.

PANSER, K., TIRIAN, L., SCHULZE, F., VILLALBA, S., JEFFERIS, G., BUHLER, K. & STRAW, A. D. 2016. Automatic Segmentation of Drosophila Neural Compartments Using GAL4 Expression Data Reveals Novel Visual Pathways. *Curr Biol,* 26, 1943-1954.

PATELLA, P. & WILSON, R. I. 2018. Functional Maps of Mechanosensory Features in the Drosophila Brain. *Curr Biol,* 28, 1189-1203 e5.

PAULK, A. C., PHILLIPS-PORTILLO, J., DACKS, A. M., FELLOUS, J. M. & GRONENBERG, W. 2008. The processing of color, motion, and stimulus timing are anatomically segregated in the bumblebee brain. *J Neurosci,* 28, 6319-32.

PFEIFFER, K. & KINOSHITA, M. 2012. Segregation of visual inputs from different regions of the compound eye in two parallel pathways through the anterior optic tubercle of the bumblebee (Bombus ignitus). *Journal of Comparative Neurology,* 520, 212-229.

PFEIFFER, K., KINOSHITA, M. & HOMBERG, U. 2005. Polarization-sensitive and light-sensitive neurons in two parallel pathways passing through the anterior optic tubercle in the locust brain. *J Neurophysiol,* 94, 3903-15.

RIBEIRO, I. M. A., DREWS, M., BAHL, A., MACHACEK, C., BORST, A. & DICKSON, B. J. 2018. Visual Projection Neurons Mediating Directed Courtship in Drosophila. *Cell,* 174, 607-621 e18.

SANCER, G., KIND, E., PLAZAOLA-SASIETA, H., BALKE, J., PHAM, T., HASAN, A., MUNCH, L. O., COURGEON, M., MATHEJCZYK, T. F. & WERNET, M. F. 2019. Modality-Specific Circuits for Skylight Orientation in the Fly Visual System. *Curr Biol.*

SANCER, G., KIND, E., UHLHORN, J., VOLKMANN, J., HAMMACHER, J., PHAM, T., PLAZAOLA-SASIETA, H. & WERNET, M. F. 2020. Cellular and synaptic adaptations of neural circuits processing skylight polarization in the fly. *J Comp Physiol A Neuroethol Sens Neural Behav Physiol,* 206, 233-246.

SCHNELL, B., JOESCH, M., FORSTNER, F., RAGHU, S. V., OTSUNA, H., ITO, K., BORST, A. & REIFF, D. F. 2010. Processing of horizontal optic flow in three visual interneurons of the Drosophila brain. *J Neurophysiol,* 103, 1646-57.

SEELIG, J. D. & JAYARAMAN, V. 2013. Feature detection and orientation tuning in the Drosophila central complex. *Nature,* 503, 262-6.

SEELIG, J. D. & JAYARAMAN, V. 2015. Neural dynamics for landmark orientation and angular path integration. *Nature,* 521, 186-91.

SHIMOSAKO, N., HADJIECONOMOU, D. & SALECKER, I. 2014. Flybow to dissect circuit assembly in the Drosophila brain. *Methods Mol Biol,* 1082, 57-69.

SHINZA-KAMEDA, M., TAKASU, E., SAKURAI, K., HAYASHI, S. & NOSE, A. 2006. Regulation of layer-specific targeting by reciprocal expression of a cell adhesion molecule, capricious. *Neuron,* 49, 205-13.

SHIOZAKI, H. M. & KAZAMA, H. 2017. Parallel encoding of recent visual experience and self-motion during navigation in Drosophila. *Nat Neurosci,* 20, 1395-1403.

SILIES, M., GOHL, D. M. & CLANDININ, T. R. 2014. Motion-detecting circuits in flies: coming into view. *Annu Rev Neurosci,* 37, 307-27.

STRAUSFELD, N. J. 1989. Insect Vision and Olfaction - Common Design Principles of Neuronal Organization. *Neurobiology of Sensory Systems*, 319-353.

STRAUSS, R. 2002. The central complex and the genetic dissection of locomotor behaviour. *Curr Opin Neurobiol,* 12, 633-8.

STUART, A. E. 1999. From fruit flies to barnacles, histamine is the neurotransmitter of arthropod photoreceptors. *Neuron,* 22, 431-3.

SUN, Y., NERN, A., FRANCONVILLE, R., DANA, H., SCHREITER, E. R., LOOGER, L. L., SVOBODA, K., KIM, D. S., HERMUNDSTAD, A. M. & JAYARAMAN, V. 2017. Neural signatures of dynamic stimulus selection in Drosophila. *Nat Neurosci,* 20, 1104-1113.

TALAY, M., RICHMAN, E. B., SNELL, N. J., HARTMANN, G. G., FISHER, J. D., SORKAC, A., SANTOYO, J. F., CHOU-FREED, C., NAIR, N., JOHNSON, M., SZYMANSKI, J. R. & BARNEA, G. 2017. Transsynaptic Mapping of Second-Order Taste Neurons in Flies by trans-Tango. *Neuron,* 96, 783-795 e4.

TING, C. Y., MCQUEEN, P. G., PANDYA, N., LIN, T. Y., YANG, M., REDDY, O. V., O'CONNOR, M. B., MCAULIFFE, M. & LEE, C. H. 2014. Photoreceptor-derived activin promotes dendritic termination and restricts the receptive fields of first-order interneurons in Drosophila. *Neuron,* 81, 830-846.

TSUBOUCHI, A., YANO, T., YOKOYAMA, T. K., MURTIN, C., OTSUNA, H. & ITO, K. 2017. Topological and modality-specific representation of somatosensory information in the fly brain. *Science,* 358, 615-623.

TURNER-EVANS, D. B. & JAYARAMAN, V. 2016. The insect central complex. *Curr Biol,* 26, R453-7.

VARGA, A. G., KATHMAN, N. D., MARTIN, J. P., GUO, P. & RITZMANN, R. E. 2017. Spatial Navigation and the Central Complex: Sensory Acquisition, Orientation, and Motor Control. *Front Behav Neurosci,* 11, 4.

WADA, S. 1971. Special Rhabdomeric Type in Compound Eye of Flies. *Experientia,* 27, 1237-&.

WADA, S. 1974. Special Marginal Ommatidia of Flies (Diptera-Brachycera) - Architecture and Distribution in Compound Eyes. *Zeitschrift Fur Morphologie Der Tiere,* 77, 87-125.

WEIR, P. T. & DICKINSON, M. H. 2015. Functional divisions for visual processing in the central brain of flying Drosophila. *Proc Natl Acad Sci U S A,* 112, E5523-32.

WERNET, M. F., LABHART, T., BAUMANN, F., MAZZONI, E. O., PICHAUD, F. & DESPLAN, C. 2003. Homothorax switches function of Drosophila photoreceptors from color to polarized light sensors. *Cell,* 115, 267-79.

WOLFF, T., IYER, N. A. & RUBIN, G. M. 2015. Neuroarchitecture and neuroanatomy of the Drosophila central complex: A GAL4-based dissection of protocerebral bridge neurons and circuits. *J Comp Neurol,* 523, 997-1037.

WU, M., NERN, A., WILLIAMSON, W. R., MORIMOTO, M. M., REISER, M. B., CARD, G. M. & RUBIN, G. M. 2016. Visual projection neurons in the Drosophila lobula link feature detection to distinct behavioral programs. *Elife,* 5.

Figure Legends

Figure 1: Organization of afferent projections within olfactory and optic glomeruli

A. Overview over sensory glomeruli. Three pathways are shown, connecting medulla, lobula and antenna with their respective target neuropils (for clarity, lobula-AOTU connections are not drawn). Open circles represent the position of the cell body, closed circles a target glomerulus and arrows indicate dendritic arborizations. AOTU, anterior optic tubercle; PVLP, posterior ventrolateral protocerebrum; PLP, posterior lateral protocerebrum; **B, C.** Axon terminals of OR67d-expressing olfactory receptor neurons in the antennal lobe are branching throughout their target glomerulus and intermingle with each other. **D.** Schematic overview of visual projection neurons contributing to optic glomeruli (horizontal section). Only a subset of optic glomeruli are shown (the AOTU and five representatives in the PVLP). Afferents are illustrated by a single medullar (MeTu; red) and four lobular (LC; green, grey [terminals only]) neurons. Me, medulla; La, lamina; Lo, lobula; Lp, lobula plate. **E.** Optic glomeruli are marked by combinatorial expression of different cell-adhesion molecules (Connectin, magenta; Capricious; green). **F.** LC06 terminals (marked with syt:GFP) contribute to a characteristic optic glomerulus in the PVLP. **G.** Two individual LC06 clones innervate the complete glomerulus. **H.** Co-labeled LC10 and LC12 neurons. Somato-dendritic (magenta) and presynaptic compartments (green) are labeled using DenMark and syt:GFP, respectively. Cell bodies of LC10 are marked with an arrow, LC12 with an arrowhead. **J.** Single cell morphologies of LC10 and LC12. While LC12 neurons branch throughout their target glomerulus (J'), LC10 neuron terminals are dorso-ventrally restricted within the LU (J''). Arrowheads indicate position of cell bodies. **K, L.** AOTU compartments innervated either by MeTu or LC10 neurons. **M.** Schematic summary of pathways innervating AOTU and PVLP. Afferent medulla innervation indicated by blue neurons. **N-O.** Single cell clones of MeTu cells with spatially restricted (N) or broad axon terminals (O). Different subtypes of MeTu neurons can be defined based on the position and size of terminal arborizations and whether the lobula is also innervated (arrow in O). CB, cell body. For genotypes, see Supplemental Information.

Figure 2: Classification of MeTu neuron subtypes

A. Subdivision of AOTU's small unit (SU) can readily be observed with neuropil markers (anti-CadN). Arrowheads indicate borders of subdomains. In contrast, the large unit (LU) has a uniform appearance. **B.** Glial labeling using repo-Gal4 reflects the compartmentalization of the AOTU's SU (arrowheads). **C-E.** Each SU domain is characterized by a unique combination of three cell-adhesion molecules: Teneurin-m (blue) is strongly expressed in the lateral domain (C), with lower intensity in the medial domain and the LU. The lateral domain is further divided into an anterior, Teneurin-m negative (asterisk) and a posterior, Teneurin-m-positive compartment (C'). Connectin expression (red) defines the central domain (D, D'). Capricious-Gal4 (yellow) marks the medial domain (E, E'). **F, G.** Domain borders are respected by terminals of MeTu subtypes: different Gal4-labeled MeTu neurons innervate either the lateral (F-F') or medial domain (G-G'), without overlapping into the central, Connectin-positive (red) domain. **H-K.** Further division of the lateral and central domain into anterior and posterior compartments: A combination of LexA- (green) and Gal4- (magenta) lines reveals a subdivision of the central domain (H). A small subset of LexA-expressing neurons also innervates the anterior part of the lateral domain (asterisk). Anti-Connectin (blue) labels the complete central domain (H'). The posterior part of the lateral domain is exclusively innervated by a population of MeTu-l neurons, and likewise defined by Teneurin-m expression (green) (J). The arrowhead marks turning MeTu-l axons (these are not innervating the central domain). The complete central, Connectin-positive (green), domain is labeled by a line specific for MeTu-c neurons (magenta) (K). **L, L'.** Dendrites of MeTu-c neurons (green) are restricted in medulla layer M6, in a sublayer below R7 terminals and Dm8 neurons (magenta). **M, M'.** Three medulla layers are occupied by MeTu-m (arrowheads). Photoreceptors are labeled with anti-Chaoptin (24B10). SL, serpentine layer. **N-P'.** MeTu-c/-l neurons and MeTu-m neurons do not overlap in the medulla (N'-P'). Asterisks indicate the respective unlabeled SU-domain. MeTu-c and MeTu-l terminals are separated in the SU, while sharing the same medulla layer. Arrowhead in N' points to MeTu-m dendrites in M2. **Q.** Schematic overview over MeTu neuron

subtype morphology in medulla and SU. Caps: Capricious; Con: Connectin; Ten-m: Teneurin-m. For genotypes, see Supplemental Information.

Figure 3: Connectivity between photoreceptors and MeTu neurons

A. R7-specific transTango experiment using (rh3+rh4)-Gal4 ('panR7') reveals tomato-positive transTango signal in MeTu processes to the SU of the AOTU (dashed area in A' and A''). **B.** No transTango signal is detectable in (rh5+rh6 / 'panR8') > transTango experiments (B' and B''). **C.** Single cell MeTu-l clone visualized via R94G05 > MCFO-1 reveals an exemplary neuron with dendrites in multiple medulla layers and processes reaching to higher medulla levels (arrowhead in layer M3). **D.** Expression of the newly generated ort-mCD8:GFP transgene in the AOTU. The domains of the SU are labeled (SU-l_a, SU-c_a, SU-c_p), whereas the LU is not labeled (D'). **E.** MeTu-l driver R94G05 labels both MeTu-l_a and MeTu-l_p populations, yet only MeTu-l_a are post-synaptic to photoreceptors (E'). **F.** MeTu-l driver R52H03 specifically labels MeTu-l_p and MeTu-c_a populations, of which only MeTu-c_a are post-synaptic to photoreceptors (F'). **G.** MeTu-c driver R67C09 specifically labels MeTu-c_a cells, which are post-synaptic to photoreceptors (G'). **H.** MeTu-c driver R25H10 specifically labels MeTu-l_a and MeTu-c_p populations, both of which are post-synaptic to photoreceptors (H'). **I.** MeTu-l driver R20B05 labels MeTu-m cells, which are not post-synaptic to photoreceptors (I'). **J.** Schematic summary of the results from D-I. For genotypes, see Supplemental Information.

Figure 4: Topographic organization of AOTU projections

A-C. FLYBOW-labeling of MeTu-neurons innervating their respective domain of the SU (magnified in A', B', C'). Arrow in (C) indicates innervation of the lobula by MeTu-m neurons. **D.** Two neighboring cells (blue arrowheads) innervate different positions within the dorsal medulla and target the lateral and the central SU-domain, respectively (white arrowheads). CB, cell body. **E.** Two MeTu clones with overlapping dendritic fields at the posterior edge of the medulla target to the dorsal edge of either the lateral domain (yellow neuron) or the central domain (magenta neuron), respectively. **F.** Anterior-posterior, but not dorso-ventral positions

in the medulla correlate with topographic projections in the AOTU: MeTu-c neurons at the same a-p position in the medulla target into the same area of the central SU-domain (different angles of the same brain are shown). **G-J.** Topographic projections of MeTu-c neurons: Central dendritic fields in the medulla correlate with central termination the AOTU (G'), anterior dendritic positions in the medulla correlate with ventral targeting (H'), while posterior medullar dendrites correlate with dorsal termination (J'). Size of dendritic fields and size of innervated target area did not correlate (blue arrowheads indicate cell bodies). **K.** Dendritic fields of neighboring clones at the anterior rim of the medulla maintain their topography in the AOTU: The red clone, being located more posteriorly in the medulla, terminates at a more dorsal position in the AOTU. **L.** The size of dendritic fields varies amongst MeTu-l neurons. **M.** Overlap of dendritic fields between two MeTu-l clones (different angles of the same brain are shown). **N.** Summary of the FLYBOW-pairs described above (colors accordingly) and model of topographic relationships between medulla dendritic fields and SU axis of innervation. For genotypes, see Supplemental Information.

Figure 5: Bulb-innervating neurons descending from the AOTU maintain domain identity

A. The bulb neuropil receives input from all three SU-domains. **B.** Terminals of TuBu-l and TuBu-c neurons are spatially separated within the bulb (asterisks mark the unlabeled anterior-lateral and posterior-central SU-domains). **C, D.** Pre- to postsynaptic matching of domain-specific expression lines in the SU revealed by synGRASP: Anti-GFP (yellow) detects the presynaptic moiety of TuBu-l, expressed under Gal4-control. Positive GRASP-signal is obtained in combination with MeTu-l neurons (C'). **D.** TuBu-c neurons (yellow) are synaptic partners of MeTu-c neurons (D'), whereas no synaptic connections are formed with MeTu-l neurons (D''). **E.** Scheme depicting how afferent MeTu neurons and efferent TuBu neuron subtypes form circuits in their respective SU-domains. **F-J'.** FLYBOW-labeling using a reporter for the majority of TuBu neurons. TuBu innervations are virtually absent from the BU_i (dashed circle). CB, cell body. TuBu-l dendrites and axonal terminals are spatially restricted (F'). Three TuBu-m clones innervate a ventral area in the bulb (BU_i), separate from TuBu-l & -c neurons

(G'). TuBu-m arborization size is variable both in AOTU and bulb, ranging from covering larger areas (H) to spatially restricted (J). **K.** Schematic describing the distribution of three TuBu classes in the bulb neuropil. The innervation of the BU_a has not been analyzed in this study. For genotypes, see Supplemental Information.

Figure 6: Variability of innervation patterns across TuBu neurons

A-C. The axon terminals of neighboring TuBu-l neurons maintain their proximity in the bulb, but their orientation is variable, both when labeling all TuBu neurons (A,B), or TuBu-c specifically (C). **D.** Example of a FLYBOW-induced TuBu-l single cell clone (magenta), while co-labeling all TuBu-l_p neurons (green). Color coding of arrowheads indicates dorso-ventral distribution in the AOTU as well as positions in the BU_s (dorsal, ventro-lateral, ventro-medial), same as in subsequent panels. **E.** Schematic depicting the lack of stereotypic orientation of terminals from adjacent TuBu-l_p neurons in the bulb. **F.** There is no topographic correlation between dendritic position in the AOTU and target field in the bulb. Neurons with dorsal positions in the AOTU target to various positions within the lateral sector of the BUs (column I). Likewise, a similar position in the bulb are innervated from various positions along the d-v axis in the AOTU (column II). For genotypes, see Supplemental Information.

Figure 7: Distinct AOTU pathways connect with specific R neuron classes

In the BU_s, different TuBu classes connect to a set of R neurons. Two LexA expression lines label the posterior lateral domain and the anterior central domain of the SU, respectively. The BU_a and BU_i are not covered in this analysis. **A-C.** TuBu-l_p neurons innervate the BU_s, where they exclusively contact R4d neurons (A), but not R2 (B) or R5 (C) neurons. **D-F.** TuBu-c_a neurons partially overlap with R2 neurons (E), but not with R4d (D) or R5 (F). White and black arrows in (E) indicate the presence or absence of co-labeling of expression lines, respectively. **G-J.** Co-labeling of R neurons reveals the coverage of different fields within the BU. R3 neurons do not contribute to the BU_i. **K.** Proposed segregation of visual information of TuBu-l_p and TuBu-c_a neurons in the superior bulb. Innervation of the BU_a in reference to Omoto et

al. (2017). Filled dark stars in the BU_s indicate terminal endings of TuBu neurons (microglomeruli). EBoc, outer central domain; EBa, anterior domain of EB. For genotypes, see Supplemental Information.

Figure 8: The Anterior Visual Pathway circuit.

In the graphic, two features of the pathway - retinotopy and parallel channels - are highlighted. **A.** The retinotopy of the pathway is demonstrated by single neurons. Three spatially separate visual stimuli are transmitted by yellow, orange and red cells, respectively. Innervation patterns in the SU_m domain and in the EB indicate a loss of retinotopic arrangements. **B.** Parallel channels exist among several synaptic steps. In the medulla, five neuron classes, innervating separate AOTU compartments, detect visual stimuli from the same medulla columns. For two classes, the target areas in the BUs are shown, where corresponding ring neurons (R) transfer the information into the EB. Inhibitory neurons from the opposite hemisphere are possible regulators in the BU_s and the AOTU.

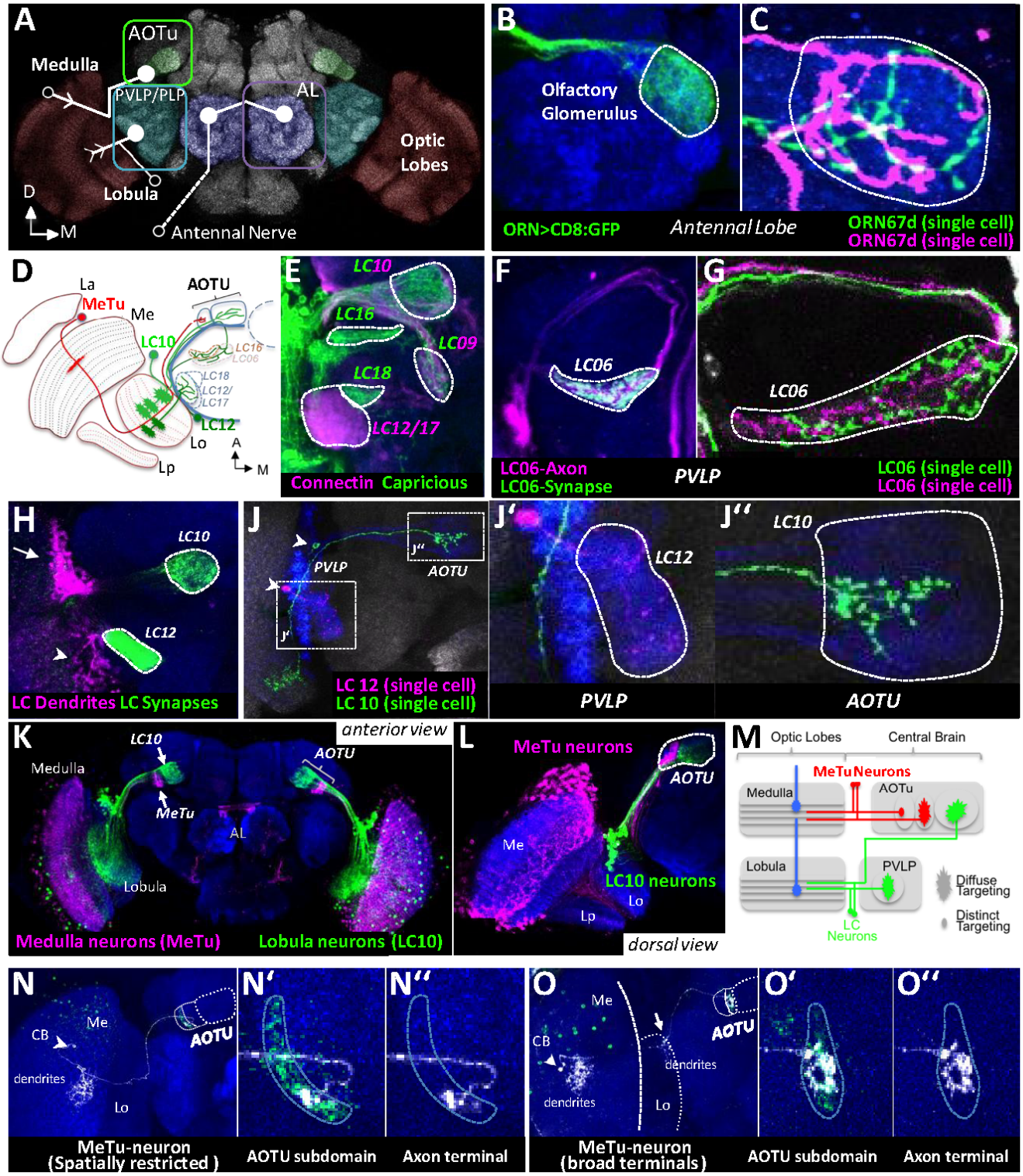
A
AOTu
Medulla
PVLP/PLP
AL
Optic Lobes
Lobula
D
M
Antennal Nerve
B
Olfactory Glomerulus
ORN>CD8:GFP
Antennal Lobe
C
ORN67d (single cell)
ORN67d (single cell)
D
La
AOTU
MeTu
Me
LC10
LC16
LC06
LC18
LC12/ LC17
LC12
Lo
A
Lp
M
E
LC10
LC16
LC09
LC18
LC12/17
Connectin Capricious
F
LC06
LC06-Axon
LC06-Synapse
PVLP
G
LC06
LC06 (single cell)
LC06 (single cell)
H
LC10
LC12
LC Dendrites LC Synapses
J
PVLP
AOTU
J'
J''
LC 12 (single cell)
LC 10 (single cell)
J'
LC12
PVLP
J''
LC10
AOTU
K
anterior view
LC10
Medulla
AOTU
MeTu
AL
Lobula
Medulla neurons (MeTu)
Lobula neurons (LC10)
L
MeTu neurons
AOTU
Me
LC10 neurons
Lo
Lp
dorsal view
M
Optic Lobes
Central Brain
MeTuNeurons
Medulla
AOTu
Lobula
PVLP
Diffuse Targeting
Distinct Targeting
LC Neurons
N
CB
Me
AOTU
dendrites
Lo
N'
N''
MeTu-neuron (Spatially restricted)
AOTU subdomain
Axon terminal
O
Me
CB
AOTU
dendrites
dendrites
Lo
O'
O''
MeTu-neuron (broad terminals)
AOTU subdomain
Axon terminal

Figure 1

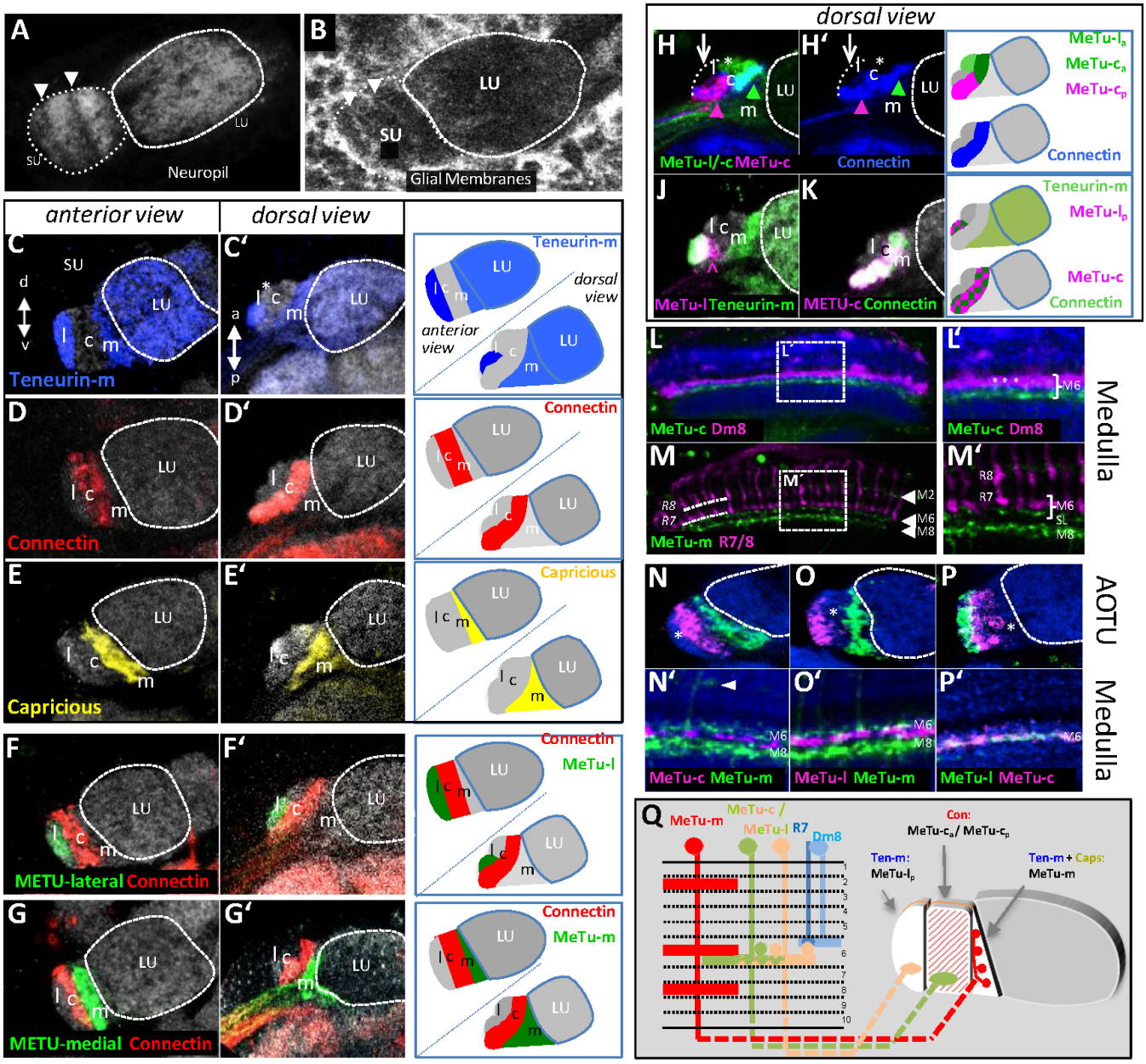
A
LU
SU
Neuropil
B
LU
SU
Glial Membranes
anterior view
dorsal view
C
SU
d
v
LU
l c m
Teneurin-m
C'
a
p
l c m
LU
Teneurin-m
dorsal view
anterior view
D
LU
l c
m
Connectin
D'
Connectin
E
Capricious
E'
Capricious
F
METU-lateral Connectin
F'
Connectin
MeTu-l
G
METU-medial Connectin
G'
Connectin
MeTu-m
dorsal view
H
H'
MeTu-l/-c MeTu-c
Connectin
MeTu-l$_a$
MeTu-c$_a$
MeTu-c$_p$
Connectin
J
K
MeTu-l Teneurin-m
METU-c Connectin
Teneurin-m
MeTu-l$_p$
MeTu-c
Connectin
L
L'
MeTu-c Dm8
M6
M
M'
MeTu-m R7/8
R8
R7
M2
M6
M8
SL
Medulla
N
O
P
N'
O'
P'
MeTu-c MeTu-m
MeTu-l MeTu-m
MeTu-l MeTu-c
AOTU
Medulla
Q
MeTu-m
MeTu-c /
MeTu-l
R7
Dm8
Con:
MeTu-c$_a$/ MeTu-c$_p$
Ten-m:
MeTu-l$_p$
Ten-m + Caps:
MeTu-m

Figure 2

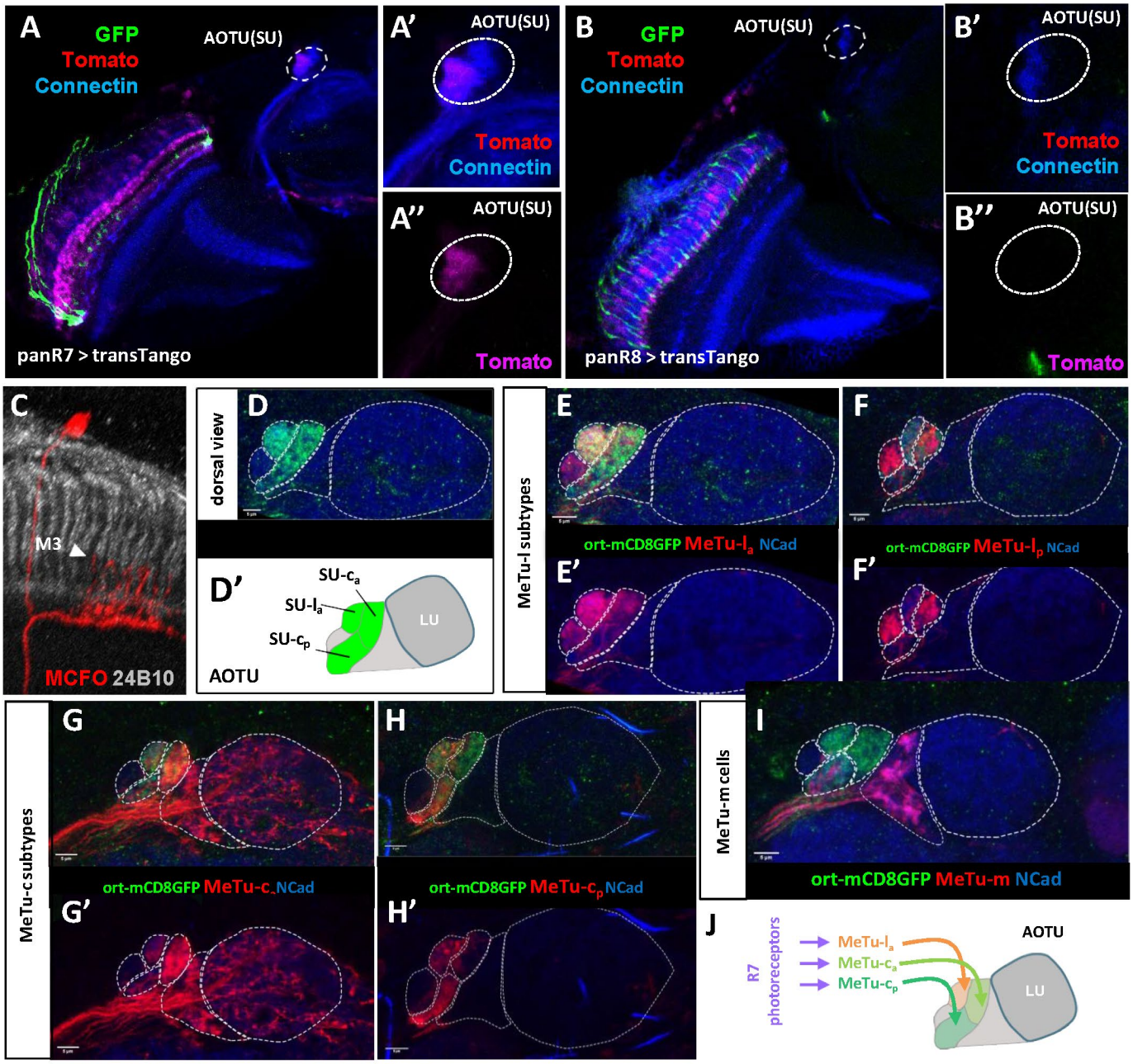
A
GFP
Tomato
Connectin
AOTU(SU)
panR7 > transTango
A'
AOTU(SU)
Tomato
Connectin
A''
AOTU(SU)
Tomato
B
GFP
Tomato
Connectin
AOTU(SU)
panR8 > transTango
B'
AOTU(SU)
Tomato
Connectin
B''
AOTU(SU)
Tomato
C
M3
MCFO 24B10
dorsal view
D
D'
SU-ca
SU-la
SU-cp
LU
AOTU
MeTu-l subtypes
E
ort-mCD8GFP MeTu-la NCad
E'
F
ort-mCD8GFP MeTu-lp NCad
F'
MeTu-c subtypes
G
ort-mCD8GFP MeTu-ca NCad
G'
H
ort-mCD8GFP MeTu-cp NCad
H'
MeTu-m cells
I
ort-mCD8GFP MeTu-m NCad
J
R7
photoreceptors
MeTu-la
MeTu-ca
MeTu-cp
AOTU
LU

Figure 3

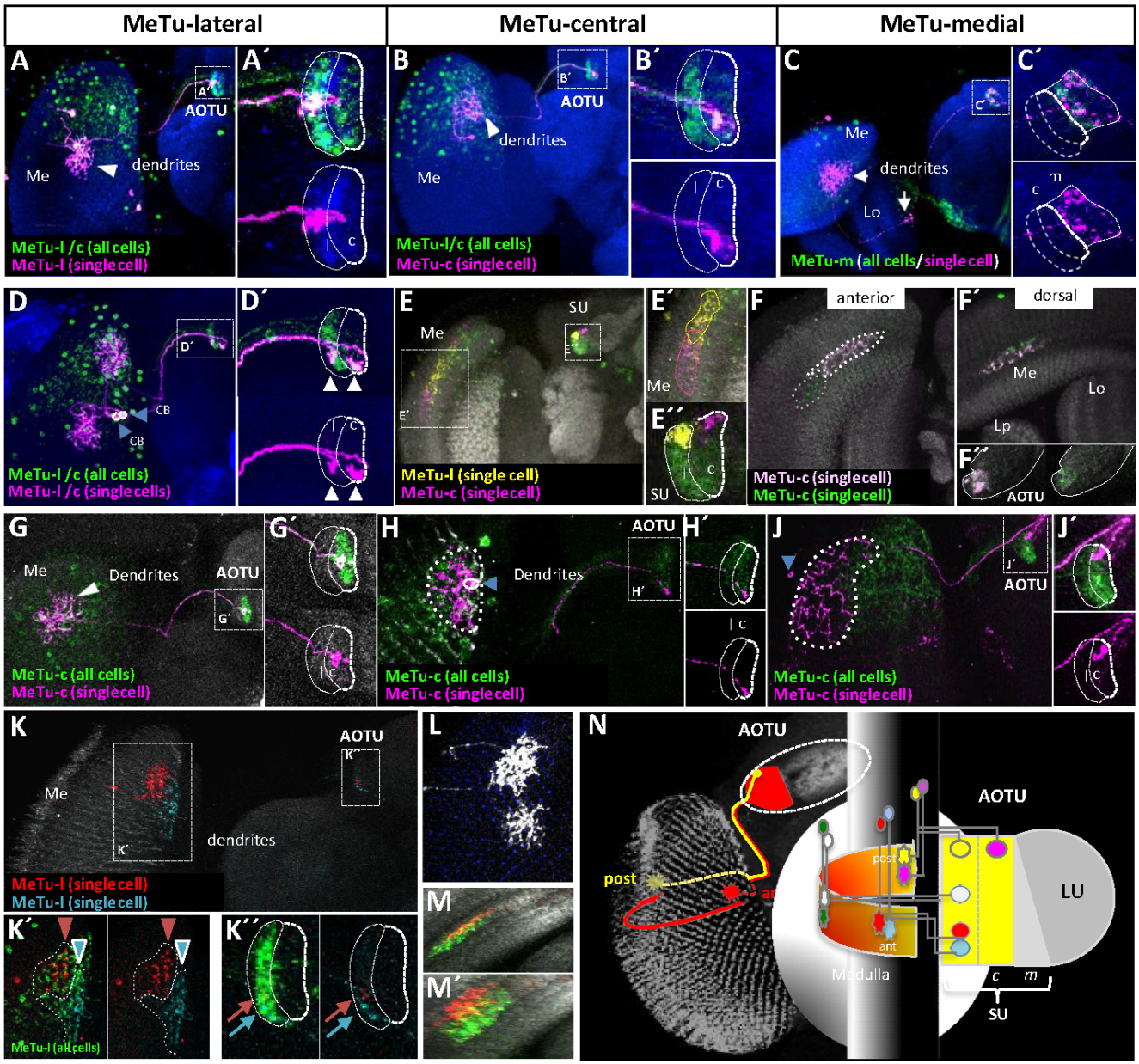
MeTu-lateral
MeTu-central
MeTu-medial
A
A´
B
B´
C
C´
AOTU
dendrites
Me
MeTu-l /c (all cells)
MeTu-l (single cell)
MeTu-l/c (all cells)
MeTu-c (single cell)
MeTu-m (all cells/single cell)
Lo
m
c
D
D´
CB
MeTu-l /c (all cells)
MeTu-l /c (single cells)
E
E´
E´´
SU
MeTu-l (single cell)
MeTu-c (single cell)
F
F´
F´´
anterior
dorsal
Lp
MeTu-c (single cell)
G
G´
Dendrites
MeTu-c (all cells)
H
H´
J
J´
K
K´
K´´
L
M
M´
N
post
ant
Medulla
LU

Figure 4

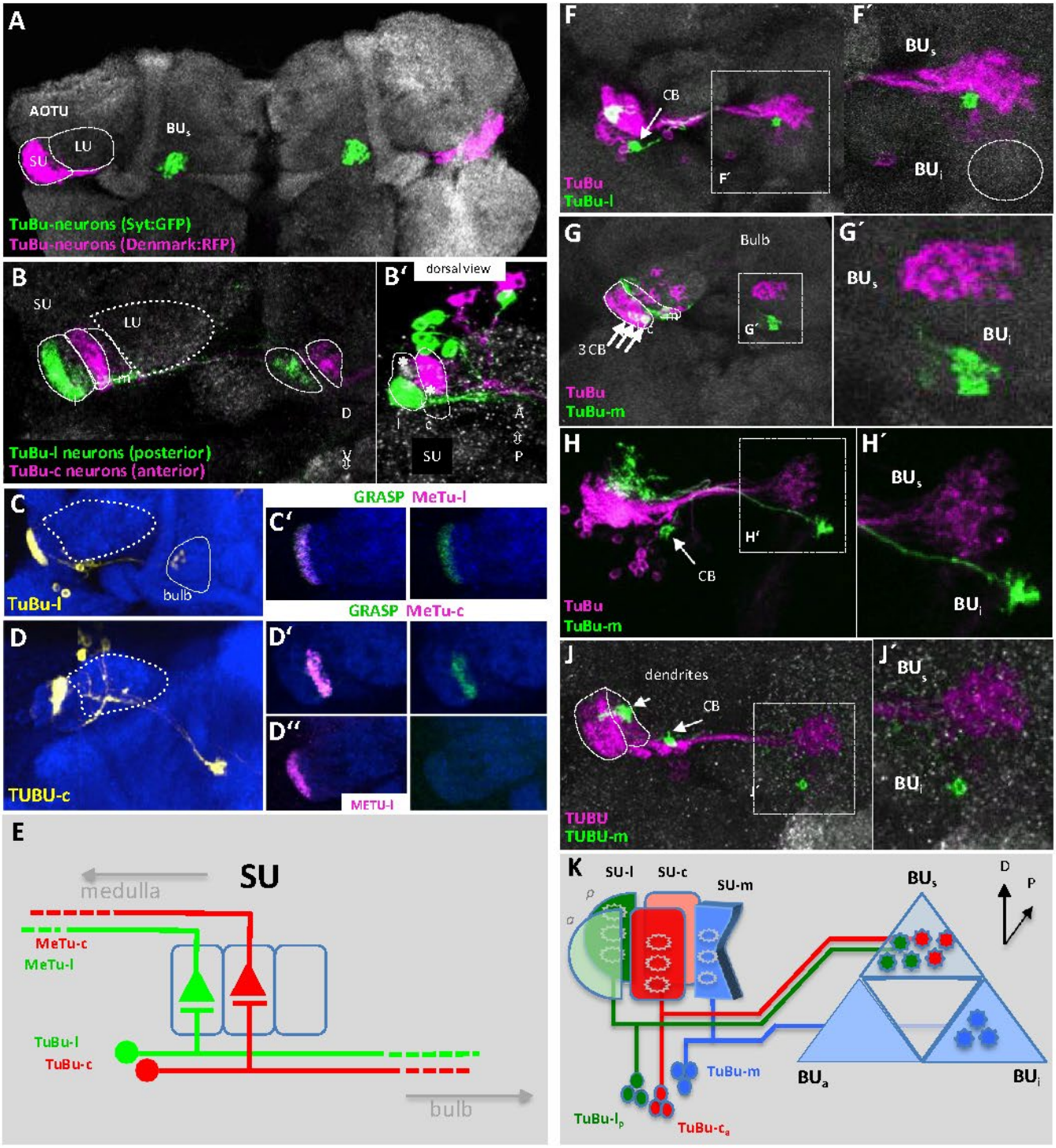
A
AOTU
SU
LU
BUs
TuBu-neurons (Syt:GFP)
TuBu-neurons (Denmark:RFP)
B
SU
LU
D
V
TuBu-l neurons (posterior)
TuBu-c neurons (anterior)
B'
dorsal view
l
c
A
P
SU
C
TuBu-l
bulb
C'
GRASP MeTu-l
D
TUBU-c
D'
GRASP MeTu-c
D''
METU-l
E
medulla
SU
MeTu-c
MeTu-l
TuBu-l
TuBu-c
bulb
F
CB
F'
TuBu
TuBu-l
F'
BUs
BUi
G
Bulb
3 CB
G'
TuBu
TuBu-m
G'
BUs
BUi
H
CB
H'
TuBu
TuBu-m
H'
BUs
BUi
J
dendrites
CB
TUBU
TUBU-m
J'
BUs
BUi
K
SU-l
SU-c
SU-m
BUs
D
P
TuBu-m
BUa
BUi
TuBu-lp
TuBu-ca

Figure 5

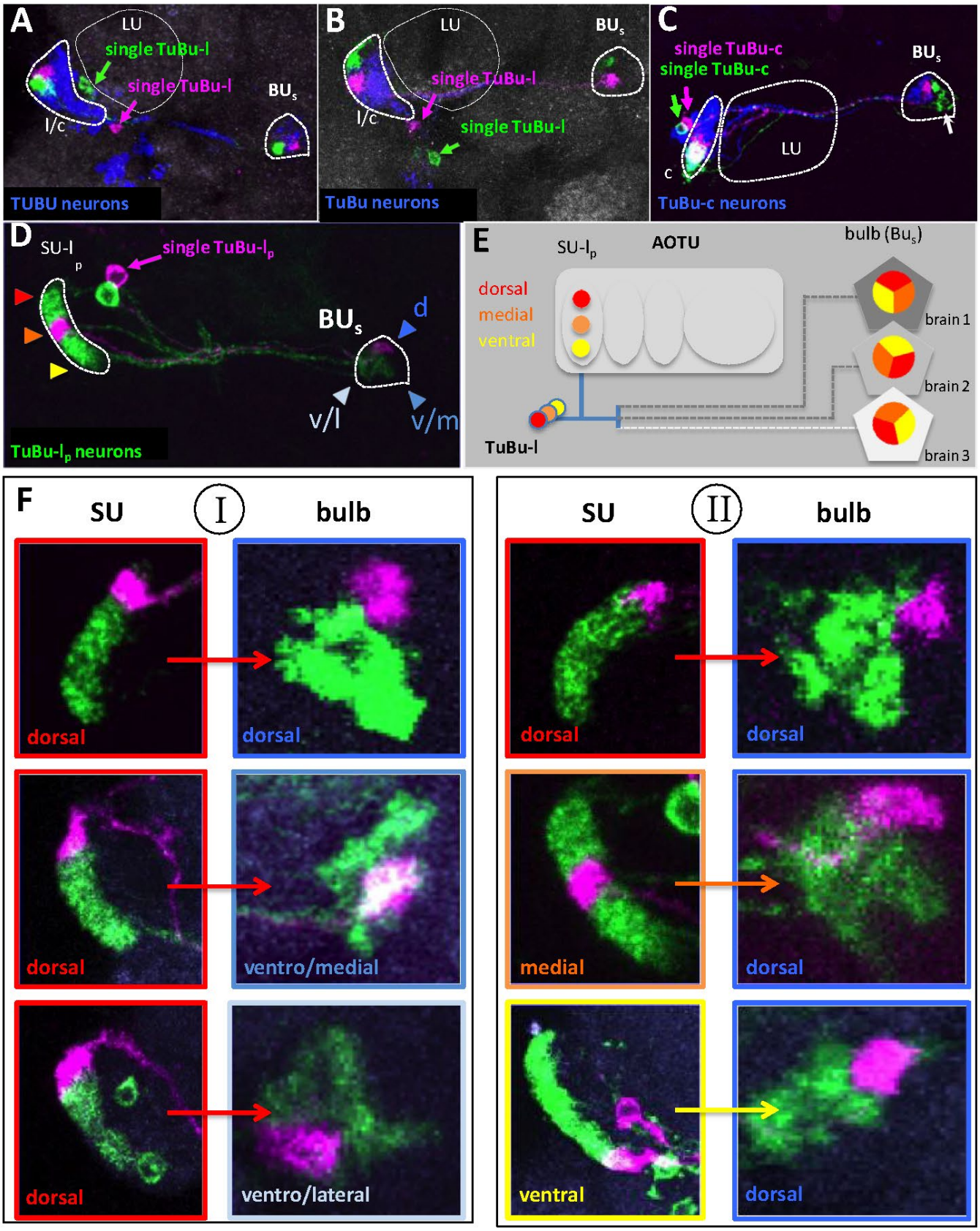
A
LU
single TuBu-l
single TuBu-l
BU$_s$
l/c
TUBU neurons
B
LU
BU$_s$
single TuBu-l
l/c
single TuBu-l
TuBu neurons
C
single TuBu-c
single TuBu-c
BU$_s$
LU
c
TuBu-c neurons
D
SU-l$_p$
single TuBu-l$_p$
BU$_s$
d
v/l
v/m
TuBu-l$_p$ neurons
E
SU-l$_p$
AOTU
bulb (Bu$_s$)
dorsal
medial
ventral
brain 1
brain 2
brain 3
TuBu-l
F
SU
I
bulb
dorsal
dorsal
dorsal
ventro/medial
dorsal
ventro/lateral
SU
II
bulb
dorsal
dorsal
medial
dorsal
ventral
dorsal

Figure 6

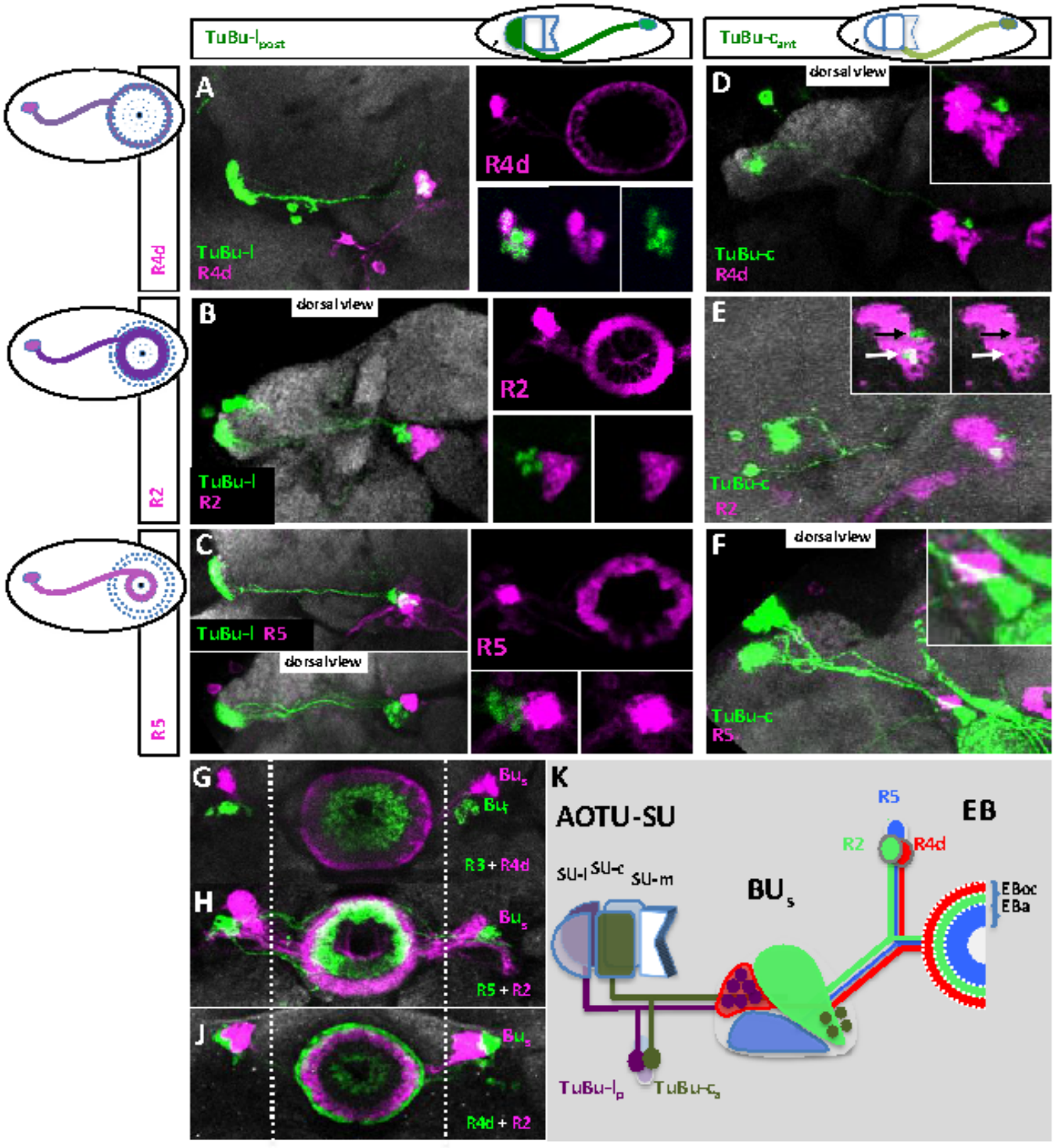
TuBu-l post
TuBu-c ant
R4d
R2
R5
A
TuBu-l
R4d
R4d
B
dorsal view
TuBu-l
R2
R2
C
TuBu-l R5
dorsal view
R5
D
dorsal view
TuBu-c
R4d
E
TuBu-c
R2
F
dorsal view
TuBu-c
R5
G
Bus
Bu
R3 + R4d
H
Bus
R5 + R2
J
Bus
R4d + R2
K
AOTU-SU
SU-l SU-c SU-m
BUs
R5
R2
R4d
EB
EBoc
EBa
TuBu-lp
TuBu-cs

Figure 7

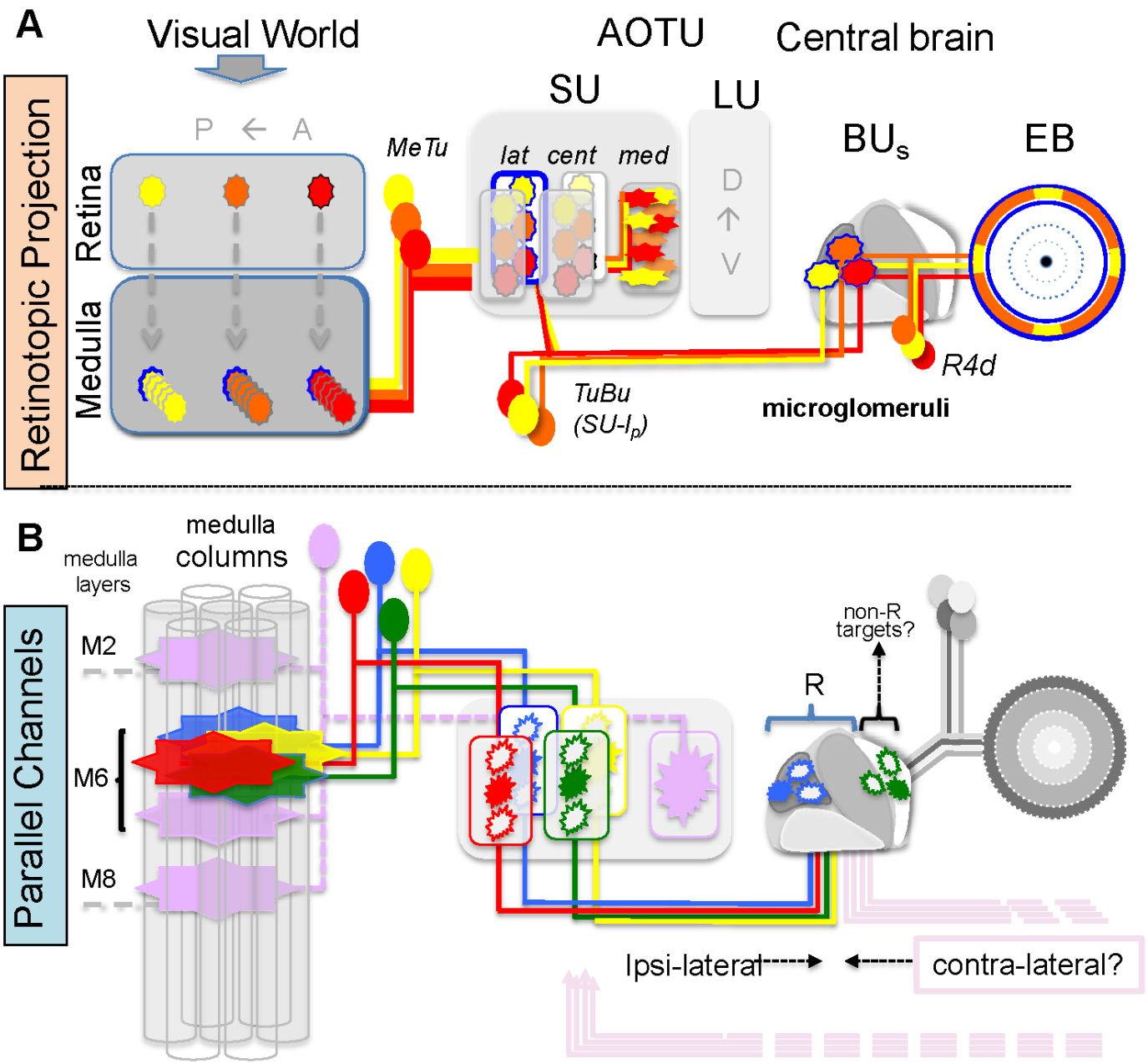
A
Visual World
AOTU
Central brain
SU
LU
Retinotopic Projection
Retina
Medulla
P ← A
MeTu
lat cent med
D
V
BUs
EB
R4d
TuBu
(SU-Ip)
microglomeruli
B
medulla
columns
medulla
layers
M2
M6
M8
non-R
targets?
R
Parallel Channels
Ipsi-lateral
contra-lateral?

Figure 8

Supplemental Figures

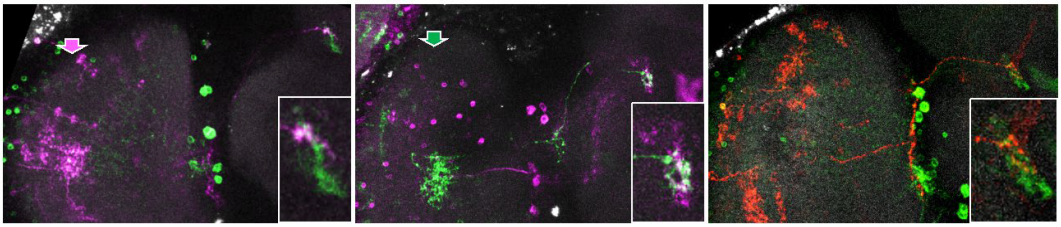

Figure S1. Morphology of MeTu-m neurons. Related to Fig. 1. FLYBOW clones of MeTu-m neurons with restricted innervation of the SU-m domain. Approximate center of dendritic area in the medulla is indicated by colored arrows. In the last image, the area of medullar innervation could not be resolved. Genotype: *hs-mFlp5; R20B05>FLYBOW1.1*.

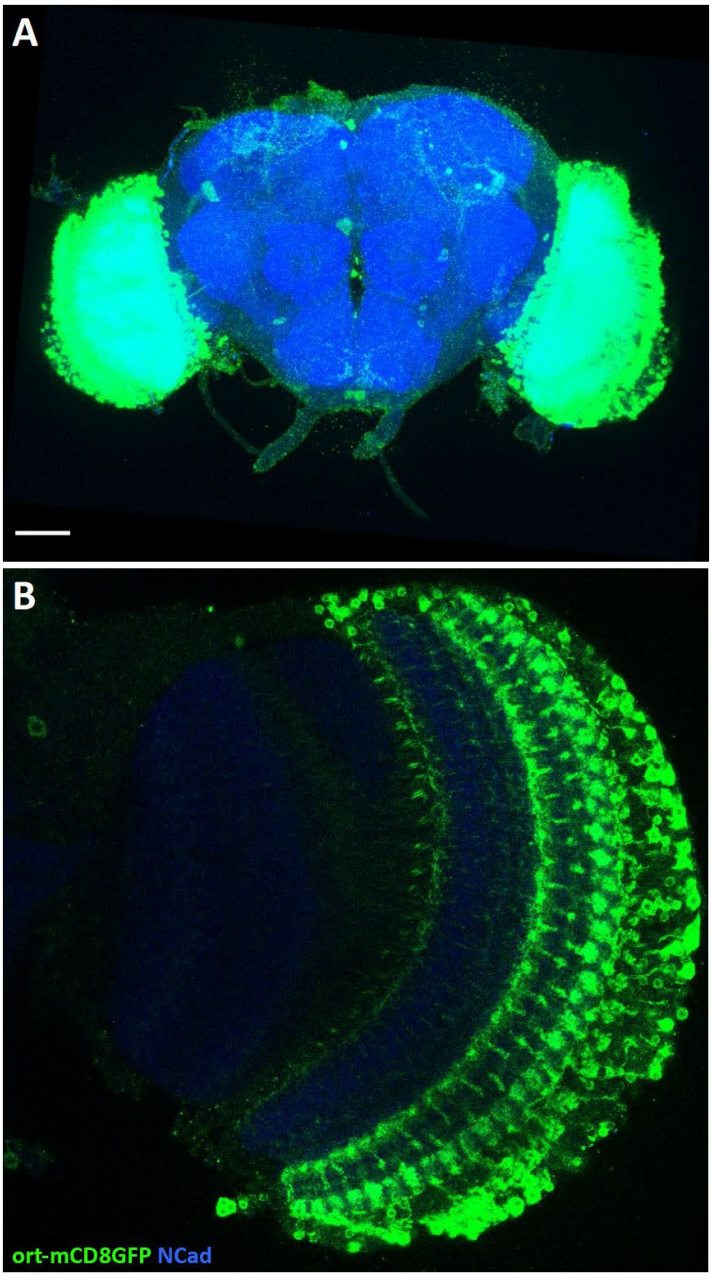

Figure S2. Expression pattern of the ort-mCD8GFP construct. A. Overview of neurons labeled by the ort-construct in the brain. Scale bar, 50µm. **B.** Expression of ort-mCD8GFP in the medulla. Genotype: *ort-mCD8GFP*.

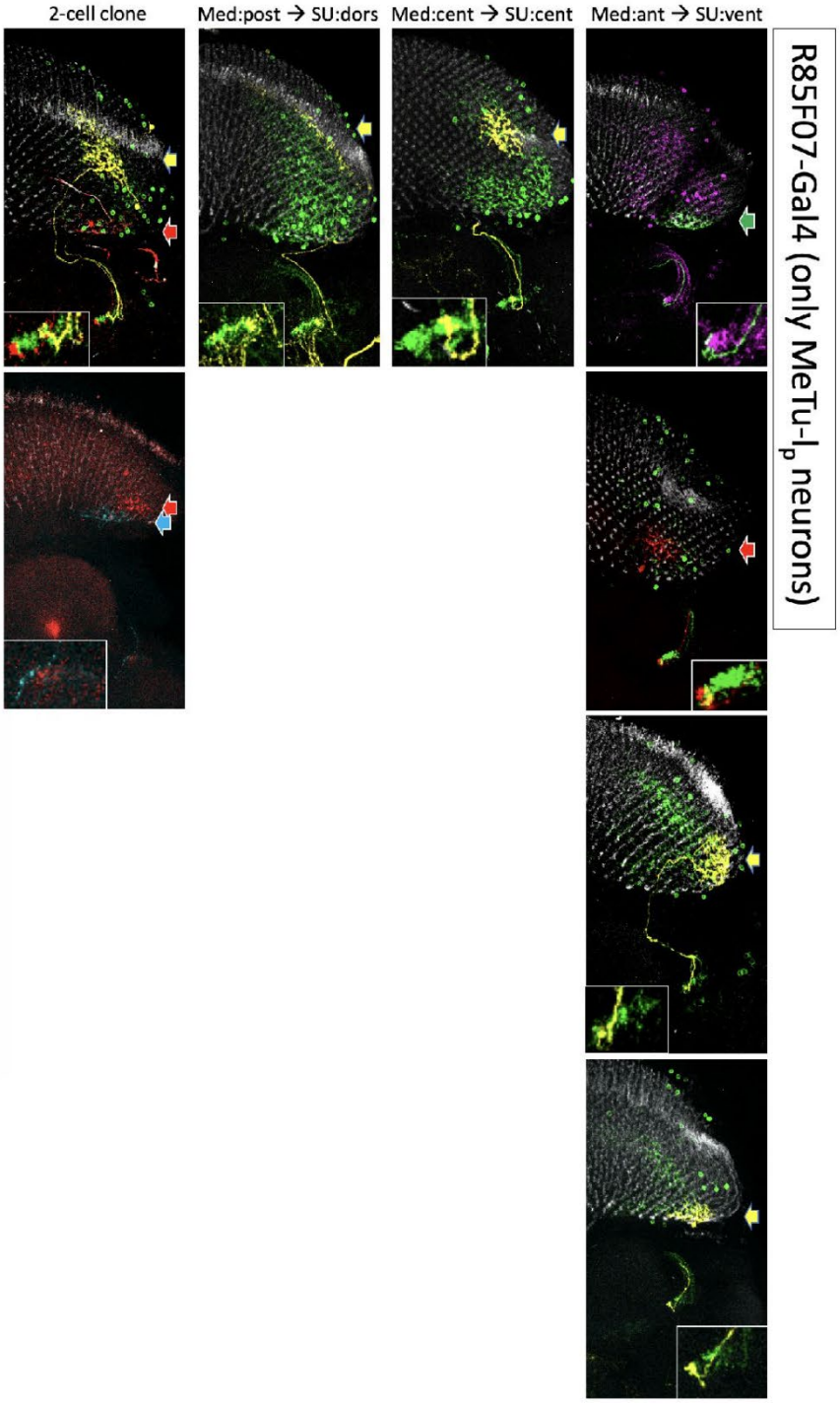
2-cell clone
Med:post → SU:dors
Med:cent → SU:cent
Med:ant → SU:vent
R85F07-Gal4 (only MeTu-l$_p$ neurons)

Figure S3. Topographic relations (medulla → SU) of FLYBOW single or two cell clones in a driver line labeling MeTu-l_p neurons. Related to Fig. 4. Three categories of dendritic (anterior, central, posterior) and axon terminal position (dorsal, central, ventral) where chosen for the medulla and the SU, respectively. The approximate center of the dendritic area (in a-p axis) is indicated by the colored arrows. Cell pairs in the same color where included in the study when their dendritic areas where in close proximity to each other. R85F07-Gal4 exclusively labels MeTu neurons innervating the SU-l_p. Genotype: *hs-mFlp5; R85F07>FLYBOW1.1*.

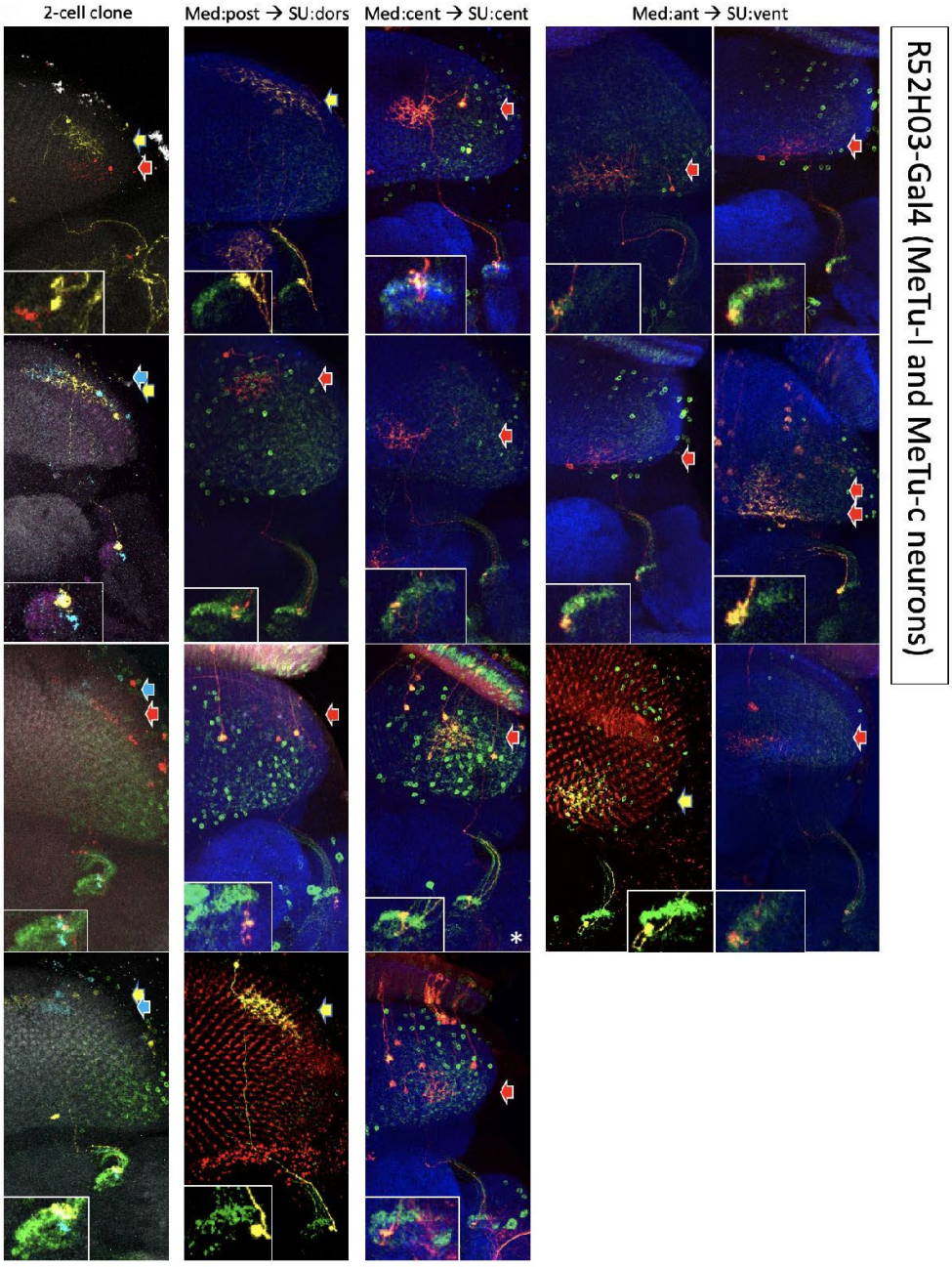
2-cell clone
Med:post → SU:dors
Med:cent → SU:cent
Med:ant → SU:vent
R52H03-Gal4 (MeTu-l and MeTu-c neurons)
*

Figure S4. Topographic relations (medulla → SU) of FLYBOW single or two cell clones in a driver liner labeling MeTu-l and -c neurons. Related to Fig. 4. Compare legend to Fig. S3 for more information. The driver line R52H03-Gal4 labels most MeTu-l and MeTu-c neurons. Different cell populations where not distinguished in this analysis. An asterisk marks the sample with the highest number of medullar columns covered in the central medulla (see main text). Genotype: *hs-mFlp5; R52H03>FLYBOW1.1*.

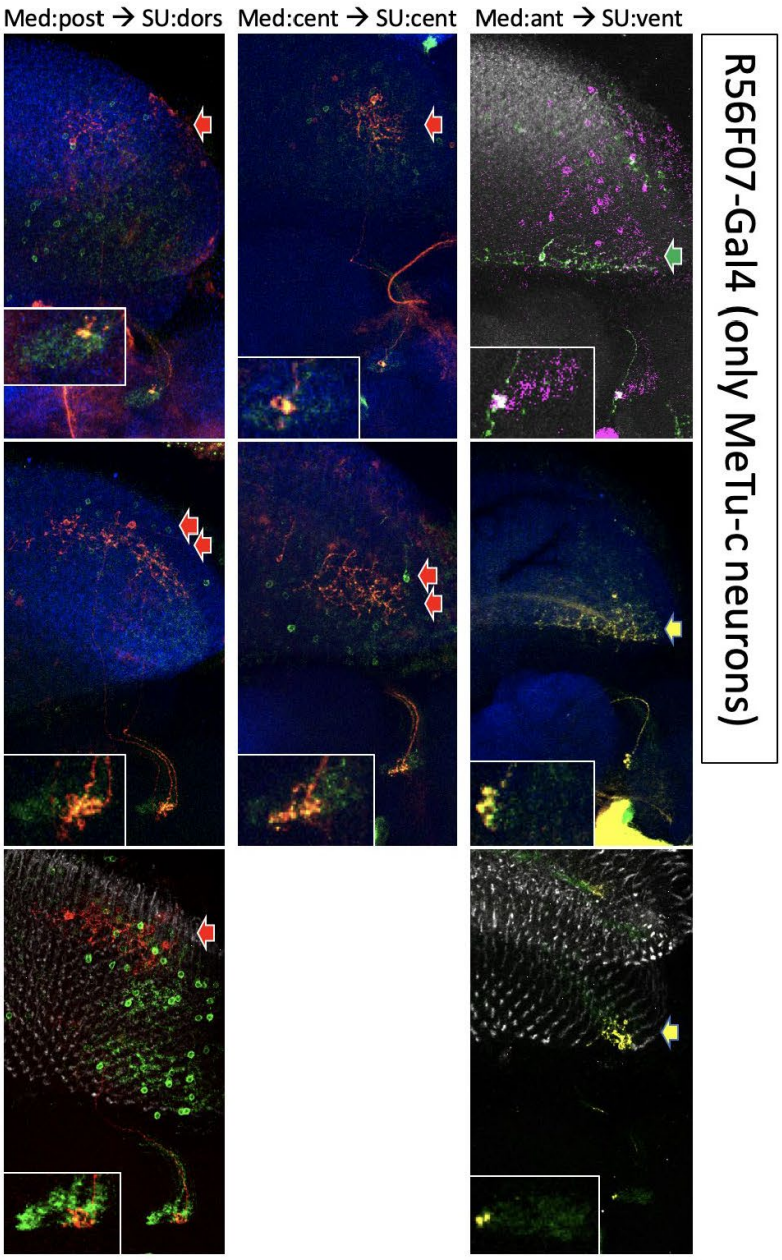

Figure S5. Topographic relations (medulla → SU) of FLYBOW single cell clones in a driver liner labeling MeTu-c neurons. Related to Fig. 4. Compare legend to Fig. S3 for more information. Populations of MeTu neurons labeled by R56F07-Gal4 innervate the SU-c_a and SU-c_p domains. Genotype: *hs-mFlp5; R56F07>FLYBOW1.1*.

Transparent Methods

Fly rearing

Flies were maintained in vials containing standard fly food medium at 25°C at 60% relative humidity unless otherwise mentioned. Canton-S flies were used as a wild type strain.

Fly stocks

Visual circuit analysis was largely based on commercially available enhancer-fragment driver lines. The following lines were generated at the Fly Light Gal4-/LexA-Collection (Jenett et al., 2012) and obtained from Bloomington Drosophila Stock Center (BDSC). One driver line was obtained from the Vienna Tiles (VT) collection (Kvon et al., 2014).

	Gal4	**LexA**	**labeling purpose**
OPTIC GLOMERULI:			
	R41C07		LC06
	R35D04		LC12 & LC10
		VT29314	LC10
METU-NEURONS:			
	R52H03		MeTu-l & MeTu-c
	R85F05		MeTu-l
		R94G05	MeTu-l
	R44A03		MeTu-c
		R67C09	MeTu-c
	R25H10		MeTu-c
	R56F07		MeTu-c
	R20B05	R20B05	MeTu-m
TUBU-NEURONS:			
	R86C02		TuBu
	R71E07		TuBu-l & TuBu-c
	R25F06	R25F06	TuBu-l
	R64F06	R64F06	TuBu-c
R-NEURONS:			
	R14A12	R14A12	R3
	R12B01		R4d
		R85E07	R4d
	R49B02		R5
		R48H04	R5

Stocks for clonal analysis and effector lines for cell labeling:

FRT42D; FRT42D TubP-Gal80; UAS-mCD8::GFP and UAS-mCherry strains were obtained from BDSC. The UAS-DenMark construct was provided by Bassem Hassan, LexAop::GFP was a

gift from Andrew Straw. Flies for synaptic-GRASP experiments (UAS-Syb::spGFP1-10 & LexAop spGFP11::CD4) (Karuppudurai et al., 2014) were a gift from Chi-Hon Lee. The FLYBOW components where provided by Iris Salecker.

Generation of ort-mCD8 transgenic flies

A ~3.5 fragment from the ort gene spanning the entire 5' intergenic region, as well as the 1st untranslated exon and the transcription start was PCR-amplified, with appropriate restriction endonuclease recognition sites attached to the primers. The fragment was subcloned, sequenced and ligated into a promoterless injection vector (pCasper-mCD8:GFP-SV40). Insertions on 2nd and 3rd chromosomes were obtained via commercial embryo injection. Interestingly, expression was not variegated as seen for many ort-Gal4 constructs. Further information is available upon request.

Specific cell labeling:

In addition to the enhancer-fragment expression lines listed above, these lines were used to visualize specific neuron types: Or67d::GFP and OR67d-Gal4 (Couto et al., 2005) were used for olfactory class visualization, glia cells were marked by repo-Gal4, and Chi-Hon Lee provided the ortC1a-LexA::VP16 (Ting et al., 2014) construct for labeling of Dm8 neurons. PanR7-Gal4 (rh3+rh4-Gal4) was used for R7 TransTango, and panR8-Gal4 (rh5+rh6-Gal4) for R8 TransTango experiments (both gifts from Claude Desplan). Caps-Gal4 (Shinza-Kameda et al., 2006) was used in a MARCM background to visualize different optic glomeruli.

Antibodies used in this study:

Primary antibodies used were: 24B10/Mouse anti-Chaoptin (1:50, DSHB), DN-Ex #8/Rat anti-CadN (1:20, DSHB), Flamingo#74/Mouse anti-flamingo (1:20, DSHB), Rabbit anti-GFP (1:1000, Invitrogen, Carlsbad, CA). Mouse anti-Teneurin-m (1:20) was a kind gift from Stefan Baumgartner, anti-Connectin (1:20) was kindly provided by Robert AH White.
Secondary antibodies used: Goat anti-Rabbit Alexa-488 (1:500), Goat anti-Rabbit Alexa-568 (1:300), Goat anti-Mouse Alexa-488 (1:300), Goat anti-Mouse Alexa-647 (1:500), Goat anti-Rat Alexa-647 (1:300). All secondary antibodies were obtained from ThermoFisher Scientific (Alexa Fluor®, Molecular Probes™).

Clonal analysis

Two approaches for visualization of large and small genetic mosaics were used respectively. For inducing larger mosaics, MARCM clones with an ey-Flp insertion on the X chromosome were generated (Lee and Luo, 1999). This approach was possible because Flp under the control of the ey-promoter is not only expressed in peripheral sensory neurons, but we found it also to be active in medulla and lobula projecting neurons innervating the optic glomeruli. For small clones and single-cell analysis, we used the temperature-sensitive hs-mFlp5 promotor in combination with a FLYBOW (FB1.1B)-construct (Hadjieconomou et al., 2011, Shimosako, Hadjieconomou et al., 2014). Prior to screening for brains with single cell labeling, a heat shock was given to developing flies (L2-stage, L3-stage, early pupal) for 30min, 1h or 2h at 38°C. The exact timing protocol was under undergoing adjustment for each experiment. The pupae were then allowed to further develop at 25°C and dissected within two days after eclosion.

Immunohistochemistry

Drosophila brains were dissected in phosphate-buffered saline (PBS) and fixed in 4% paraformaldehyde (PFA) in PBS for 20 min. Samples were washed 3 x 15 min with PBST (PBS containing 0.3 % Triton X-100) and blocked for 3 hours (10% Goat serum in PBST) under constant shaking on a horizontal shaker, before incubating in primary antibody solution for two days at 4°C. Washing procedure was repeated before incubating with secondary antibody for two days at 4°C. Following three times washing, the brains were mounted in Vectashield® (Vector Laboratories, Burlingame, CA) anti-fade mounting medium prior to confocal microscopy. Images were obtained using a TCS SP5II confocal microscope (Leica) using 20x and 63x glycerol immersion objectives. Image processing was performed using ImageJ and Adobe Photoshop® CS6.

Activity GRASP

Flies were grown in a 12h-12h dark-light cycle incubator at 25°C in normal vials. 1-day old flies were kept in a 25°C, 20 h – 4 h light-dark cycle custom-made light box for 3 days to ensure sufficient activation of visual neurons. Brains were stained with polyclonal GFP (anti GFP goat pAB) and monoclonal GFP (anti-GFP rat mAB) antibody to visualize pre-synaptic cells and GRASP signal, respectively. Post-synaptic cells were visualized by staining with CD4 antibody.

TransTango

Flies for TransTango experiments were either kept in 18°C, in a 12h-12h dark-light cycle incubator and dissected when they were either 15 days old.

Drosophila genotypes used in the respective figures

Figure 1

B) *OR47d::GFP*, C) *hs-mFlp5; OR67d-Gal4>FLYBOW1.1*, E) *ey-Flp; FRT40, Gal80/FRT40*; *Caps-Gal4>mCD8::GFP* (MARCM), F) *R41C07-Gal4>mCherry, >syt::GFP*, G) *hs-mFlp5*; *R41C07-Gal4>FLYBOW1.1*, H) *R35D04-Gal4>DenMark, >syt::GFP*, J) *hs-mFlp5; R35D04-Gal4>FLYBOW1.1,* K, L) *VT29314-LexA>mCD8::GFP; R44A03-Gal4>mCherry*, N) *hs-mFlp5; R52H03-Gal4>FLYBOW1.1*, O) *hs-mFlp5; R20B05-Gal4>FLYBOW1.1*

Figure 2

B) *Repo-Gal4>mCD8::GFP*, E) *Caps-Gal4>mCD8::GFP*, F, F') *R85F05-Gal4>mCD8::GFP*, G, G') *R20B05-LexA>mCD8::GFP*, H) *R25H10-Gal4>mCherry; R67C09-LexA>mCD8::GFP*, J) *R85F05-Gal4>mCD8::GFP*, K) *R44A03-Gal4>mCD8::GFP*, L) *R56F07-Gal4>mCherry, Dm8-LexA>mCD8::GFP*, M) *R20B05-LexA>mCD8::GFP*, N, N') *R56F07-Gal4>mCherry, R20B05-LexA>mCD8::GFP*, O, O') *R56F07-Gal4>mCherry, R20B05-LexA>mCD8::GFP*, P, P') *R44A03-Gal4>mCherry, R94G05-LexA>mCD8::GFP*

Figure 3

A) *panR7-Gal4>transTango*, B) *panR8-Gal4>transTango*, C) *R94G05-Gal4>MCFO-1*, D) *ort-mCD8::GFP*, E) *ort-mCD8::GFP; R94G05-Gal4>myrTomato*, F) *ort-mCD8GFP; R52H03-Gal4>myrTomato*, G) *ort-mCD8::GFP; R67C09-Gal4>myrTomato*, H) *ort-mCD8::GFP; R25H10-Gal4>myrTomato*, I) *ort-mCD8::GFP; R20B05-Gal4>myrTomato*

Figure 4

A, B) *hs-mFlp5; R52H03-Gal4>FLYBOW1.1*, C) *hs-mFlp5; R20B05-Gal4>FLYBOW1.1*, D-F) *hs-mFlp5; R52H03-Gal4>FLYBOW1.1*, G-J) *hs-mFlp5; R56F07-Gal4>FLYBOW1.1*, K-M) *hs-mFlp5; R85F05-Gal4>FLYBOW1.1*

Figure 5

A) *R86C02-Gal4>DenMark, >syt::GFP*, B) *R25F06-LexA>GFP; R64F06-Gal4>mCherry*, C) *R25F06-LexA>GFP*, C') *R85F05-Gal4>syb::spGFP1-10; R25F06-LexA>CD4::spGFP11*, D) *R64F06-LexA>GFP*, D') *R56F07> syb::spGFP1-10; R64F06-LexA>CD4::spGFP11*, D'') *R85F05-Gal4>syb::spGFP1-10; R64F06-LexA>CD4::spGFP11*, F-J) *hs-mFlp5; R86C02-Gal4>FLYBOW1.1*

Figure 6

A) *hs-mFlp5; R71E07-Gal4>FLYBOW1.1*, B) *hs-mFlp5; R86C02-Gal4>FLYBOW1.1*, C) *hs-mFlp5; R64F06-Gal4>FLYBOW1.1*, D, F) *R25F06-Gal4>FLYBOW1.1*

Figure 7

A) *R25F06-LexA>GFP; R12B01-Gal4>mCherry*, B) *R25F06-LexA>GFP; EB1-Gal4>mCherry*, C) *R25F06-LexA>GFP; R49B02-Gal4>mCherry*, D) *R64F06-LexA>GFP; R12B01-Gal4>mCherry*, E) *R64F06-LexA>GFP; EB1-Gal4>mCherry*, F) *R64F06-LexA>GFP; R49B02-Gal4>mCherry*, G) *R14A12-LexA>GFP; R12B01-Gal4>mCherry*, H) *R48H04-LexA>GFP; EB1-Gal4>mCherry*, J) *R85E07-LexA>GFP; EB1-Gal4>mCherry*

Supplemental References

COUTO, A., ALENIUS, M. & DICKSON, B. J. 2005. Molecular, anatomical, and functional organization of the Drosophila olfactory system. *Curr Biol,* 15, 1535-1547.

HADJIECONOMOU, D., ROTKOPF, S., ALEXANDRE, C., BELL, D. M., DICKSON, B. J. & SALECKER, I. 2011. Flybow: genetic multicolor cell labeling for neural circuit analysis in Drosophila melanogaster. *Nat Methods* 8, 260-266.

JENETT, A., RUBIN, G. M., NGO, T. T., SHEPHERD, D., MURPHY, C., DIONNE, H., PFEIFFER, B. D., CAVALLARO, A., HALL, D., JETER, J., IYER, N., FETTER, D., HAUSENFLUCK, J. H., PENG, H., TRAUTMAN, E. T., SVIRSKAS, R. R., MYERS, E. W., IWINSKI, Z. R., ASO, Y., DEPASQUALE, G. M., ENOS, A., HULAMM, P., LAM, S. C., LI, H. H., LAVERTY, T. R., LONG, F., QU, L., MURPHY, S. D., ROKICKI, K., SAFFORD, T., SHAW, K., SIMPSON, J. H., SOWELL, A., TAE, S., YU, Y. & ZUGATES, C. T. 2012. A GAL4-driver line resource for Drosophila neurobiology. *Cell Rep,* 2, 991-1001.

KARUPPUDURAI, T., LIN, T. Y., TING, C. Y., PURSLEY, R., MELNATTUR, K. V., DIAO, F., WHITE, B. H., MACPHERSON, L. J., GALLIO, M., POHIDA, T & LEE, C. H. 2014. A hard-wired glutamatergic circuit pools and relays UV signals to mediate spectral preference in Drosophila. *Neuron,* 81, 603-615.

KVON, E. Z., KAZMAR, T., STAMPFEL, G., YANEZ-CUNA, J. O., PAGANI, M., SCHERNHUBER, K., DICKSON, B. J. & STARK, A. 2014. Genome-scale functional characterization of Drosophila developmental enhancers in vivo. *Nature,* 512, 91-95.

LEE, T. & LUO, L. 1999. Mosaic analysis with a repressible cell marker for studies of gene function in neuronal morphogenesis. *Neuron,* 22, 451-461.

SHIMOSAKO, N., HADJIECONOMOU, D. & SALECKER, I. 2014. Flybow to dissect circuit assembly in the Drosophila brain. *Methods Mol Biol*, 1082, 57-69.

SHINZA-KAMEDA, M., TAKASU, E., SAKURAI, K., HAYASHI, S. & NOSE, A. 2006. Regulation of layer-specific targeting by reciprocal expression of a cell adhesion molecule, capricious. *Neuron*, 49, 205-213.

TING, C. Y., MCQUEEN, P. G., PANDYA, N., LIN, T. Y., YANG, M., REDDY, O. V., O'CONNOR, M. B., MCAULIFFE, M. & LEE, C. H. 2014. Photoreceptor-derived activin promotes dendritic termination and restricts the receptive fields of first-order interneurons in Drosophila. *Neuron* 81, 830-846.

JU

4.4. Manuscript IV

The development and function of neuronal subtypes processing color and skylight polarization in the optic lobes of *Drosophila melanogaster*

Gizem Sancer, Mathias F. Wernet

Contribution:

I generated the figures under the supervision of Prof. Dr. Mathias Wernet and wrote the manuscript together with Prof. Dr. Mathias Wernet.

This manuscript is submitted, and it is under review at Arthropod Structure & Development.

Highlights

- Color and skylight polarization are processed via similar yet different cell types in the optic lobe of *Drosophila melanogaster*
- Amacrine-like Dm8 cells fall into two subtypes with different spectral inputs in their center, while integrating over a presumably similar surrounding area of mixed inputs
- A duplicated set of modality-specific Dm8-like cell types exists in the 'dorsal rim area' of the adult eye, where skylight polarization is being processed
- Transcriptomic and developmental studies shine light on the molecular mechanisms behind assembling these visual circuits
- By receiving photoreceptor inputs from multiple facets, as well as providing feedback synapses, Dm9 cells provide a second layer of inter-ommatidial integration

The development and function of neuronal subtypes processing color and skylight polarization in the optic lobes of *Drosophila melanogaster*

Gizem Sancer and Mathias F. Wernet *

Freie Universität Berlin

Fachbereich Biologie, Chemie und Pharmazie

Institut für Biologie – Neurobiologie

Königin-Luise Strasse 1-3

14195 Berlin, Germany

*: Corresponding author.

E-mail address: mathias.wernet@fu-berlin.de (M.F. Wernet)

Highlights

- Color and skylight polarization are processed via similar yet different cell types in the optic lobe of *Drosophila melanogaster*
- Amacrine-like Dm8 cells fall into two subtypes with different spectral inputs in their center, while integrating over a presumably similar surrounding area of mixed inputs
- A duplicated set of modality-specific Dm8-like cell types exists in the 'dorsal rim area' of the adult eye, where skylight polarization is being processed
- Transcriptomic and developmental studies shine light on the molecular mechanisms behind assembling these visual circuits
- By receiving photoreceptor inputs from multiple facets, as well as providing feedback synapses, Dm9 cells provide a second layer of inter-ommatidial integration

Keywords

Neural circuits

Color vision

Skylight polarization vision

Neuronal cell types

Circuit assembly

Circuit function

Drosophila melanogaster

Abstract

The retinal mosaics of many insects contain different ommatidial subtypes harboring photoreceptors that are both molecularly and morphologically specialized for comparing between different wavelengths versus detecting the orientation of skylight polarization. The neural circuits underlying these different inputs and the characterization of their specific cellular elements are the subject of intense research. Here we review recent progress on the description of both assembly and function of color and skylight polarization circuitry, by focusing on two cell types located in the distal portion of the medulla neuropil of the fruit fly *Drosophila melanogaster*'s optic lobes, called Dm8 and Dm9. In the main part of the retina, Dm8 cells fall into two molecularly distinct subtypes whose center becomes specifically connected to either one of randomly distributed 'pale' or 'yellow' R7 photoreceptor fates during development. Only in the 'dorsal rim area' (DRA), both polarization-sensitive R7 and R8 photoreceptors are connected to different Dm8-like cell types, called Dm-DRA1 and Dm-DRA2, respectively. An additional layer of interommatidial integration is introduced by Dm9 cells, which receive input from multiple neighboring R7 and R8 cells, as well as providing feedback synapses back into these photoreceptors. As a result, the response properties of color-sensitive photoreceptor terminals are sculpted towards being both maximally decorrelated, as well as harboring several levels of opponency (both columnar as well as intercolumnar). In the DRA, individual Dm9 cells appear to mix both polarization and color signals, thereby potentially serving as the first level of integration of different celestial stimuli. The molecular mechanisms underlying the establishment of these synaptic connections are beginning to be revealed, by using a combination of live imaging, developmental genetic studies, and cell type-specific transcriptomics.

1. Introduction

Despite its homogenous external morphology with ~800 unit eyes (ommatidia), the adult compound eye of the fly *Drosophila melanogaster* contains different ommatidial subtypes of that manifest specialization ideally suited for serving specific tasks (Kind, Belušič, & Wernet, 2020). Tightly regulated expression of either one out of four different rhodopsin genes, as well as, in some cases, morphological differences in the ultrastructure of light-gathering rhabdomeric membranes of the central photoreceptors R7 and R8, together generate at least three subtypes of ommatidia (Figure 1A): In the main part of the retina so-called 'pale' and 'yellow' subtype are distributed randomly, yet in an uneven ratio of 35% to 65%, which is conserved in larger fly species (Bell, Earl, & Britt, 2007; Feiler et al., 1992; Fortini & Rubin, 1990; Franceschini, Kirschfeld, & Minke, 1981; Hilbrant et al., 2014). Interestingly, expression of the UV opsin Rh3 in pale R7 is always paired with expression of a blue-sensitive Rh5 in pale R8 photoreceptors of the same ommatidium (Chou et al., 1996; Papatsenko, Sheng, & Desplan, 1997), whereas R7 and R8 in yellow ommatidia always the UV opsin Rh4 (in R7) paired with a green-sensitive Rh6 in R8 (Chou et al., 1999; Huber et al., 1997; Salcedo et al., 1999). Although the genetic mechanisms behind pale/yellow choice in R7 and R8 have been elucidated (Johnston & Desplan, 2014; Jukam et al., 2013; Mikeladze-Dvali et al., 2005; Wernet et al., 2006), the communication of these choices between R7 and R8 remains incompletely understood (Wells, Pistillo, Barnhart, & Desplan, 2017). Due to their different spectral sensitivities, pale and yellow photoreceptor subtypes are perfectly suited to extract different kinds of spectral comparisons from the visual environment (Salcedo et al., 1999). Furthermore, behavior experiments as well as physiological studies have confirmed that the pale/yellow mosaic is crucial for mediating *Drosophila* color vision (Heath et al., 2019; Melnattur et al., 2014; Schnaitmann, Garbers, Wachtler, & Tanimoto, 2013; Schnaitmann et al., 2018; Yamaguchi, Desplan, & Heisenberg, 2010). The occurrence of the third ommatidial subtype is always restricted to one or two rows of ommatidia along the dorsal rim of the eye, hence called 'dorsal rim area' (DRA) (Labhart & Meyer, 1999; Tomlinson, 2003; Wada, 1974; Wernet et al.,

2003). Only in DRA ommatidia, R7 and R8 are monochromatic and therefore not suitable for directly comparing spectral information, as they both express the same UV sensitive opsin Rh3 (Fortini & Rubin, 1990, 1991). However, like in many other insect species, DRA.R7 and DRA.R8 are specialized to detect the angle of polarized skylight due to the strict alignment of opsin molecules along their untwisted rhabdomeric membranes (Smola & Tscharntke, 1979; Wernet et al., 2012; Wunderer & Smola, 1982). Rhabdomeres of R7 vs R8 from the same ommatidia form orthogonal analyzers (Wernet et al., 2012), whereas analyzer directions of neighboring DRA ommatidia gradually change along the DRA, forming a fan-shaped array of skylight polarization detectors (Weir et al., 2016). In the DRA, R7 and R8 therefore detect a separate modality of light (i.e. skylight polarization) and compare orthogonal angles of polarized light instead of different wavelengths. Indeed, even a behavioral generalist like Drosophila melanogaster is able to keep stable headings over long periods of time (Coyne et al., 1982; Coyne, Bryant, & Turelli, 1987; Dickinson, 2014), and its navigation skills using polarized light have been confirmed both under the real sky (Weir & Dickinson, 2012), as well as when walking (Velez, Gohl, Clandinin, & Wernet, 2014; Velez, Wernet, Clark, & Clandinin, 2014; Wernet et al., 2012), or flying under laboratory conditions (Thomas F. Mathejczyk & Wernet, 2017; T. F. Mathejczyk & Wernet, 2019, 2020; Warren, Giraldo, & Dickinson, 2019; Warren, Weir, & Dickinson, 2018; Wolf, Gebhardt, Gademann, & Heisenberg, 1980). Just like for pale and yellow ommatidia, the genetic mechanisms specifying DRA ommatidia has been elucidated (Wernet & Desplan, 2014; Wernet et al., 2003; Wernet et al., 2014), resulting in a complete understanding of how the retinal mosaic of flies is patterned (Wernet, Celik, Mikeladze-Dvali, & Desplan, 2007), some of which are evolutionary conserved (Perry et al., 2016; Wernet, Perry, & Desplan, 2015).

The different kinds of visual information collected by these different ommatidial subtypes is transmitted to the optic lobe for further processing (I. Meinertzhagen & Hanson, 1993). The optic lobes in *Drosophila* consist of four successive, retinotopically organized neuropils called lamina, medulla, lobula and lobula plate (Fischbach & Dittrich, 1989). Photoreceptors R7 and R8

send axons directly to the medulla which is the most complex neuropil of the optic lobe with more than 80 different cell types and ~40,000 neurons (Fischbach & Dittrich, 1989). Many of these neurons occur once in every retinotopic column (hence ~800 times per optic lobe), which corresponds to the visual field of single ommatidia from the adult eye (columnar neurons), while other neuron types occur at fewer numbers while innervating many columns (multicolumnar neurons). Via precise synaptic connectivity, the columnar organization of the optic lobes ensures that retinotopy is maintained as information flows from the eye to higher brain regions. Usually, each neuron type also stratifies in specific medulla layers (named M1-M10, from distal to proximal) (Fischbach & Dittrich, 1989). The axons of pale and yellow R7 and R8 photoreceptors terminate in layers M6 and M3, respectively (Fischbach & Dittrich, 1989). Only in the DRA, both R7 and R8 terminate in the same deeper layer M6, yet R8 still terminating slightly more distally (Fischbach & Dittrich, 1989; Pollack & Hofbauer, 1991; Sancer et al., 2019) (Figure 1B). Despite several studies systematically characterizing both morphology and connectivity of specific cell types in the optic lobes (Nern, Pfeiffer, & Rubin, 2015; S. Y. Takemura, Lu, & Meinertzhagen, 2008; S. Y. Takemura et al., 2015; Tuthill, Nern, Holtz, Rubin, & Reiser, 2013; Wu et al., 2016), relatively little is known about the differences between those neural circuits processing color versus polarized light inputs. More specifically, our knowledge remains limited about the importance of similarities versus differences in circuit architecture within columns of different and similar subtype identity, as well as their organization of cell types into distinct layers for informing color versus polarized light vision. More recently, several studies have investigated the circuit structure and photoreceptor connectivity in medulla columns located in both pale and yellow (Carrillo et al., 2015a; Courgeon & Desplan, 2019; Heath et al., 2019; Karuppudurai et al., 2014; Lin et al., 2016; Schnaitmann et al., 2018; Tan et al., 2015), as well as in the DRA (Sancer et al., 2019; Sancer et al., 2020). Here we review recent progress on the description of both assembly and function of color and skylight polarization circuitry, by focusing on two cell types that are

photoreceptor targets located in the distal medulla of the *Drosophila* optic lobes, called Dm8 and Dm9 (Figure 1C,D) (Fischbach & Dittrich, 1989; S. Takemura et al., 2013).

2. Assembly and function color vision circuitry: Lessons from Dm8 cells

In *Drosophila*, pale and yellow R7 cells (both UV-sensitive), pale R8 (blue-sensitive), and yellow R8 (green-sensitive) serve as detectors for the color vision (Gao et al., 2008; Salcedo et al., 1999; Schnaitmann et al., 2013; Schnaitmann et al., 2018; Yamaguchi et al., 2010). Beyond the spectral sensitivity of these photoreceptors, it is crucial to understand the computations executed by the downstream neural for the comparison of chromatic information (Schnaitmann, Pagni, & Reiff, 2020; Song & Lee, 2018). Using behavior assays like UV-versus-Green spectral preference tests, fruit flies were shown to be strongly attracted to UV light (Gao et al., 2008; Otsuna, Shinomiya, & Ito, 2014), probably interpreting it as a celestial cue thereby potentially informing an innate escape response. Systematic genetic screens revealed that this behavior is mediated by UV-sensitive R7 cells (both pale and yellow), as well as an amacrine-like cell in distal medulla (Dm) named Dm8 that is directly postsynaptic to R7 (Fischbach & Dittrich, 1989; Gao et al., 2008; Karuppudurai et al., 2014; Nern et al., 2015; S. Y. Takemura et al., 2015). Cell type specific synaptic silencing of Dm8 cells in combination with rescue experiments for restoring their synaptic input cell type specifically revealed that this cell type is indeed necessary and sufficient for mediating UV spectral preference (Gao et al., 2008). A detailed analysis of Dm8 morphology revealed prominent lateral arborizations within the M6 layer, i.e. the target layer of R7 photoreceptors (Fischbach & Dittrich, 1989; Gao et al., 2008). Furthermore, studies using light microscopy and serial EM reconstruction showed that one Dm8 cell receives inhibitory synaptic input from R7 photoreceptors in ~13 adjacent ommatidia (Karuppudurai et al., 2014; S. Y. Takemura et al., 2015), using histamine as neurotransmitter (Stuart, 1999). Therefore, synaptic connections suggest that one given Dm8 cell pools UV information from these adjacent columns. On the output side, Dm8 then conveys this pooled information to a columnar transmedullary cell

named Tm5c via an excitatory glutamatergic connection located in its center (Karuppudurai et al., 2014). When glutamatergic synaptic output of Dm8 cells is blocked or the expression of Kainate (glutamate) receptors is knocked down in Tm5c cells, flies show a reduced UV preference, suggesting that this circuit including an excitatory connection between Dm8 and Tm5c is important or UV preference (Karuppudurai et al., 2014). Remarkably, Tm5c also receives direct columnar input from blue- or green-sensitive R8 cells thereby completing the minimal architecture of the circuit mediating spectral preference and color vision (Karuppudurai et al., 2014; I. A. Meinertzhagen et al., 2009) (Figure 2A).

In order for this circuit to function properly, both dendritic size of Dm8 cells, as well as distribution of synapses across this field needs must be regulated during development. To ensure this, the R7 photoreceptors play an important role in the determination of the dendritic branch size of their Dm8 targets. They provide the morphogen Activin which acts through its receptor Baboon expressed in Dm8 to limit the development of arborizations and thereby restricting the dendritic field size of their respective postsynaptic partner (Ting et al., 2014). While its limitation is controlled by the presynaptic partner of Dm8, the growth of the dendritic field size is controlled via a separate mechanism: A recent study identified an important role for the lamina monopolar cell type L5, which is a not synaptically connected to either photoreceptors or to Dm8 (Luo et al., 2020). During early developmental stages, L5 cells provide an insulin like peptide (called DILP2) signal to the nearby Dm8 cells which has a facilitating effect on the dendritic expansion of Dm8 cells. In combination, antagonistic regulatory inputs via DILP2 (from L5) and Activin (from R7) together regulate the stereotyped morphology of Dm8 dendrites, presumably in order to ensure proper dendritic size for proper circuit function (Luo et al., 2020).

Interestingly, synaptic inputs from R7 onto Dm8 are not evenly distributed along the Dm8 cell surface. In the center of most Dm8 single cell clones exists a prominent dendritic projection extending distally from M6, reaching all the way into layers M4 at which defines Dm8's so-called home column (Carrillo et al., 2015b; Courgeon & Desplan, 2019; Fischbach & Dittrich, 1989;

Menon, Kulkarni, Takemura, Anaya, & Zinn, 2019; Nern et al., 2015; Tan et al., 2015). Although lateral branches of one given Dm8 contact ~13 R7 terminals in layer M6, the home column contains an unproportionally high number of R7-to-Dm8 synapses (Menon et al., 2019; S. Y. Takemura et al., 2015). While lateral branches of neighboring Dm8 cells overlap extensively, their home columns tile in the medulla, thereby providing Dm8 cells with both unicolumnar and multicolumnar attributes (Nern et al., 2015; Tan et al., 2015). As a result, almost every medulla column is home to one dedicated Dm8 cell (S. Y. Takemura et al., 2015). Since Dm8 cells show strict preference for one R7 cell in their home column, the question was raised whether Dm8 cells also fall into specific pale- and yellow-specific subtypes. Recent developmental studies focusing on the cell-type specific expression of cell surface molecules revealed that such Dm8 subtypes indeed exist and investigated how they could be matched with R7 pale and yellow subtypes (Carrillo et al., 2015a; Courgeon & Desplan, 2019; Menon et al., 2019; Tan et al., 2015). Pale and yellow fates are stochastically determined in R7 cells during development (Johnston & Desplan, 2014; Wernet et al., 2006), through the evolutionarily-conserved expression of the transcription factor Spineless (Perry et al., 2016). Therefore, it seemed hard to imagine how the Dm8 cells of each medulla column would assume their pale/yellow identity before contacting its future presynaptic partner. Important insight came from the finding that matching pairs of cell surface molecules are expressed in yellow R7 cells and the Dm8 cells that they are synaptically connected to: the immunoglobin family cell member Dpr11 is expressed in yellow R7, whereas one of its specific binding partners called DIP-γ (for interacting partner gamma, another immunoglobulin transmembrane protein) is expressed in a distinct population of Dm8 cells, long before synapses are formed (Carrillo et al., 2015a, 2015b; Courgeon & Desplan, 2019; Menon et al., 2019). It turns out that two Dm8 subtypes (DIP-γ positive and DIP-γ negative) are produced in excess during development, originating from distinct neural progenitors (Courgeon & Desplan, 2019). In each medulla column, these subtypes then appear to compete for presynaptic R7 partners. When a yellow R7 photoreceptor terminal encounters a DIP-γ positive Dm8, interaction between Dpr11

and DIP-γ promotes the survival of this Dm8, whereas unmatched Dm8 subtypes are eliminated by apoptosis (Courgeon & Desplan, 2019). Therefore, excess production of alternative postsynaptic partners and target derived trophic support via DIP/Dpr cell surface molecules provide an elegant molecular mechanism for ensuring correct matching between stochastically specified presynaptic elements (yellow R7) and their prospective postsynaptic partners (DIP-γ or yellow Dm8) (Figure 2B).

3. Modality-specific circuit elements for processing skylight polarization

Like in many other insects, R7 and R8 residing in DRA form an orthogonal analyzer pair morphologically and molecularly specialized for detecting the celestial polarization pattern (Labhart & Meyer, 1999; Labhart & Wehner, 2006; Wernet et al., 2012; Wunderer & Smola, 1982). These two photoreceptors therefore produce similar yet opponent outputs, yet little is known about how these polarization-opponent signals are processed by cell types in the DRA columns of the medulla of any insect (el Jundi, Pfeiffer, & Homberg, 2011; Labhart, 1988). Two recent studies investigated basic aspects of circuit structure in DRA columns by comparing both photoreceptor and Dm8 morphology there with the rest of the medulla columns (Sancer et al., 2019; Sancer et al., 2020). Interestingly, DRA.R8 morphology is rather unique, differing from non-DRA counterparts not only in Rhodopsin expression (expressing the R7 UV-Rhodopsin Rh3) and layer targeting (axons terminating in the R7 layer M6) but also in the distribution of its presynaptic sites, which resembles that of normal R7 cells (Sancer et al., 2019). Based on all these features, it appears that R8 photoreceptors in the DRA assume an R7-like fate which is in good agreement with their function: To provide an orthogonal analyzer channel to DRA.R7 cells of equal weight (Sancer et al., 2019). But two R7-like photoreceptors terminating in layer M6 immediately raises two important questions: Are both DRA.R7 and DRA.R8 connected to the same Dm8 cell(s), despite having orthogonally opponent analyzer directions? And since one Dm8 cell usually pools from ~13 neighboring ommatidia – do Dm8 cells in the DRA integrate both polarization and color

information? It was recently revealed that indeed there exist significant differences in Dm8 morphology in the DRA, when compared to non-DRA columns (Sancer et al., 2019). Since *Drosophila* optic lobe cell type nomenclature is based mostly on unambiguous morphological classification, this Dm8-like distal medulla cell in the DRA was renamed Dm-DRA1. Importantly, this cell new type restricts its photoreceptor contacts in layer M6 exclusively to DRA inner photoreceptor inputs, while avoiding contacts from color sensitive R7 photoreceptors (Courgeon & Desplan, 2019; Sancer et al., 2019). As a result, lateral arborizations of Dm-DRA1 cells reaching towards the center of the medulla were restricted to a medulla layer below M6, resulting in 'deep projections', a hallmark feature characteristic of Dm-DRA1 cells (Figure 3A)(Sancer et al., 2019). Importantly, the columnar sites of Dm-DRA1 photoreceptor contacts never overlapped with the dendritic fields color sensitive Dm8 cells (Figure 3 A' and A''). Since Dm-DRA1 cells heavily overlapped amongst their own kind (as Dm8 cells do amongst themselves), the DRA/non-DRA boundary is in fact the only place in the medulla neuropil where Dm8-like cells do not overlap, thereby reflecting a modality-specific boundary between color and polarization-sensitive inputs (Sancer et al., 2019).

Despite these differences, developmental studies suggest that Dm-DRA1 and Dm8 cells share a similar developmental origin (Courgeon & Desplan, 2019), hence Dm-DRA1 can probably be considered a third kind of 'true' Dm8 cells (in addition to DIP-γ positive and negative Dm8s). Unexpectedly, a second Dm8-like cell type was described in the M6 layer only in DRA medulla column which is morphologically different from Dm-DRA1 and was therefore named Dm-DRA2 (Sancer et al., 2019). All the arborizations of these cells were restricted to DRA columns (hence not forming 'deep projections' while instead forming very prominent and characteristic vertical projection that follows photoreceptor axon terminals (Figure 3B). Photoreceptor contacts of this second Dm8-like cell type also never overlapped with pale or yellow Dm8 cells and therefore represented a second kind of modality specific cell type for processing skylight information (Figure 3 B' and B''). Interestingly, both Dm-DRA1 and Dm-DRA2 cell types overlap heavily with their own

kind as well as between types, along the entire DRA (Sancer et al., 2019). However, Dm-DRA1 and Dm-DRA2 located at the same position stratify within slightly different layers within M6 (Dm-DRA1 always being located proximally of Dm-DRA2)(Figure 3C). In fact the distance between them exactly matches the distance DRA.R7 and DRA.R8 axon termination sites within M6 (Sancer et al., 2019). The possibility of Dm-DRA1 and Dm-DRA2 being specific postsynaptic partners of DRA.R7 and DRA.R8, respectively was indeed confirmed via molecular genetic tools, like GFP reconstitution across synaptic partners (GRASP) (Feinberg et al., 2008; Macpherson et al., 2015) and by using the trans-synaptic tracer tool trans-tango (Sancer et al., 2019; Talay et al., 2017). Therefore, only in the DRA region of the medulla neuropil, both R7 and R8 cells are synaptically connected to different subtypes of morphologically distinct Dm8-like subtypes, further supporting the observation that DRA.R8 cells become R7-like both in function and circuitry, when processing polarized skylight information.

The fact that Dm-DRA1 and Dm-DRA2 stratify in close proximity within two M6 sublayers of M6 while being connected to different presynaptic partners (DRA.R7 versus DRA.R8) raises the question how such synaptic specificity is achieved during development. So far, no immunoglobulin proteins are known to be specifically expressed in DRA circuit elements. Important insight into a possible mechanism facilitating the formation of specific synaptic connections in close proximity came from the intravital imaging of sparsely labeled inner photoreceptor terminals as they grow into their medulla target layers (Sancer et al., 2019). Normal non-DRA R7 growth cones target swiftly to M6, whereas R8 growth cones pause at the distal end of the medulla (M0) and then actively extend towards M3 (Ozel, Langen, Hassan, & Hiesinger, 2015). Although in adult DRA.R8 become more R7-like, developmental dynamics of DRA.R8 remain “normal R8” until mid-pupal stages. As a result, DRA.R7 and DRA.R8 axon terminals reach layer M6 at different times, which might enable a temporal separation for synaptic partner choice (Figure 3D). Certainly, specific expression of cell surface molecules might still play an

important role, and more live imaging is needed to get a better understanding of how partner choice and transient cell-cell contacts influence the generation of synaptic specificity in the DRA.

4. An additional layer of inter-ommatidial integration: Dm9 cells

In most cases, true color vision involves color opponent elements collecting information from at least two distinct chromatic channels (Longden, 2018). In recent years it became clear that in *Drosophila*, color opponency already starts in the level of photoreceptor terminals: Ultrastructural studies revealed that color-sensitive R7 and R8 photoreceptor terminals from the same ommatidium are bidirectionally synaptically connected to each other (S. Y. Takemura et al., 2008; S. Y. Takemura et al., 2015). More recently, functional imaging of R7 and R8 terminals using cell-type specific expression of genetically encoded indicators of activity revealed short-UV/blue opponent signals in pale columns and long-UV/green opponency in yellow columns (Schnaitmann et al., 2018). This intra-ommatidial color opponency was shown to depend on direct reciprocal inhibition mediated by a specific isoform of a histamine gated chloride channel expressed rather specifically in inner photoreceptor terminals (while being absent from most inner photoreceptor target cells in the optic lobe) (Davis et al., 2020; Tan et al., 2015). In addition to this direct reciprocal intra-ommatidial inhibition, it has been suggested that medulla neurons expressing another histamine gated chloride channel isoform (called Ort) also provide feedback inhibition to photoreceptors (Schnaitmann et al., 2018). Hence, the outputs of histaminergic inner photoreceptors R7 and R8 are already opponent in nature, which must be taken into account when interpreting the functional properties of the cholinergic R7 → Dm8 → Tm5c circuit described above.

One recent study offered important new insight into the cellular mechanism providing feedback inhibition into R7 and R8 photoreceptor terminals. In fact, this study also revealed that inter-columnar interactions between neighboring ommatidia play an important role in shape the color sensitive responses of R7 and R8 terminals (Heath et al., 2019). Once again, functional

imaging of the photoreceptor terminals was used to reveal that neighboring columns provide additional (indirect) inhibitory input. For instance, inhibition is observed for blue-sensitive pale R8 terminals when stimulating with longer wavelengths, suggesting that yellow R8 photoreceptor input from neighboring ommatidia also shapes pale R8 output. Such inter-columnar inhibition could only be provided by horizontal cell types that contact several medulla columns, while also providing synaptic input into the photoreceptor terminals. The distal medulla cell type Dm9 was identified as the likely candidate, each cell spanning seven columns on, tiling in layers M2-M5 while overlapping in M1 and M6 (Figure 4A)(Nern et al., 2015; S. Takemura et al., 2013). More importantly, Dm9 is the only medulla cell type that both receives synaptic input from R7 and R8 while also providing strong synaptic feedback onto both photoreceptor terminals (Figure 4B)(Uhlhorn & Wernet, 2020). Indeed, functional imaging of R7 and R8 axon terminals while silencing the synaptic output of Dm9 cells specifically led to a disappearance of inter-ommatidial inhibition (Heath et al., 2019). Strikingly, Dm9 was shown to be both necessary and sufficient for mediating inter-ommatidial antagonism and thereby enabling additional color comparisons (Figure 4C). Hence, this dual opponent system via intra-columnar and inter-columnar inhibition provides an efficient mechanism for 'sculpting' photoreceptor responses, thereby decorrelating photoreceptor signals with overlapping opsin sensitivity while keeping adequate information for the reconstruction of chromatic stimuli.

Surprisingly, unlike Dm8, Dm9 does not manifest any modality-specific morphology in the DRA region of the medulla, meaning that Dm9 cells located there appear to contact R7 and R8 photoreceptors from both DRA and non-DRA ommatidia (see Figure 1 E) (Sancer et al., 2020). This is particularly interesting, since intra-ommatidial opponency has also been demonstrated in DRA photoreceptor terminals, resulting in polarization-opponent signals in both DRA.R7 and DRA.R8 terminals from the same ommatidium with preferred e-vector orientations being orthogonal to each other (Weir et al., 2016). It is therefore possible that Dm9 cells in the DRA might mix color and polarization information in the photoreceptor terminals they innervate. Hence,

color and skylight polarization information might already be integrated at this early stage in the visual circuit, as suggested by data from other insects (el Jundi, Pfeiffer, Heinze, & Homberg, 2014). However, Dm9 crossing the DRA boundary do manifest specific differences in the localization of both pre- and post-synaptic membranes located within DRA columns as compared to those in non-DRA columns, hinting at possible differences in the synaptic connectivity within one cell (Sancer et al., 2020). For now, it therefore remains unknown whether Dm9 affects DRA photoreceptors and adjacent color-sensitive photoreceptor output and more studies are needed to answer this question.

5. Summary and outlook

The neural circuit elements post-synaptic to R7 and R8 photoreceptors are crucial for processing color and polarized light signals. In recent years it became apparent that synaptic interconnections between photoreceptors themselves, as well as their targets result in rather complex properties of the photoreceptors themselves. It is now crucial to extend the anatomical and physiological characterization of these circuits towards all cell types directly or indirectly post-synaptic to R7 and R8. Beyond Dm8 and Dm9, several synaptic targets of either R7, R8, or both have been reported (S. Y. Takemura et al., 2008; S. Y. Takemura et al., 2015). However, significantly less is known about their physiological properties, as well as their relevance for guiding behavioral responses (Longden, 2018; Otsuna et al., 2014; Schnaitmann et al., 2020; Song & Lee, 2018). So far, most systematic dissection has focused on the circuits for detecting moving stimuli (Borst, 2014; Silies, Gohl, & Clandinin, 2014; Tuthill et al., 2013). The ongoing anatomical study of visual circuitry will greatly benefit from the recent publication of an electron microscopic dataset spanning the entire adult female fly brain (Zheng et al., 2018). Using this data, virtually any circuit can be reconstructed at synaptic resolution. Molecular genetic tools specifically labeling the newly identified cell types can then be retrieved from existing databases (Jenett et al., 2012; Pfeiffer et al., 2008), to be used for the physiological characterization, or

manipulation in the behaving animal. Importantly, the same tools are currently being used to identify all the genes expressed by a particular optic lobe cell type, for instance neurotransmitters or their receptors (Davis et al., 2020), which in turn provides very useful information for understanding the computations they execute. Alternative approaches even aim at extracting such transcriptomes in an unbiased way from single cells, by collecting clusters of expression profiles which must then be matched with their presumptive cell types (Konstantinides et al., 2018). Together with state-of-the art light microscopic techniques (Macpherson et al., 2015; Talay et al., 2017), as well as immunohistochemistry in combination with expansion microscopy (Wassie, Zhao, & Boyden, 2019), these combined approaches will reveal crucial insight into both the similarities and differences of the anatomical structure of those neural circuits processing color versus polarized light.

In addition to studies on the structure and function of optic lobe cell types, the ongoing studies on both the development and the assembly of these neural circuits will provide crucial information that complements those datasets. For instance, the developmental origin of many lamina, medulla, and lobula cell types is currently being identified, thereby revealing their sibling relationship (neuroblast origin), as well as the transcriptional code and the mechanisms regulating the number and location of cell types (Apitz & Salecker, 2018; Bertet et al., 2014; Chen et al., 2016; Erclik et al., 2017; Holguera & Desplan, 2018; Li et al., 2013; Mora et al., 2018; Pinto-Teixeira et al., 2018). Transcriptomic data from specific cell types, collected at successive time points during development will reveal new transcription factors as well as the dynamic expression of cell surface molecules specifically expressed in any type of interest. Developmental studies will further clarify the exact role of adhesion molecules: Which ones act as specific cues for informing the formation of new synapses? Which ones are necessary for stabilizing transient synaptic connections? Which ones regulate the sorting of cell types during development? Which ones are necessary for inducing or suppressing apoptosis by mediating cell/cell contacts? Of particular importance are live imaging studies for revealing the dynamic nature of cell/cell interactions, as

well as axon outgrowth and synaptic stabilization (Langen et al., 2015; Ozel et al., 2015).The growing number of studies related to these questions will reveal the common principles, as well as the cell type specific differences behind establishing specific synaptic connections. Finally, although visual input has been shown to play no significant role in the generation of synaptic specificity in the periphery of the fly visual system (Hiesinger et al., 2006), a recent study using genetically encoded indicators of activity during circuit assembly in the optic lobes revealed spontaneous activity waves in cell types that will be connected in the adult brain (Akin, Bajar, Keles, Frye, & Zipursky, 2019). Therefore, it turns out the combination of similar tools (molecular biology, physiology, anatomy) bear the potential to provide answers on multiple aspects of neural circuit development and assembly, as well as adult circuit structure and function.

Author contributions

GS and MFW together planned the outline of text and figures. GS generated the figures. GS and MFW together wrote the manuscript. MFW acquired the funds.

Acknowledgments

The authors would like to thank the Wernet and Hiesinger Lab members for helpful suggestions on the manuscript. This work was supported by the Deutsche Forschungsgemeinschaft (DFG) through grants WE 5761/2-1, and SPP2205, through AFOSR grant FA9550-19-1-7005, through the Berlin Excellency Cluster NeuroCure, with support from the Fachbereich Biologie, Chemie & Pharmazie of the Freie Universität Berlin, as well as the Division of Neurobiology at Freie Universität Berlin (support of FU Berlin and the National Institute of Health to Robin Hiesinger).

References

Akin, O., Bajar, B. T., Keles, M. F., Frye, M. A., & Zipursky, S. L. (2019). Cell-type-Specific Patterned Stimulus-Independent Neuronal Activity in the Drosophila Visual System during Synapse Formation. *Neuron, 101*(5), 894-904 e895. doi:10.1016/j.neuron.2019.01.008

Apitz, H., & Salecker, I. (2018). Spatio-temporal relays control layer identity of direction-selective neuron subtypes in Drosophila. *Nat Commun, 9*(1), 2295. doi:10.1038/s41467-018-04592-z

Bell, M. L., Earl, J. B., & Britt, S. G. (2007). Two types of Drosophila R7 photoreceptor cells are arranged randomly: a model for stochastic cell-fate determination. *J Comp Neurol, 502*(1), 75-85. doi:10.1002/cne.21298

Bertet, C., Li, X., Erclik, T., Cavey, M., Wells, B., & Desplan, C. (2014). Temporal patterning of neuroblasts controls Notch-mediated cell survival through regulation of Hid or Reaper. *Cell, 158*(5), 1173-1186. doi:10.1016/j.cell.2014.07.045

Borst, A. (2014). In search of the Holy Grail of fly motion vision. *Eur J Neurosci, 40*(9), 3285-3293. doi:10.1111/ejn.12731

Carrillo, R. A., Ozkan, E., Menon, K. P., Nagarkar-Jaiswal, S., Lee, P. T., Jeon, M., . . . Zinn, K. (2015a). Control of Synaptic Connectivity by a Network of Drosophila IgSF Cell Surface Proteins. *Cell, 163*(7), 1770-1782. doi:10.1016/j.cell.2015.11.022

Carrillo, R. A., Ozkan, E., Menon, K. P., Nagarkar-Jaiswal, S., Lee, P. T., Jeon, M., . . . Zinn, K. (2015b). Control of Synaptic Connectivity by a Network of Drosophila IgSF Cell Surface Proteins. *Cell, 163*(7), 1770-1782. doi:10.1016/j.cell.2015.11.022

Chen, Z., Del Valle Rodriguez, A., Li, X., Erclik, T., Fernandes, V. M., & Desplan, C. (2016). A Unique Class of Neural Progenitors in the Drosophila Optic Lobe Generates Both Migrating Neurons and Glia. *Cell Rep, 15*(4), 774-786. doi:10.1016/j.celrep.2016.03.061

Chou, W. H., Hall, K. J., Wilson, D. B., Wideman, C. L., Townson, S. M., Chadwell, L. V., & Britt, S. G. (1996). Identification of a novel Drosophila opsin reveals specific patterning of the R7 and R8 photoreceptor cells. *Neuron, 17*(6), 1101-1115. doi:10.1016/s0896-6273(00)80243-3

Chou, W. H., Huber, A., Bentrop, J., Schulz, S., Schwab, K., Chadwell, L. V., . . . Britt, S. G. (1999). Patterning of the R7 and R8 photoreceptor cells of Drosophila: evidence for induced and default cell-fate specification. *Development, 126*(4), 607-616. Retrieved from http://www.ncbi.nlm.nih.gov/pubmed/9895309

Courgeon, M., & Desplan, C. (2019). Coordination between stochastic and deterministic specification in the Drosophila visual system. *Science, 366*(6463). doi:10.1126/science.aay6727

Coyne, J. A., Boussy, I. A., Prout, T., Bryant, S. H., Jones, J. S., & Moore, J. A. (1982). Long-distance migration of Drosophila. *Am. Nat.*(119), 589–595.

Coyne, J. A., Bryant, S. H., & Turelli, M. (1987). Long-distance migration of Drosophila. 2. Presence in desolate sites and dispersal near a desert oasis. *Am. Nat.*(129), 847–861.

Davis, F. P., Nern, A., Picard, S., Reiser, M. B., Rubin, G. M., Eddy, S. R., & Henry, G. L. (2020). A genetic, genomic, and computational resource for exploring neural circuit function. *Elife, 9*. doi:10.7554/eLife.50901

Dickinson, M. H. (2014). Death Valley, Drosophila, and the Devonian toolkit. *Annu Rev Entomol, 59*, 51-72. doi:10.1146/annurev-ento-011613-162041

el Jundi, B., Pfeiffer, K., Heinze, S., & Homberg, U. (2014). Integration of polarization and chromatic cues in the insect sky compass. *J Comp Physiol A Neuroethol Sens Neural Behav Physiol, 200*(6), 575-589. doi:10.1007/s00359-014-0890-6

el Jundi, B., Pfeiffer, K., & Homberg, U. (2011). A distinct layer of the medulla integrates sky compass signals in the brain of an insect. *PLoS One, 6*(11), e27855. doi:10.1371/journal.pone.0027855

Erclik, T., Li, X., Courgeon, M., Bertet, C., Chen, Z., Baumert, R., . . . Desplan, C. (2017). Integration of temporal and spatial patterning generates neural diversity. *Nature, 541*(7637), 365-370. doi:10.1038/nature20794

Feiler, R., Bjornson, R., Kirschfeld, K., Mismer, D., Rubin, G. M., Smith, D. P., . . . Zuker, C. S. (1992). Ectopic expression of ultraviolet-rhodopsins in the blue photoreceptor cells of Drosophila: visual physiology and photochemistry of transgenic animals. *J Neurosci, 12*(10), 3862-3868. Retrieved from http://www.ncbi.nlm.nih.gov/pubmed/1403087

Feinberg, E. H., Vanhoven, M. K., Bendesky, A., Wang, G., Fetter, R. D., Shen, K., & Bargmann, C. I. (2008). GFP Reconstitution Across Synaptic Partners (GRASP) defines cell contacts and synapses in living nervous systems. *Neuron, 57*(3), 353-363. doi:10.1016/j.neuron.2007.11.030

Fischbach, K. F., & Dittrich, A. P. M. (1989). The Optic Lobe of Drosophila-Melanogaster .1. A Golgi Analysis of Wild-Type Structure. *Cell and Tissue Research, 258*(3), 441-475. Retrieved from <Go to ISI>://WOS:A1989CC25600001

Fortini, M. E., & Rubin, G. M. (1990). Analysis of Cis-Acting Requirements of the Rh3 and Rh4 Genes Reveals a Bipartite Organization to Rhodopsin Promoters in Drosophila-Melanogaster. *Genes & Development, 4*(3), 444-463. Retrieved from <Go to ISI>://WOS:A1990DD09600013

Fortini, M. E., & Rubin, G. M. (1991). The Optic Lobe Projection Pattern of Polarization-Sensitive Photoreceptor Cells in Drosophila-Melanogaster. *Cell and Tissue Research, 265*(1), 185-191. Retrieved from <Go to ISI>://WOS:A1991FU79300021

Franceschini, N., Kirschfeld, K., & Minke, B. (1981). Fluorescence of photoreceptor cells observed in vivo. *Science, 213*(4513), 1264-1267. Retrieved from http://www.ncbi.nlm.nih.gov/pubmed/7268434

Gao, S., Takemura, S. Y., Ting, C. Y., Huang, S., Lu, Z., Luan, H., . . . Lee, C. H. (2008). The neural substrate of spectral preference in Drosophila. *Neuron, 60*(2), 328-342. doi:10.1016/j.neuron.2008.08.010

Heath, S. L., Christenson, M. P., Oriol, E., Saavedra-Weisenhaus, M., Kohn, J. R., & Behnia, R. (2019). Circuit mechanisms underlying chromatic encoding in Drosophila photoreceptors. *bioRxiv*, 790295. doi:10.1101/790295

Hiesinger, P. R., Zhai, R. G., Zhou, Y., Koh, T. W., Mehta, S. Q., Schulze, K. L., . . . Bellen, H. J. (2006). Activity-independent prespecification of synaptic partners in the visual map of Drosophila. *Curr Biol, 16*(18), 1835-1843. doi:10.1016/j.cub.2006.07.047

Hilbrant, M., Almudi, I., Leite, D. J., Kuncheria, L., Posnien, N., Nunes, M. D., & McGregor, A. P. (2014). Sexual dimorphism and natural variation within and among species in the Drosophila retinal mosaic. *BMC Evol Biol, 14*, 240. doi:10.1186/s12862-014-0240-x

Holguera, I., & Desplan, C. (2018). Neuronal specification in space and time. *Science, 362*(6411), 176-180. doi:10.1126/science.aas9435

Huber, A., Schulz, S., Bentrop, J., Groell, C., Wolfrum, U., & Paulsen, R. (1997). Molecular cloning of Drosophila Rh6 rhodopsin: the visual pigment of a subset of R8 photoreceptor cells. *FEBS Lett, 406*(1-2), 6-10. doi:10.1016/s0014-5793(97)00210-x

Jenett, A., Rubin, G. M., Ngo, T. T., Shepherd, D., Murphy, C., Dionne, H., . . . Zugates, C. T. (2012). A GAL4-driver line resource for Drosophila neurobiology. *Cell Rep, 2*(4), 991-1001. doi:10.1016/j.celrep.2012.09.011

Johnston, R. J., Jr., & Desplan, C. (2014). Interchromosomal communication coordinates intrinsically stochastic expression between alleles. *Science, 343*(6171), 661-665. doi:10.1126/science.1243039

Jukam, D., Xie, B., Rister, J., Terrell, D., Charlton-Perkins, M., Pistillo, D., . . . Cook, T. (2013). Opposite feedbacks in the Hippo pathway for growth control and neural fate. *Science, 342*(6155), 1238016. doi:10.1126/science.1238016

Karuppudurai, T., Lin, T. Y., Ting, C. Y., Pursley, R., Melnattur, K. V., Diao, F., . . . Lee, C. H. (2014). A hard-wired glutamatergic circuit pools and relays UV signals to mediate spectral preference in Drosophila. *Neuron, 81*(3), 603-615. doi:10.1016/j.neuron.2013.12.010

Kind, E., Belušič, G., & Wernet, M. F. (2020). Retinal Mosaics Across Fly Species: Variations on a Theme *Reference Module in Neuroscience and Biobehavioral Psychology*: Elsevier.

Konstantinides, N., Kapuralin, K., Fadil, C., Barboza, L., Satija, R., & Desplan, C. (2018). Phenotypic Convergence: Distinct Transcription Factors Regulate Common Terminal Features. *Cell, 174*(3), 622-635 e613. doi:10.1016/j.cell.2018.05.021

Labhart, T. (1988). Polarization-Opponent Interneurons in the Insect Visual-System. *Nature, 331*(6155), 435-437. doi:DOI 10.1038/331435a0

Labhart, T., & Meyer, E. P. (1999). Detectors for polarized skylight in insects: a survey of ommatidial specializations in the dorsal rim area of the compound eye. *Microsc Res Tech, 47*(6), 368-379. doi:10.1002/(SICI)1097-0029(19991215)47:6<368::AID-JEMT2>3.0.CO;2-Q

Labhart, T., & Wehner, R. (2006). Polarization Vision. In E. J. Warrant & D. E. Nilsson (Eds.), *Invertebrate vision* (pp. 291-348). Cambridge: Cambridge University Press.

Langen, M., Agi, E., Altschuler, D. J., Wu, L. F., Altschuler, S. J., & Hiesinger, P. R. (2015). The Developmental Rules of Neural Superposition in Drosophila. *Cell, 162*(1), 120-133. doi:10.1016/j.cell.2015.05.055

Li, X., Erclik, T., Bertet, C., Chen, Z., Voutev, R., Venkatesh, S., . . . Desplan, C. (2013). Temporal patterning of Drosophila medulla neuroblasts controls neural fates. *Nature, 498*(7455), 456-462. doi:10.1038/nature12319

Lin, T. Y., Luo, J., Shinomiya, K., Ting, C. Y., Lu, Z., Meinertzhagen, I. A., & Lee, C. H. (2016). Mapping chromatic pathways in the Drosophila visual system. *J Comp Neurol, 524*(2), 213-227. doi:10.1002/cne.23857

Longden, K. D. (2018). Colour Vision: A Fresh View of Lateral Inhibition in Drosophila. *Curr Biol, 28*(7), R308-R311. doi:10.1016/j.cub.2018.02.052

Luo, J., Ting, C. Y., Li, Y., McQueen, P., Lin, T. Y., Hsu, C. P., & Lee, C. H. (2020). Antagonistic regulation by insulin-like peptide and activin ensures the elaboration of appropriate dendritic field sizes of amacrine neurons. *Elife, 9*. doi:10.7554/eLife.50568

Macpherson, L. J., Zaharieva, E. E., Kearney, P. J., Alpert, M. H., Lin, T. Y., Turan, Z., . . . Gallio, M. (2015). Dynamic labelling of neural connections in multiple colours by trans-synaptic fluorescence complementation. *Nat Commun, 6*, 10024. doi:10.1038/ncomms10024

Mathejczyk, T. F., & Wernet, M. F. (2017). Sensing Polarized Light in Insects: Oxford Encyclopedia of Neuroscience.

Mathejczyk, T. F., & Wernet, M. F. (2019). Heading choices of flying Drosophila under changing angles of polarized light. *Sci Rep, 9*(1), 16773. doi:10.1038/s41598-019-53330-y

Mathejczyk, T. F., & Wernet, M. F. (2020). Modular assays for the quantitative study of visually guided navigation in both flying and walking flies. *J Neurosci Methods, 340*, 108747. doi:10.1016/j.jneumeth.2020.108747

Meinertzhagen, I., & Hanson, T. (1993). The development of the optic lobe. In "The Development of Drosophila melanogaster"MBate, AMartinez-Arias, eds. 1363–1392: Cold Spring Harbor Laboratory Press, New York.

Meinertzhagen, I. A., Takemura, S. Y., Lu, Z., Huang, S., Gao, S., Ting, C. Y., & Lee, C. H. (2009). From form to function: the ways to know a neuron. *J Neurogenet, 23*(1-2), 68-77. doi:10.1080/01677060802610604

Melnattur, K. V., Pursley, R., Lin, T. Y., Ting, C. Y., Smith, P. D., Pohida, T., & Lee, C. H. (2014). Multiple redundant medulla projection neurons mediate color vision in Drosophila. *J Neurogenet, 28*(3-4), 374-388. doi:10.3109/01677063.2014.891590

Menon, K. P., Kulkarni, V., Takemura, S. Y., Anaya, M., & Zinn, K. (2019). Interactions between Dpr11 and DIP-gamma control selection of amacrine neurons in Drosophila color vision circuits. *Elife, 8*. doi:10.7554/eLife.48935

Mikeladze-Dvali, T., Wernet, M. F., Pistillo, D., Mazzoni, E. O., Teleman, A. A., Chen, Y. W., . . . Desplan, C. (2005). The growth regulators warts/lats and melted interact in a bistable loop to specify opposite fates in Drosophila R8 photoreceptors. *Cell, 122*(5), 775-787. doi:10.1016/j.cell.2005.07.026

Mora, N., Oliva, C., Fiers, M., Ejsmont, R., Soldano, A., Zhang, T. T., . . . Hassan, B. A. (2018). A Temporal Transcriptional Switch Governs Stem Cell Division, Neuronal Numbers, and Maintenance of Differentiation. *Dev Cell, 45*(1), 53-66 e55. doi:10.1016/j.devcel.2018.02.023

Nern, A., Pfeiffer, B. D., & Rubin, G. M. (2015). Optimized tools for multicolor stochastic labeling reveal diverse stereotyped cell arrangements in the fly visual system. *Proc Natl Acad Sci U S A, 112*(22), E2967-2976. doi:10.1073/pnas.1506763112

Otsuna, H., Shinomiya, K., & Ito, K. (2014). Parallel neural pathways in higher visual centers of the Drosophila brain that mediate wavelength-specific behavior. *Front Neural Circuits, 8*, 8. doi:10.3389/fncir.2014.00008

Ozel, M. N., Langen, M., Hassan, B. A., & Hiesinger, P. R. (2015). Filopodial dynamics and growth cone stabilization in Drosophila visual circuit development. *Elife, 4*. doi:10.7554/eLife.10721

Papatsenko, D., Sheng, G., & Desplan, C. (1997). A new rhodopsin in R8 photoreceptors of Drosophila: evidence for coordinate expression with Rh3 in R7 cells. *Development, 124*(9), 1665-1673. Retrieved from http://www.ncbi.nlm.nih.gov/pubmed/9165115

Perry, M., Kinoshita, M., Saldi, G., Huo, L., Arikawa, K., & Desplan, C. (2016). Molecular logic behind the three-way stochastic choices that expand butterfly colour vision. *Nature, 535*(7611), 280-+. Retrieved from <Go to ISI>://WOS:000379912600056

Pfeiffer, B. D., Jenett, A., Hammonds, A. S., Ngo, T. T., Misra, S., Murphy, C., . . . Rubin, G. M. (2008). Tools for neuroanatomy and neurogenetics in Drosophila. *Proc Natl Acad Sci U S A, 105*(28), 9715-9720. doi:10.1073/pnas.0803697105

Pinto-Teixeira, F., Koo, C., Rossi, A. M., Neriec, N., Bertet, C., Li, X., . . . Desplan, C. (2018). Development of Concurrent Retinotopic Maps in the Fly Motion Detection Circuit. *Cell, 173*(2), 485-498 e411. doi:10.1016/j.cell.2018.02.053

Pollack, I., & Hofbauer, A. (1991). Histamine-like immunoreactivity in the visual system and brain of Drosophila melanogaster. *Cell Tissue Res, 266*(2), 391-398. doi:10.1007/bf00318195

Salcedo, E., Huber, A., Henrich, S., Chadwell, L. V., Chou, W. H., Paulsen, R., & Britt, S. G. (1999). Blue- and green-absorbing visual pigments of Drosophila: ectopic expression and physiological characterization of the R8 photoreceptor cell-specific Rh5 and Rh6 rhodopsins. *J Neurosci, 19*(24), 10716-10726. Retrieved from http://www.ncbi.nlm.nih.gov/pubmed/10594055

Sancer, G., Kind, E., Plazaola-Sasieta, H., Balke, J., Pham, T., Hasan, A., . . . Wernet, M. F. (2019). Modality-Specific Circuits for Skylight Orientation in the Fly Visual System. *Curr Biol*. doi:10.1016/j.cub.2019.07.020

Sancer, G., Kind, E., Uhlhorn, J., Volkmann, J., Hammacher, J., Pham, T., . . . Wernet, M. F. (2020). Cellular and synaptic adaptations of neural circuits processing skylight polarization in the fly. *J Comp Physiol A Neuroethol Sens Neural Behav Physiol, 206*(2), 233-246. doi:10.1007/s00359-019-01389-3

Schnaitmann, C., Garbers, C., Wachtler, T., & Tanimoto, H. (2013). Color discrimination with broadband photoreceptors. *Curr Biol, 23*(23), 2375-2382. doi:10.1016/j.cub.2013.10.037

Schnaitmann, C., Haikala, V., Abraham, E., Oberhauser, V., Thestrup, T., Griesbeck, O., & Reiff, D. F. (2018). Color Processing in the Early Visual System of Drosophila. *Cell, 172*(1-2), 318-330 e318. doi:10.1016/j.cell.2017.12.018

Schnaitmann, C., Pagni, M., & Reiff, D. F. (2020). Color vision in insects: insights from Drosophila. *J Comp Physiol A Neuroethol Sens Neural Behav Physiol, 206*(2), 183-198. doi:10.1007/s00359-019-01397-3

Silies, M., Gohl, D. M., & Clandinin, T. R. (2014). Motion-detecting circuits in flies: coming into view. *Annu Rev Neurosci, 37*, 307-327. doi:10.1146/annurev-neuro-071013-013931

Smola, U., & Tscharntke, H. (1979). Twisted Rhabdomeres in the Dipteran Eye. *Journal of Comparative Physiology, 133*(4), 291-297. Retrieved from <Go to ISI>://WOS:A1979HU30200005

Song, B. M., & Lee, C. H. (2018). Toward a Mechanistic Understanding of Color Vision in Insects. *Front Neural Circuits, 12*, 16. doi:10.3389/fncir.2018.00016

Stuart, A. E. (1999). From fruit flies to barnacles, histamine is the neurotransmitter of arthropod photoreceptors. *Neuron, 22*(3), 431-433. doi:10.1016/s0896-6273(00)80699-6

Takemura, S., Bharioke, A., Lu, Z. Y., Nern, A., Vitaladevuni, S., Rivlin, P. K., . . . Chklovskii, D. B. (2013). A visual motion detection circuit suggested by Drosophila connectomics. *Nature, 500*(7461), 175-+. Retrieved from <Go to ISI>://WOS:000322825500028

Takemura, S. Y., Lu, Z. Y., & Meinertzhagen, I. A. (2008). Synaptic circuits of the Drosophila optic lobe: The input terminals to the medulla. *Journal of Comparative Neurology, 509*(5), 493-513. Retrieved from <Go to ISI>://WOS:000257630700003

Takemura, S. Y., Xu, C. S., Lu, Z., Rivlin, P. K., Parag, T., Olbris, D. J., . . . Scheffer, L. K. (2015). Synaptic circuits and their variations within different columns in the visual system of Drosophila. *Proc Natl Acad Sci U S A, 112*(44), 13711-13716. doi:10.1073/pnas.1509820112

Talay, M., Richman, E. B., Snell, N. J., Hartmann, G. G., Fisher, J. D., Sorkac, A., . . . Barnea, G. (2017). Transsynaptic Mapping of Second-Order Taste Neurons in Flies by trans-Tango. *Neuron, 96*(4), 783-795 e784. doi:10.1016/j.neuron.2017.10.011

Tan, L., Zhang, K. X., Pecot, M. Y., Nagarkar-Jaiswal, S., Lee, P. T., Takemura, S. Y., . . . Zipursky, S. L. (2015). Ig Superfamily Ligand and Receptor Pairs Expressed in Synaptic Partners in Drosophila. *Cell, 163*(7), 1756-1769. doi:10.1016/j.cell.2015.11.021

Ting, C. Y., McQueen, P. G., Pandya, N., Lin, T. Y., Yang, M., Reddy, O. V., . . . Lee, C. H. (2014). Photoreceptor-derived activin promotes dendritic termination and restricts the receptive

fields of first-order interneurons in Drosophila. *Neuron, 81*(4), 830-846. doi:10.1016/j.neuron.2013.12.012

Tomlinson, A. (2003). Patterning the peripheral retina of the fly: decoding a gradient. *Dev Cell, 5*(5), 799-809. Retrieved from http://www.ncbi.nlm.nih.gov/pubmed/14602079

Tuthill, J. C., Nern, A., Holtz, S. L., Rubin, G. M., & Reiser, M. B. (2013). Contributions of the 12 neuron classes in the fly lamina to motion vision. *Neuron, 79*(1), 128-140. doi:10.1016/j.neuron.2013.05.024

Uhlhorn, J., & Wernet, M. F. (2020). Colour Vision: Self-Centered Fly Photoreceptors Communicate over Distances. *Curr Biol, 30*(2), R78-R81. doi:10.1016/j.cub.2019.11.050

Velez, M. M., Gohl, D., Clandinin, T. R., & Wernet, M. F. (2014). Differences in neural circuitry guiding behavioral responses to polarized light presented to either the dorsal or ventral retina in Drosophila. *J Neurogenet, 28*(3-4), 348-360. doi:10.3109/01677063.2014.922556

Velez, M. M., Wernet, M. F., Clark, D. A., & Clandinin, T. R. (2014). Walking Drosophila align with the e-vector of linearly polarized light through directed modulation of angular acceleration. *J Comp Physiol A Neuroethol Sens Neural Behav Physiol, 200*(6), 603-614. doi:10.1007/s00359-014-0910-6

Wada, S. (1974). Special Marginal Ommatidia of Flies (Diptera-Brachycera) - Architecture and Distribution in Compound Eyes. *Zeitschrift Fur Morphologie Der Tiere, 77*(2), 87-125. Retrieved from <Go to ISI>://WOS:A1974S115800001

Warren, T. L., Giraldo, Y. M., & Dickinson, M. H. (2019). Celestial navigation in Drosophila. *J Exp Biol, 222*(Pt Suppl 1). doi:10.1242/jeb.186148

Warren, T. L., Weir, P. T., & Dickinson, M. H. (2018). Flying Drosophilamelanogaster maintain arbitrary but stable headings relative to the angle of polarized light. *J Exp Biol, 221*(Pt 9). doi:10.1242/jeb.177550

Wassie, A. T., Zhao, Y., & Boyden, E. S. (2019). Expansion microscopy: principles and uses in biological research. *Nat Methods, 16*(1), 33-41. doi:10.1038/s41592-018-0219-4

Weir, P. T., & Dickinson, M. H. (2012). Flying Drosophila Orient to Sky Polarization. *Current Biology, 22*(1), 21-27. Retrieved from <Go to ISI>://WOS:000299144200017

Weir, P. T., Henze, M. J., Bleul, C., Baumann-Klausener, F., Labhart, T., & Dickinson, M. H. (2016). Anatomical Reconstruction and Functional Imaging Reveal an Ordered Array of Skylight Polarization Detectors in Drosophila. *J Neurosci, 36*(19), 5397-5404. doi:10.1523/JNEUROSCI.0310-16.2016

Wells, B. S., Pistillo, D., Barnhart, E., & Desplan, C. (2017). Parallel Activin and BMP signaling coordinates R7/R8 photoreceptor subtype pairing in the stochastic Drosophila retina. *Elife, 6*. doi:10.7554/eLife.25301

Wernet, M. F., Celik, A., Mikeladze-Dvali, T., & Desplan, C. (2007). Generation of uniform fly retinas. *Curr Biol, 17*(23), R1002-1003. doi:10.1016/j.cub.2007.10.006

Wernet, M. F., & Desplan, C. (2014). Homothorax and Extradenticle alter the transcription factor network in Drosophila ommatidia at the dorsal rim of the retina. *Development, 141*(4), 918-928. doi:10.1242/dev.103127

Wernet, M. F., Labhart, T., Baumann, F., Mazzoni, E. O., Pichaud, F., & Desplan, C. (2003). Homothorax switches function of Drosophila photoreceptors from color to polarized light sensors. *Cell, 115*(3), 267-279. Retrieved from http://www.ncbi.nlm.nih.gov/pubmed/14636555

Wernet, M. F., Mazzoni, E. O., Celik, A., Duncan, D. M., Duncan, I., & Desplan, C. (2006). Stochastic spineless expression creates the retinal mosaic for colour vision. *Nature, 440*(7081), 174-180. doi:10.1038/nature04615

Wernet, M. F., Meier, K. M., Baumann-Klausener, F., Dorfman, R., Weihe, U., Labhart, T., & Desplan, C. (2014). Genetic dissection of photoreceptor subtype specification by the Drosophila melanogaster zinc finger proteins elbow and no ocelli. *PLoS Genet, 10*(3), e1004210. doi:10.1371/journal.pgen.1004210

Wernet, M. F., Perry, M. W., & Desplan, C. (2015). The evolutionary diversity of insect retinal mosaics: common design principles and emerging molecular logic. *Trends Genet, 31*(6), 316-328. doi:10.1016/j.tig.2015.04.006

Wernet, M. F., Velez, M. M., Clark, D. A., Baumann-Klausener, F., Brown, J. R., Klovstad, M., . . . Clandinin, T. R. (2012). Genetic dissection reveals two separate retinal substrates for polarization vision in Drosophila. *Curr Biol, 22*(1), 12-20. doi:10.1016/j.cub.2011.11.028

Wolf, R., Gebhardt, B., Gademann, R., & Heisenberg, M. (1980). Polarization Sensitivity of Course Control in Drosophila-Melanogaster. *Journal of Comparative Physiology, 139*(3), 177-191. Retrieved from <Go to ISI>://WOS:A1980KQ73100002

Wu, M., Nern, A., Williamson, W. R., Morimoto, M. M., Reiser, M. B., Card, G. M., & Rubin, G. M. (2016). Visual projection neurons in the Drosophila lobula link feature detection to distinct behavioral programs. *Elife, 5*. doi:10.7554/eLife.21022

Wunderer, H., & Smola, U. (1982). Fine-Structure of Ommatidia at the Dorsal Eye Margin of Calliphora-Erythrocephala Meigen (Diptera, Calliphoridae) - an Eye Region Specialized for the Detection of Polarized-Light. *International Journal of Insect Morphology & Embryology, 11*(1), 25-38. Retrieved from <Go to ISI>://WOS:A1982NG80400002

Yamaguchi, S., Desplan, C., & Heisenberg, M. (2010). Contribution of photoreceptor subtypes to spectral wavelength preference in Drosophila. *Proc Natl Acad Sci U S A, 107*(12), 5634-5639. doi:10.1073/pnas.0809398107

Zheng, Z., Lauritzen, J. S., Perlman, E., Robinson, C. G., Nichols, M., Milkie, D., . . . Bock, D. D. (2018). A Complete Electron Microscopy Volume of the Brain of Adult Drosophila melanogaster. *Cell, 174*(3), 730-743 e722. doi:10.1016/j.cell.2018.06.019

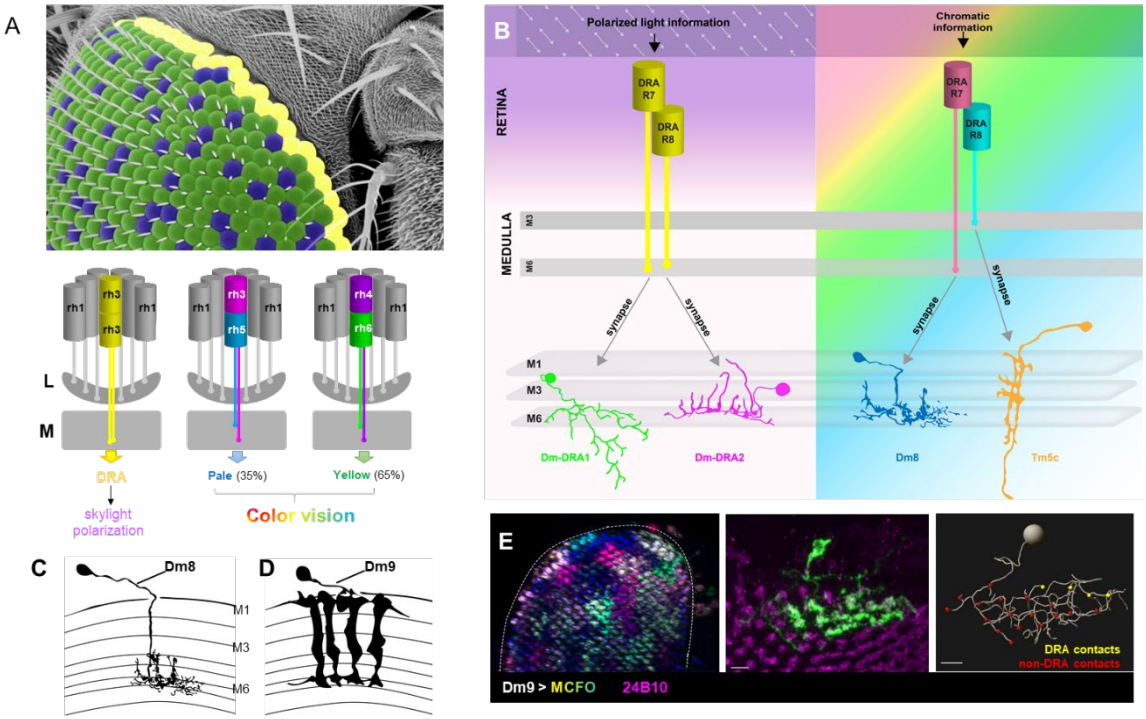

Figure 1: Neural circuit elements processing color versus skylight information in the fly

(A) Top: Electron micrograph depicting the distribution of three different ommatidial subtypes, false colored as blue (pale ommatidia), green (yellow ommatidia) and yellow (DRA ommatidia) in the adult *Drosophila* eye. Bottom: Schematic summarizing rhodopsin expression in these three ommatidial subtypes. Axons of inner photoreceptors R7 and R8 terminate in specific layers of the medulla neuropil (M). (L: Lamina, M: Medulla) **(B)** A graphical summary of the early circuit elements processing skylight polarization versus color vision. Polarization-sensitive DRA.R7 and DRA.R8 project axons to the same deep layer (M6) of the medulla where they are connected to different post-synaptic partners, the horizontal cell types Dm-DRA1 and Dm-DRA2, respectively. Non-DRA R7 and R8 detect different wavelengths and project to different layers, where only R7 connects to the horizontal cell type Dm8 within layer M6, whereas R8 connects to columnar cell typeTm5c in layer M3. Adapted from (Sancer et al., 2019). **(C)** Single cell morphology of Dm8 cell with arborizations in the distal medulla. Adapted from (Fischbach & Dittrich, 1989). **(D)** Single cell morphology of a Dm9 cell with arborizations in close proximity to R7 and R8 terminals. **(E)** Multiple-Color Flp-Out (MCFO) clones of Dm9 cells tiling across the medulla. Lateral view of a Dm9 single-cell clone (green) located at the dorsal rim of the medulla. Skeleton of the same cell with DRA photoreceptor contacts shown in yellow and non-DRA contacts shown in red. Adapted from (Sancer et al., 2020).

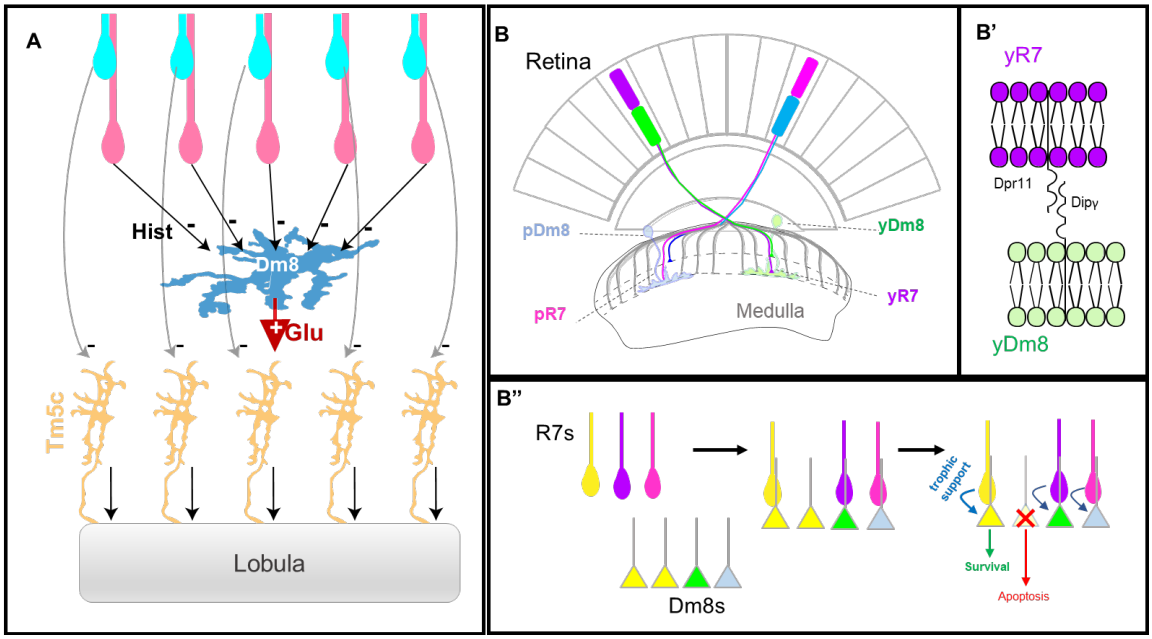

Figure 2: Connectivity and circuit assembly of color-sensitive Dm8 cells

(A) The amacrine-like Dm8 cell receives inhibitory histaminergic inputs from ~13 neighboring R7 photoreceptors and provides excitatory glutamatergic input to columnar Tm5c neuron which also receive direct photoreceptor inputs from R8. (Adapted from (Karuppudurai et al., 2014). **(B)** Top: Pale and yellow R7 cells are connected to different Dm8 subtypes (pDm8 or yDm8). Pairing is controlled by the complementary cell adhesion molecules Dpr11 and DIP-γ expressed specifically in yR7 and yDm8, respectivele (B'). Bottom: Summary of a proposed mechanism that allows correct pairing between R7 subtypes and their specific post-synaptic targets: Different Dm8 subtypes are produced in excess independent of R7 subtypes. When correct R7 and Dm8 subtypes match, interaction leads to a trophic signal (for instance via Dpr-DIP) ensuring the survival of the Dm8 cell, whereas unmatched Dm8s are eliminated via apoptosis. Adapted from (Courgeon & Desplan, 2019).

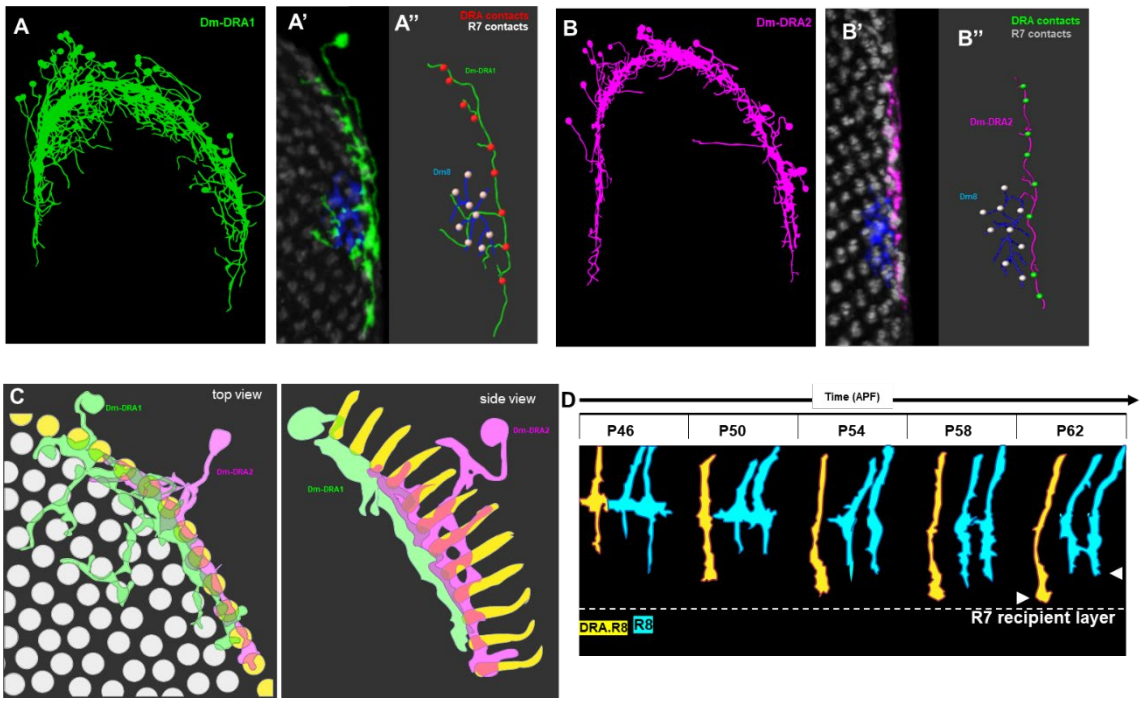

Figure 3: Modality-specific Dm8-like cells processing skylight polarization

(A) Virtual assembly of multiple Dm-DRA1 clones along the DRA region of the medulla. Neighboring MCFO clones of a Dm-DRA1 cell (green) and a color sensitive Dm8 cell (blue) in A'. These two cell types never share photoreceptor contacts, as visible from their skeletons: Dm8-R7 contacts (gray spheres) and Dm-DRA1-DRA photoreceptor contacts (red spheres) in A''. **(B)** Virtual assembly of multiple Dm-DRA2 clones along the DRA of the medulla. Neighboring MCFO clones of a Dm-DRA2 cell (magenta) and a color sensitive Dm8 cell (blue) in B'. Again, these two cells never share photoreceptor contacts, as visible from their skeletons: Dm8-R7 contacts (gray spheres) and Dm-DRA2-DRA contacts (green spheres) in B''. **(C)** Two adjacent Dm-DRA cell clones of different subtypes (Dm-DRA1: green; Dm-DRA2: purple) located at the same position along the DRA (yellow circles). (C'): side view. Note the slight difference in sublayer stratification. **(D)** Illustration summarizing the developmental layer targeting of DRA.R8 (yellow) and non-DRA R8 (cyan) growth cones from 46 hours after pupa formation(APF, P46) to 62 hours APF (P62). Arrowheads point to layers M3 and M6, respectively. All data adapted from (Sancer et al., 2019).

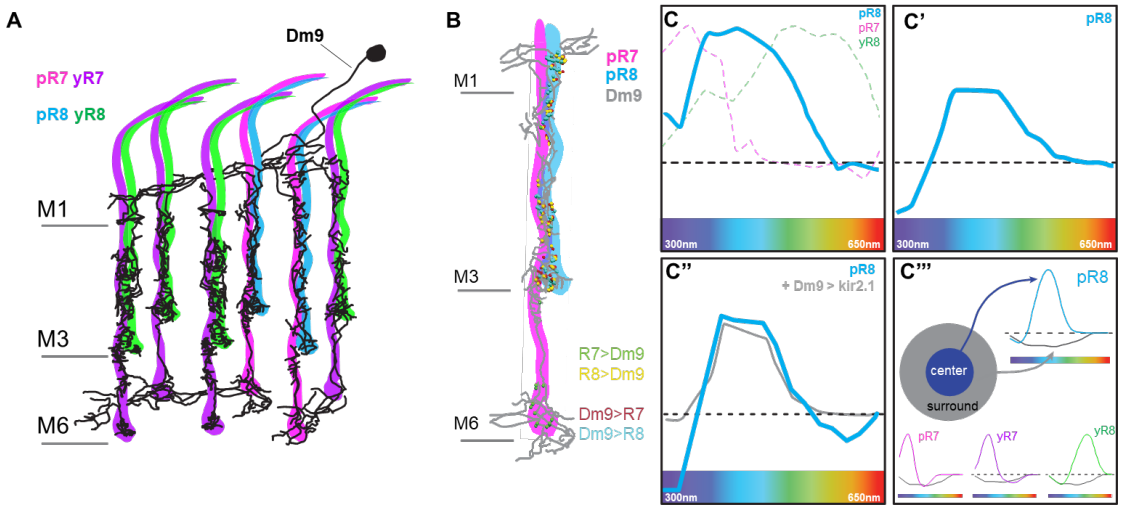

Figure 4: Inter-ommatidial integration via Dm9 cells

(A) Skeleton of a Dm9 cell (black), covering multiple 'pale' and 'yellow' columns, where blue-sensitive R8 cells are paired with UV-sensitive R7 (pale) or green-sensitive R8 with UV- sensitive R7 (yellow), respectively. Inter-ommatidial connections of Dm9 and photoreceptors (and vice versa) exist in medulla layers M1 and M6. **(B)** Intra-ommatidial connections of Dm9 and photoreceptors are distributed from M1 to M6. Feedback synapses from Dm9 onto R7 and R8 (red and light blue, respectively) and R8 synapses onto Dm9 (yellow) locate between medulla layer M1 to M3 while R7 to Dm9 synapses (green) exist mainly within layer M6. **(C)** Uncoupled tuning curve of a 'pale' R8 photoreceptor (blue). A black dashed line depicts the baseline activity of 'pale' R8. Pink and green dashed lines show tuning curves of uncoupled 'pale' R7 and 'yellow' R8 respectively. (C') Tuning curve of a 'pale' R8 photoreceptor when paired with 'pale' R7 of the same column: Intra-ommatidial inhibition is observed at short wavelengths. (C'') Tuning curve of a 'pale' R8 photoreceptor in a wild-type background reveals additional inter-ommatidial inhibition at longer wavelengths. The grey line depicts the same tuning curve after Dm9 inactivation. (C''') Spectral filtering model for inner photoreceptors: Modeled output for predicted 'pale' R8 (blue) in the center and their surround over different wavelengths is shown. The modeled outputs for 'pale' R7 (pink), 'yellow' R7 (purple) or 'yellow' R8 (green) are shown below. All data adapted from (Heath et al., 2019) and (Uhlhorn & Wernet, 2020).

5. DISCUSSION

The visual system of *Drosophila* is composed of optically isolated unit eyes or ommatidia that are repeated ~750 times across the adult retina, sampling individual points in space. Furthermore, the *Drosophila* eye contains different ommatidial subtypes with molecularly and morphologically specialized inner photoreceptors (R7 and R8), which are specialized for the detection of color versus skylight polarization. The processing of visual information occurs in the optic lobes (organized in four neuropils: lamina, medulla, lobula, and lobula complex), by the repetitive microcircuits organized in columns and layers and that receive direct or indirect input from photoreceptor cells. How are different visual modalities such as color and polarization processed by these microcircuits? Before this thesis, it was unknown whether modality-specific differences in the morphology and connectivity of circuit elements downstream of functionally specialized photoreceptors exist in *Drosophila*. I, therefore, characterized the neural circuit elements synaptically connected to polarization-sensitive photoreceptors of the 'dorsal rim area' (DRA), defined the morphological and synaptic differences of these circuit elements that process skylight polarization, when compared to their color-sensitive counterparts, and aimed at identifying the putative pathways carrying skylight information to the central brain.

5.1.1. Duplication of R7 circuitry in the DRA

In my first published manuscript (Modality-Specific Circuits for Skylight Orientation in the Fly Visual System), I focused on the initial characterization of neuronal elements post-synaptic to polarization-sensitive photoreceptors, located in DRA columns of the medulla neuropil. Despite being morphologically, molecularly, and functionally different (Hardie, 1985; Labhart and Meyer, 1999; Wernet et al., 2003), DRA and non-DRA inner photoreceptors R7 and R8 manifest important similarities: It has been shown that both R7 and R8 processing color and skylight polarization show reciprocal columnar inhibition, via histaminergic synapses between inner photoreceptors of the same ommatidium (Schnaitmann et al., 2018; Weir et al., 2016). Furthermore, both color- and polarization sensitive R7 and R8 provide direct synaptic input into several amacrine-like optic lobe neurons stratifying in the distal medulla (Gao et al., 2008; Heath et al., 2020; Karuppudurai et al., 2014; Lin et al., 2016; Sancer et

al., 2019, 2020). Of the two inner photoreceptor cells, DRA.R7 cells most resemble non-DRA R7 cells : They express the same transcription factor during development (Prospero (Cook et al., 2003), express a typical R7 UV-sensitive Rhodopsin (Rh3), and they target the typical R7 target layer in the medulla (layer M6), where ~10 neighboring R7 photoreceptors connect to similar multicolumnar cell types (Dm8 for R7 and Dm8-like Dm-DRA1 for DRA.R7) (Gao et al., 2008; Karuppudurai et al., 2014; Wernet et al., 2003). In contrast, adult DRA.R8 cells are quite different from their color sensitive R8 counterparts. During pupal development, DRA.R8 loose expression of R8 specific transcription factor Senseless and project axons to the R7 target layer M6 instead of the typical R8 target layer M3. Interestingly, DRA.R8 axon terminals always target slightly distally from DRA.R7 terminals (Chin et al., 2014; Fischbach and Dittrich, 1989).The distribution of presynaptic sites in DRA.R8 terminals is more similar to non-DRA R7 than non-DRA R8, active zones being shifted towards more deeper layers (Sancer et al., 2019). By the end of pupation, DRA.R8 then express the same UV-sensitive Rhodopsin as DRA.R7 (Rh3), which is always found in R7 cells, outside of the DRA(Fortini and Rubin, 1991; Sancer et al., 2019; Wernet et al., 2003, 2014). Finally, I found that DRA.R8 connectivity is also very different from color sensitive R8. In non-DRA columns, R8 is synaptically connected to specific columnar trans-medullary (Tm) cell types that project to the lobula neuropil (Karuppudurai et al., 2014; Takemura et al., 2008). In the DRA region, however, ~10 neighboring DRA.R8 cells connect to a specific multicolumnar Dm8-like cell (Dm-DRA2), thereby resembling DRA.R7 cells. Importantly, both Dm-DRA1 and Dm-DRA2 cells are modality-specific, i.e. they avoid contacts with color-sensitive R7 (and R8) cells. Based on my neuroanatomical work, we proposed that within DRA columns, the R7 proto circuit (R7 → Dm8) is duplicated (DRA.R7 → Dm-DRA1 and DRA.R8 →Dm.DRA2) thereby creating two channels for processing signals emanating from orthogonally tuned polarization-sensitive photoreceptors. Such circuit architecture seems ideal for comparing measuring the orientation of the incident polarized light, hence for informing polarization vision. We hypothesize that this duplication of downstream circuitry is necessary due to the opponent nature of the input signals collected by both types of DRA photoreceptors. A single type of Dm-DRA (or Dm8) cells may not be computationally convenient for comparing orthogonal angles of the polarized light, while separate Dm-DRA1 and Dm-DRA2 cells each can process either one of the two

opponent channels, since they are specifically connected to DRA.R7 or DRA.R8, respectively. Duplication of downstream elements appears logically convenient so that signals from several neighboring DRA columns with slightly different preferred e-vector orientations can be pooled and ultimately integrated via post-synaptic cells with (presumably) similar synaptic strength. In contrast, R8 cells in the color circuit are connected to single columnar units, leading to a strong amplification of R7/Dm8 mediated UV signal, ultimately resulting in the strong UV attraction observed behaviorally (Gao et al., 2008; Karuppudurai et al., 2014; Yamaguchi et al., 2010). Interestingly, it should be pointed out that many hymenopteran and lepidopteran species harbor two R7-like cells in every ommatidium (both in the DRA and outside of it), forming three color-sensitive ommatidial subtypes via independent stochastic expression between UV- and Blue-sensitive Rhodopsins (Perry et al., 2016; Wakakuwa et al., 2005; Wernet et al., 2015). Virtually nothing is known about how color information is processed downstream of two R7-like cells in these species, yet Golgi stained honeybee photoreceptor terminals suggest that these two cells terminate in slightly different sublayers, just like R7 and R8 in the fruit fly DRA. The circuit architecture described here might therefore serve as a more general design for functionally specialized insect retinas.

5.1.2. Specific cellular and synaptic adaptations in DRA circuits

Considering the clear modality-specific differences between inner photoreceptor targets in the DRA versus outside of it, we asked whether other neuron types that had previously been characterized in the main part of the medulla also manifested any specifications in DRA columns (this work was ultimately published as ‘Cellular and synaptic adaptations of neural circuits processing skylight polarization in the fly’). In this second manuscript, both morphology and connectivity of several medulla neuron types known to be downstream of color-sensitive photoreceptors, as well as different neuromodulatory and visual projection neuron types were examined. In this study, I discovered that differences between DRA and non-DRA circuits are indeed not limited to Dm-DRA cell types. Similar to what I described for Dm-DRA cells, the distal medulla cell type Dm2 appears to be modality-specific, since within the DRA of the medulla it only contacts to DRA photoreceptors. Furthermore, Dm2 cells also

manifested differences in synaptic connectivity and the distribution of pre- and post-synaptic membranes within the DRA, when compared with non-DRA counterparts. This was to be expected, since Dm2 was reported to be a post-synaptic partner of color sensitive R8 photoreceptors (Reiser, 2019; Takemura et al., 2015). Surprisingly, the multicolumnar Dm9 cell type that is known to be reciprocally connected with both R7 and R8 photoreceptors in the main part of the medulla (i.e. being both pre- and postsynaptic to inner photoreceptors) did not show any modality-specific morphology (Heath et al., 2020; Nern et al., 2015; Sancer et al., 2020). Hence, one given Dm9 cell spans both DRA and non-DRA columns without showing any modality-specific preference. Therefore, we hypothesize that Dm9 cells located at the DRA/non-DRA boundary may play a role in the integration of color and skylight polarization information. However, it should be noted that Dm9 cells manifested different patterns of pre- and postsynaptic membrane distribution in the DRA columns (when compared to non-DRA columns), possibly reflecting the different synaptic distribution of DRA.R7 and DRA.R8 (Sancer et al., 2019). Alternatively, these differences in the synaptic profile of Dm9 cells within DRA columns could also have an impact on circuit function, yet we do not know the functional role of these modality-specific synaptic differences. Surprisingly, a well-known R7 target, the cell type(s) Tm5a/b, was missing in the DRA columns (Melnattur et al., 2014; Reiser, 2019). Furthermore, other known columnar downstream elements of color sensitive R8 showed different and/or weaker synaptic connectivity to inner photoreceptors located within DRA columns(Melnattur et al., 2014; Reiser, 2019). This suggests that unlike color information, skylight polarization may not be strongly represented in the lobula neuropil where columnar Tm-cell types project (Melnattur et al., 2014). However, it should be noted that this study was restricted to a rather small number of only those Tm cells that are known post-synaptic partners of R7 and R8 and it therefore remains unknown whether other, specialized Tm cells might exist in DRA columns. Besides, it is reasonable to assume that the DRA-specific differences in morphology and synaptic distribution described here are not limited to the postsynaptic partners of R7 and R8 photoreceptors. For instance, we observed that dendrites of an Mt11-like tangential cell type that projects to ventrolateral protocerebrum (VLP) also specifically avoided DRA columns. Surprisingly, octopaminergic cells with large dendritic trees also show a very similar avoidance of DRA columns. Therefore, neuromodulation may affect the visual circuits

computing modalities like color and skylight polarization differently. Interestingly, opposing effects of octopamine and dopamine on different visually guided behaviors had previously been reported (Gorostiza et al., 2016).

5.1.3. Representation of skylight cues in the central brain

Different skylight cues like celestial bodies (sun, moon, milky way), intensity gradients, chromatic gradients and skylight polarization can be used by insects for improving orientation or navigation-related behaviors (Heinze, 2017). Despite progress centered on larger insect species like locusts, crickets, and monarch butterflies, large gaps in knowledge remain when trying to understand how these skylight cues are extracted, transferred from the eye to the central brain, and ultimately and spatially represented and integrated there. Over the past years, much progress has been made towards understanding the representation of visual landmarks in the central complex of *Drosophila*, by using genetically encoded indicators of activity. In a series of publications, it became apparent that the central complex receives visual input via ring neurons that show retinotopic organization (Seelig and Jayaraman, 2013). However, it is not clear how visual information reaches the central complex, for this information to become represented in ring neurons or the downstream so-called 'compass neurons. I contributed to the dissection of synaptic pathways connecting the retina and the central complex, culminating in a third manuscript ('Parallel visual pathways with topographic versus non-topographic organization connect the *Drosophila* eyes to the central brain'). In this publication, we aimed at describing the cellular and synaptic organization of the neurons forming the evolutionarily conserved 'anterior visual pathway' (or 'compass pathway'). Interestingly, at least four subclasses of MeTu (medulla to tubercle) neurons that relay visual information to different subdomains of lateral and central regions within the small unit (SU) of anterior optic tubercle (AOTU) showed topographic organization, which so far had only been observed (in a mild form) for LC10 cells projecting to the large unit of the same optic glomeruli (Wu et al., 2016). In this case, topography meant that individual MeTu cells with adjacent dendritic trees in the medulla would project axons to the SU of the AOTu where they would terminate next to each other along the dorsoventral axis, thereby maintaining their neighboring relationships. Interestingly, only some of these topographically projecting MeTu neurons were also directly post-synaptic to R7

photoreceptors. While this suggests that spatial information (along the anterior-posterior axis, yet not along the dorsoventral axis) from the eye is preserved in anterior visual pathway via topographic MeTu neuron projections, it could also hint at parallel channels transmitting different modalities of light (being represented in different subdomains of the SU of the AOTU). Regarding the layering of MeTu dendrites in the medulla, some of these cells may receive input from color-sensitive Dm8 neurons versus polarization-sensitive Dm-DRA neurons, instead of direct R7 inputs. Hence, different skylight cues might be processed via direct or indirect MeTu connections to the SU of the AOTU. In agreement with this, MeTu cell terminals of different classes are spatially restricted within discrete AOTU subdomains. Still it remains unknown whether individual modalities (or rather: skylight cues) are indeed represented in these AOTU subdomains. Nevertheless, this data supports a hypothesis in which different skylight cues would be processed along parallel channels, becoming represented in spatially distinct subregions of the SU of the AOTU. Little is known about the functional properties connecting the eye to the central complex: Three previous studies showed that both TuBu (tubercle to bulb) and R (Ring-)neurons manifest response to bright objects, indicating that the location of the sun may be encoded within the AVP (Omoto et al., 2017; Seelig and Jayaraman, 2013; Shiozaki and Kazama, 2017). However, other celestial cues were not tested as stimuli, during these experiments. It must also be noted that while ‘compass neurons’ in the central complex of larger insects (crickets, locusts and monarch butterflies) (Heinze and Homberg, 2007; Homberg et al., 2011; Reppert et al., 2010) show clear responses to linearly polarized light, no such responses were detected in *Drosophila* (Weir and Dickinson, 2015). Therefore, it remains unknown what kind of visual information is represented (and integrated) in the central complex of fruit flies. In summary, parallel anatomical pathways exist within the AVP that might encode different skylight cues. The exact target neurons of most of these pathways within the central complex remain largely unknown for n as well as the circuit motifs responsible for integrating different modalities along the pathway.

6. FUTURE DIRECTIONS

In this thesis, I have described previously unknown circuit elements that are specialized for processing of the skylight polarization pattern. Although this work, for the first time, revealed the modality-specific differences in the *Drosophila* visual system by showing that color and skylight polarization are computed via different and specialized pathways, we still don't know how these computations are executed on a cellular, synaptic, and physiological level. Similarly, the contributions of all these circuit elements to the orientation behavior of the fly also remain to be demonstrated.

As shown in manuscript I, DRA.R7 and DRA.R8 are connected to their own respective post-synaptic Dm8–like target cells. Similar to Dm8, these Dm-DRA cells collect information from several adjacent columns (~10 columns). It was shown that one given Dm8 cell is most strongly connected to one R7 cell through its home column, while peripheral branches of the Dm8 cell receive weaker input from surrounding R7 cells. (Courgeon and Desplan, 2019; Karuppudurai et al., 2014; Menon et al., 2019). It remains unknown whether this is also the case for Dm-DRA cells, i.e. whether they are more strongly connected to one single DRA.R7/R8 and are therefore biased towards a certain preferred angle of polarized light represented within fan-shaped array of DRA detectors. In theory, one given Dm-DRA cell could also get equal amount of synaptic input from all 10 innervating DRA photoreceptors, which would result in a broader, pooled signal by averaging over 10 DRA columns with slightly different preferred e-vector orientations. Using the light microscopic techniques used in this study (GRASP and trans-tango), it is not possible to determine the exact distribution of synaptic inputs into Dm-DRA1 and Dm-DRA2, thereby distinguishing between the above scenarios. However, detailed connectomic information about these neurons can be gained by using published electron microscopy data (Zheng et al., 2018), thereby better understanding the computational role of circuit elements. Indeed, data is currently being extracted via EM reconstruction for both Dm-DRA1 and Dm-DRA2 (unpublished, Emil Kind). Preliminary data points towards both Dm-DRA cell types averaging over several DRA columns. Furthermore, Dm-DRA1 and Dm-DRA2 membranes are overlapping considerably within medulla layer M6, suggesting possible synaptic connections between these two cell types. Such interconnections

between Dm-DRAs might be essentially important in early processing of the polarized skylight signal as these cells could produce a multicolumnar, polarization-opponent signal. Preliminary EM data also show that connection between Dm-DRA cells might indeed be unidirectional. However, the nature of this input remains unknow, i.e. whether this synaptic connection is excitatory or inhibitory (the same being true for potential interconnections within Dm-DRA1 or Dm-DRA2 cell types). Therefore, identification of the neurotransmitter and their receptors expressed by these cells, as well as functional imaging of their responses to different angles of polarized skylight will be crucial. Also, contribution of these newly identified Dm-DRA neuron types to orientation behavior should be tested by manipulating activity of these neurons (for instance via cell-type specific expression of dominant-negative, temperature-sensitive dynamin, with tetanus toxin, or using inwardly rectifying potassium channels) in the behaving animal (for instance in virtual flight arenas (Mathejczyk and Wernet, 2019, 2020; Warren et al., 2018).

Although my thesis revealed distinct differences in the circuits for color vision versus skylight polarization vision, it will be important to understand how these modalities are integrated. This study mostly focused on differences in circuit architecture, but it also revealed cell types that may play a role in the integration of different modalities. For example, Dm9 cells located at the DRA/non-DRA boundary within the medulla do not show any modality-specific morphology and might be a good candidate for integrating color and skylight polarization early in the circuit. It remains unknown for now, how Dm9 cells in DRA columns respond to polarized light and this should be investigated using functional imaging techniques using the cell-type specific expression of genetically encoded indicators of neuronal activity. Ultimately, a systematic connectomic reconstruction of the neuronal pathways connecting the eye to the central complex will reveal the potential sites of integration between color, polarization, as well as additional celestial cues.

How is skylight polarization information (being one of several skylight cues used for navigation) transferred to central brain? Although we cannot answer this question right now, it seems reasonable to assume that skylight polarization enters the central brain via anterior visual pathway (through putative synaptic connections between Dm-

DRA cells and MeTu neurons). However, we do not know yet how this DRA input is represented in the MeTu neurons which are stratifying at the correct sublayer of medulla layer M6 to connect Dm-DRAs. Therefore, the SU of the AOTU may either get direct polarization-sensitive information from DRA photoreceptors, or indirect input from Dm-DRAs (or both). Alternatively, additional cell types (as described in manuscript II) could be intercalated as well. Also, it remains unknown how skylight polarization information is represented within AOTU. In manuscript III we showed topographical organization in AOTU for lateral and central MeTu cells. However, it remains to be seen which of the parallel channels may transport skylight polarization information in order to understand actual representation of angle of polarized skylight in AOTu. In all mentioned cases, activity imaging of the cell types identified and described in this thesis using linearly polarized stimuli will provide crucial insight into the organization of the AVP.

7. SUMMARY

The fly eye contains different subtypes of unit eyes (ommatidia) with molecularly and morphologically specialized photoreceptors for comparing either between different wavelengths (color vision) or between different angles of the linearly polarized skylight (polarization vision). However, microcircuit differences between those parts of the columnar medulla neuropil computing color versus polarization remain largely unknown. There is virtually nothing known about the circuit elements immediately downstream of polarization-sensitive photoreceptors in the 'dorsal rim area' (DRA). In this work, I described the cellular and synaptic architecture of medulla columns that receive skylight polarization input from DRA photoreceptors. I showed that only in the DRA region, R7 and R8 photoreceptors resemble each other by targeting their axons to the same medulla layer. However, within this layer DRA R7 and R8 connect to morphologically distinct Dm target cells (called Dm-DRA1 and Dm-DRA2, respectively). Both Dm-DRA cell types are modality-specific by avoiding contact with color-sensitive photoreceptors. Using the genetic toolbox of *Drosophila* such as activity-dependent GFP-reconstitution across synaptic partners (GRASP) and the genetically inducible trans-synaptic tracer 'trans-Tango', I confirmed that Dm-DRA1 and Dm-DRA2 are the specific post-synaptic targets of DRA.R7 or DRA.R8, respectively. Neither Dm-DRAs overlap with the main synaptic targets of color-sensitive R7 cells (called Dm8 cells), revealing for the first time that skylight polarization is processed by separate modality-specific circuits in the early visual system. These modality-specific differences are not limited only Dm-DRA cells. I described modality-specific cellular and synaptic specializations in other optic lobe cell types in the DRA region of the medulla: the dendritic arbors of certain cell types (neuromodulatory cells and visual projection neurons) specifically avoid the DRA region. Furthermore, Transmedullary (Tm) cells that are post-synaptic to color-sensitive photoreceptors showed modality-specific differences in connectivity or were absent from the DRA. Finally, I contributed a study describing the cellular organization of the 'anterior visual pathway' that carries skylight information from the eye to the central brain. In this study, I showed that an optic glomerulus called the anterior optic tubercle (AOTU) receives direct information via different classes of medulla-to-tubercle (MeTu) neurons, terminating in different subdomains of the AOTU. Finally,

we hypothesize that different classes of MeTu cells carry different types of skylight information to the central brain via parallel pathways.

8. ZUSAMMENFASSUNG

Das Fliegenauge enthält verschiedene ommatidiale Subtypen mit molekular und morphologisch spezialisierten Photorezeptoren zum Vergleich zwischen verschiedenen Wellenlängen (Farbensehen) oder zwischen verschiedenen Orientierungen des linear polarisierten Himmelslichts (Polarisationssehen). Die spezifischen Unterschiede der Mikroschaltkreise zwischen jenen Teilen des in retinotopen Säulen organiserten Medulla- Neuropils, welche dem Farbensehen oder dem Polarisationseehen dienen, bleiben weitgehend unbekannt. Insbesondere weiss man praktisch nichts über die zellulären Elemente welche den polarisationsempfindlichen Photorezeptoren im "dorsalen Randbereich" (Dorsal Rim Area, DRA). unmittelbar nachgeschaltet sind. In dieser Arbeit beschreibe ich die zelluläre und synaptische Architektur jener Medulla-Säulen, welche die den polarisationssensitiven DRA Photorezeptoren nachgeschaltet sind. Ich zeige, dass R7 und R8 Photorezeptoren nur in DRA einander ähneln und Axone in dieselbe Medullaschicht schicken, wo sie jedoch mit zwei morphologisch unterschiedlichen Dm-Zellen (Dm-DRA1 und Dm-DRA2) synaptisch verbunden sind. Beide Dm-DRA Zelltypen sind modalitätsspezifisch da sie Kontakte mit farbempfindlichen Photorezeptoren vermeiden. Unter Verwendung molekulargenetischer *Drosophila* Methoden wie aktivitätsabhängigem GRASP und trans-tango bestätige ich, dass Dm-DRA1 und Dm-DRA2 die spezifischen post-synaptischen Partner von DRA.R7 bzw. DRA.R8 sind. Beide Dm-DRA Zelltypen überlappen nicht mit den postsynaptischen Partnersn farbempfindlicher R7 Photorezeptoren (sogenannten Dm8-Zellen). Polarisiertes Himmelslichts wird also bereits im frühen visuellen System von spezifischen, modalitätsspezifischen Schaltkreisen verarbeitet. Modalitätsspezifische Unterschiede dieser Art sind nicht auf Dm-DRA-Zellen beschränkt. Ich beschreibe weitere zelluläre und synaptische Unterschiede modalitätsspezifischer Art für andere Zelltypen in der DRA Region des Medulla Neuropils: So vermeiden die dendriten mancher Zelltypen (neuromodulatorische Zellen und visuelle Projektionsneuronen) spezifisch die DRA Region. Transmedulläre (Tm) Zellen, die post-synaptische zu farbempfindlichen Photorezeptoren sind, zeigen in der DRA ebenfalls

modalitätsspezifische Unterschiede in ihrer Verschaltung, oder gehlen dort ganz.. Schließlich beschreibe ich die zelluläre Organisation der ‚anterioren visuellen Sehbahn', welche Himmelsreize vom Auge zum Zentralhirn weiter leitet. Ich zeige, dass ein spezifischer optischer Glomerulus, der sogenannte anteriore optische Tuberkel (AOTu), direkte Afferenzen über mehrere Subtypen von Nervenzellen vom Medulla Neuropil zum AOTU (sogenannte MeTu Zellen) erhält. Schließlich formulieren wir die Hypothese, dass verschiedene Klassen von MeTu-Zellen unterschiedliche Arten von Himmelsreizen über parallele Bahnen zum Zentralhirn transportieren.

9. REFERENCES

Borst, A. (2014). Neural Circuits for Motion Vision in the Fly. Cold Spring Harb. Symp. Quant. Biol. *79*, 131–139.

Chin, A.-L., Lin, C.-Y., Fu, T.-F., Dickson, B.J., and Chiang, A.-S. (2014). Diversity and wiring variability of visual local neurons in {theDrosophilamedulla} M6 stratum. J. Comp. Neurol. *522*, 3795–3816.

Chou, W.-H., Hall, K.J., Wilson, D.B., Wideman, C.L., Townson, S.M., Chadwell, L. V, and Britt, S.G. (1996). Identification of a Novel Drosophila Opsin Reveals Specific Patterning of the R7 and R8 Photoreceptor Cells. Neuron *17*, 1101–1115.

Clark, D.A., Freifeld, L., and Clandinin, T.R. (2013). Mapping and Cracking Sensorimotor Circuits in Genetic Model Organisms. Neuron *78*, 583–595.

Courgeon, M., and Desplan, C. (2019). Coordination between stochastic and deterministic specification in the Drosophila visual system. Science (80-.). *366*, eaay6727.

Dewar, A.D.M., Wystrach, A., Philippides, A., and Graham, P. (2017). Neural coding in the visual system of Drosophila melanogaster: How do small neural populations support visually guided behaviours? PLOS Comput. Biol. *13*, 1–21.

Fischbach, K.-F., and Dittrich, A.P.M. (1989). The optic lobe of Drosophila melanogaster. I. A Golgi analysis of wild-type structure. Cell Tissue Res. *258*.

Fortini, M.E., and Rubin, G.M. (1990). Analysis of cis-acting requirements of the Rh3 and Rh4 genes reveals a bipartite organization to rhodopsin promoters in Drosophila melanogaster. Genes Dev. *4*, 444–463.

Fortini, M.E., and Rubin, G.M. (1991). The optic lobe projection pattern of polarization-sensitive photoreceptor cells in Drosophila melanogaster. Cell Tissue Res. *265*, 185–191.

Gao, S., Takemura, S., Ting, C.-Y., Huang, S., Lu, Z., Luan, H., Rister, J., Thum, A.S., Yang, M., Hong, S.-T., et al. (2008). The Neural Substrate of Spectral Preference in Drosophila. Neuron *60*, 328–342.

Giraldo, Y.M., Leitch, K.J., Ros, I.G., Warren, T.L., Weir, P.T., and Dickinson, M.H. (2018). Sun Navigation Requires Compass Neurons in Drosophila. Curr. Biol. *28*, 2845-2852.e4.

Gkanias, E., Risse, B., Mangan, M., and Webb, B. (2019). From skylight input to behavioural output: A computational model of the insect polarised light compass. PLoS Comput. Biol. *15*, 1–30.

Gorostiza, E.A., Colomb, J., and Brembs, B. (2016). A decision underlies phototaxis in an insect. Open Biol.

Green, J., Adachi, A., Shah, K.K., Hirokawa, J.D., Magani, P.S., and Maimon, G. (2017). A neural circuit architecture for angular integration in Drosophila. Nature *546*, 101–106.

Hardie, R.C. (1985). Functional Organization of the Fly Retina. p.

Heath, S.L., Christenson, M.P., Oriol, E., Saavedra-Weisenhaus, M., Kohn, J.R., and Behnia, R. (2020). Circuit Mechanisms Underlying Chromatic Encoding in Drosophila Photoreceptors. Curr. Biol. *30*, 264--275.e8.

Heinze, S. (2017). Unraveling the neural basis of insect navigation. Curr. Opin. Insect Sci. *24*, 58–67.

Heinze, S., and Homberg, U. (2007). Maplike Representation of. Science (80-.). *431*, 2004–2006.

Heinze, S., and Homberg, U. (2009). Linking the Input to the Output: New Sets of Neurons Complement the Polarization Vision Network in the Locust Central Complex. J. Neurosci. *29*, 4911–4921.

Heisenberg, M., and Buchner, E. (1977). The role of retinula cell types in visual behavior {ofDrosophila} melanogaster. J. Comp. Physiol. ? A *117*, 127–162.

Homberg, U. (2004). In search of the sky compass in the insect brain. Naturwissenschaften *91*, 199–208.

Homberg, U., Heinze, S., Pfeiffer, K., Kinoshita, M., and el Jundi, B. (2011). Central neural coding of sky polarization in insects. Philos. Trans. R. Soc. B Biol. Sci. *366*, 680–687.

Huber, A., Schulz, S., Bentrop, J., Groell, C., Wolfrum, U., and Paulsen, R. (1997). Molecular cloning of Drosophila Rh6 rhodopsin: the visual pigment of a subset of R8 photoreceptor cells 1. FEBS Lett. *406*, 6–10.

Hurvich, L.M., and Jameson, D. (1957). An opponent-process theory of color vision. Psychol. Rev. *64*, 384–404.

Immonen, E.-V., Dacke, M., Heinze, S., and el Jundi, B. (2017). Anatomical organization of the brain of a diurnal and a nocturnal dung beetle. J. Comp. Neurol. *525*, 1879–1908.

Ito, K., Shinomiya, K., Ito, M., Armstrong, J.D., Boyan, G., Hartenstein, V., Harzsch, S., Heisenberg, M., Homberg, U., Jenett, A., et al. (2014). A systematic nomenclature for the insect brain. Neuron *81*, 755–765.

Jagadish, S., Barnea, G., Clandinin, T.R., and Axel, R. (2014). Identifying Functional Connections of the Inner Photoreceptors in Drosophila using Tango-Trace. Neuron *83*.

el Jundi, B., Pfeiffer, K., and Homberg, U. (2011). A distinct layer of the medulla integrates Sky compass signals in the brain of an insect. PLoS One *6*.

el Jundi, B., Pfeiffer, K., Heinze, S., and Homberg, U. (2014). Integration of polarization and chromatic cues in the insect sky compass. J. Comp. Physiol. A.

el Jundi, B., Warrant, E.J., Byrne, M.J., Khaldy, L., Baird, E., Smolka, J., and Dacke, M. (2015). Neural coding underlying the cue preference for celestial orientation. Proc. Natl. Acad. Sci. *112*, 11395 LP – 11400.

Karuppudurai, T., Lin, T.Y., Ting, C.Y., Pursley, R., Melnattur, K. V., Diao, F., White, B.H., Macpherson, L.J., Gallio, M., Pohida, T., et al. (2014). A Hard-Wired Glutamatergic Circuit Pools and Relays UV Signals to Mediate Spectral Preference in Drosophila. Neuron *81*, 603–615.

Kim, S.S., Hermundstad, A.M., Romani, S., Abbott, L.F., and Jayaraman, V. (2019). Generation of stable heading representations in diverse visual scenes. Nature.

Kind, E., Belušič, G., and Wernet, M.F. (2020). Retinal Mosaics Across Fly Species: Variations on a Theme. In Reference Module in Neuroscience and Biobehavioral Psychology, (Elsevier), p.

Klapoetke, N.C., Nern, A., Peek, M.Y., Rogers, E.M., Breads, P., Rubin, G.M., Reiser, M.B., and Card, G.M. (2017). Ultra-selective looming detection from radial motion opponency. Nature *551*, 237–241.

Kulkarni, A., Ertekin, D., Lee, C.-H., and Hummel, T. (2016). Birth order dependent growth cone segregation determines synaptic layer identity in the Drosophila visual system. Elife *5*.

Labhart, T. (1988). Polarization-opponent interneurons in the insect visual system. Nature *331*, 435–437.

Labhart, T., and Meyer, E.P. (1999). Detectors for polarized skylight in insects: A survey of ommatidial specializations in the dorsal rim area of the compound eye. Microsc. Res. Tech. *47*, 368–379.

Lambrinos, D., Möller, R., Labhart, T., Pfeifer, R., and Wehner, R. (2000). A mobile robot employing insect strategies for navigation. Rob. Auton. Syst. *30*, 39–64.

Langen, M., Agi, E., Altschuler, D.J., Wu, L.F., Altschuler, S.J., and Hiesinger, P.R. (2015). The Developmental Rules of Neural Superposition in Drosophila. Cell *162*.

Lin, T.-Y.Y., Luo, J., Shinomiya, K., Ting, C.-Y.Y., Lu, Z., Meinertzhagen, I.A., and Lee, C.-H.H. (2016). Mapping chromatic pathways in the Drosophila visual system. J. Comp. Neurol. *524*, 213–227.

Liu, G., Seiler, H., Wen, A., Zars, T., Ito, K., Wolf, R., Heisenberg, M., and Liu, L. (2006). Distinct memory traces for two visual features in the Drosophila brain. Nature *439*, 551–556.

Longden, K. (2016). Central Brain Circuitry for Color-Vision-Modulated Behaviors. Curr. Biol. *26*, R981--R988.

Longden, K.D. (2018). Colour Vision: A Fresh View of Lateral Inhibition in Drosophila. Curr. Biol. *28*, R308–R311.

Maisak, M.S., Haag, J., Ammer, G., Serbe, E., Meier, M., Leonhardt, A., Schilling, T., Bahl, A., Rubin, G.M., Nern, A., et al. (2013). A directional tuning map of Drosophila elementary motion detectors. Nature *500*, 212–216.

Mappes, M., and Homberg, U. (2004). Behavioral analysis of polarization vision in tethered flying locusts. J. Comp. Physiol. A Neuroethol. Sensory, Neural, Behav. Physiol.

Mappes, M., and Homberg, U. (2007). Surgical lesion of the anterior optic tract abolishes polarotaxis in tethered flying locusts, Schistocerca gregaria. J. Comp. Physiol. A Neuroethol. Sensory, Neural, Behav. Physiol.

Mathejczyk, T., and Wernet, M.F. (2019). New modular assays for the quantitative study of skylight navigation in flying flies.

Mathejczyk, T.F., and Wernet, M.F. (2020). Modular assays for the quantitative study of visually guided navigation in both flying and walking flies. J. Neurosci. Methods *340*, 108747.

Mauss, A.S., Vlasits, A., Borst, A., and Feller, M. (2017). Visual Circuits for Direction Selectivity. Annu. Rev. Neurosci. *40*, 211–230.

Melnattur, K. V, Pursley, R., Lin, T.-Y., Ting, C.-Y., Smith, P.D., Pohida, T., and Lee, C.-H. (2014). Multiple Redundant Medulla Projection Neurons Mediate Color Vision in Drosophila. J. Neurogenet. *7063*, 1–15.

Menon, K.P., Kulkarni, V., Takemura, S.-Y., Anaya, M., and Zinn, K. (2019). Interactions between Dpr11 and DIP-γ control selection of amacrine neurons in Drosophila color vision circuits. Elife *8*.

Millard, S.S., and Pecot, M.Y. (2018). Strategies for assembling columns and layers in the Drosophila visual system. Neural Dev.

Mota, T., Gronenberg, W., Giurfa, M., and Sandoz, J.-C. (2013). Chromatic Processing in the Anterior Optic Tubercle of the Honey Bee Brain. J. Neurosci. *33*,

4–16.

Nern, A., Pfeiffer, B.D., and Rubin, G.M. (2015). Optimized tools for multicolor stochastic labeling reveal diverse stereotyped cell arrangements in the fly visual system. Proc. Natl. Acad. Sci. *112*, E2967–E2976.

Ofstad, T.A., Zuker, C.S., and Reiser, M.B. (2011). Visual place learning in Drosophila melanogaster. Nature *474*, 204–207.

Omoto, J.J., Keleş, M.F., Nguyen, B.-C.M., Bolanos, C., Lovick, J.K., Frye, M.A., and Hartenstein, V. (2017). Visual Input to the Drosophila Central Complex by Developmentally and Functionally Distinct Neuronal Populations. Curr. Biol. 1098–1110.

Otsuna, H., Shinomiya, K., and Ito, K. (2014). Parallel neural pathways in higher visual centers of the Drosophila brain that mediate wavelength-specific behavior . Front. Neural Circuits *8*, 8.

Papatsenko, D., Sheng, G., and Desplan, C. (1997). A new rhodopsin in R8 photoreceptors of Drosophila: evidence for coordinate expression with Rh3 in R7 cells. Development *124*, 1665–1673.

Paulk, A., Millard, S.S., and van Swinderen, B. (2013). Vision in Drosophila: Seeing the World Through a Model's Eyes. Annu. Rev. Entomol. *58*, 313–332.

Paulk, A.C., Phillips-Portillo, J., Dacks, A.M., Fellous, J.-M., and Gronenberg, W. (2008). The Processing of Color, Motion, and Stimulus Timing Are Anatomically Segregated in the Bumblebee Brain. J. Neurosci. *28*, 6319–6332.

Perry, M., Kinoshita, M., Saldi, G., Huo, L., Arikawa, K., and Desplan, C. (2016). Molecular logic behind the three-way stochastic choices that expand butterfly colour vision. Nature *535*, 280–284.

Pfeiffer, K., Kinoshita, M., and Homberg, U. (2005). Polarization-Sensitive and Light-Sensitive Neurons in Two Parallel Pathways Passing Through the Anterior Optic Tubercle in the Locust Brain. J. Neurophysiol. *94*, 3903–3915.

von Philipsborn, A., and Labhart, T. (1990). A behavioural study of polarization vision in the fly, Musca domestica. J. Comp. Physiol. A *167*, 737–743.

Reiser, M. (2019). colorVision2.pdf.

Reppert, S.M., Gegear, R.J., and Merlin, C. (2010). Navigational mechanisms of migrating monarch butterflies. Trends Neurosci. *33*, 399–406.

Ribeiro, I.M.A., Drews, M., Bahl, A., Machacek, C., Borst, A., and Dickson, B.J. (2018). Visual Projection Neurons Mediating Directed Courtship in Drosophila. Cell *174*, 607--621.e18.

Ryglewski, S., Vonhoff, F., Scheckel, K., Duch, C., Bainbridge, S.P., Bownes, M., Ben-Ari, Y., Boerner, J., Duch, C., Brembs, B., et al. (2017). Intra-neuronal Competition for Synaptic Partners Conserves the Amount of Dendritic Building Material. Neuron *0*, 57–80.

Salay, L.D., Ishiko, N., and Huberman, A.D. (2018). A midline thalamic circuit determines reactions to visual threat. Nature *557*, 183–189.

Salcedo, E., Huber, A., Henrich, S., Chadwell, L. V, Chou, W.-H., Paulsen, R., and Britt, S.G. (1999). Blue- and Green-Absorbing Visual Pigments {ofDrosophila}: Ectopic Expression and Physiological Characterization of the R8 Photoreceptor Cell-Specific Rh5 and Rh6 Rhodopsins. J. Neurosci. *19*, 10716–10726.

Sancer, G., Kind, E., Plazaola-Sasieta, H., Balke, J., Pham, T., Hasan, A., Münch, L.O., Courgeon, M., Mathejczyk, T.F., and Wernet, M.F. (2019). Modality-Specific Circuits for Skylight Orientation in the Fly Visual System. Curr. Biol. *29*, 2812--2825.e4.

Sancer, G., Kind, E., Uhlhorn, J., Volkmann, J., Hammacher, J., Pham, T., Plazaola-Sasieta, H., and Wernet, M.F. (2020). Cellular and synaptic adaptations of neural circuits processing skylight polarization in the fly. J. Comp. Physiol. A Neuroethol. Sensory, Neural, Behav. Physiol. *206*, 233–246.

Schnaitmann, C., Garbers, C., Wachtler, T., and Tanimoto, H. (2013). Color discrimination with broadband photoreceptors. Curr. Biol. *23*, 2375–2382.

Schnaitmann, C., Haikala, V., Abraham, E., Oberhauser, V., Thestrup, T., Griesbeck, O., and Reiff, D.F. (2018). Color Processing in the Early Visual System of Drosophila. Cell *172*, 318--330.e18.

Seelig, J.D., and Jayaraman, V. (2013). Feature detection and orientation tuning in the Drosophila central complex. Nature *503*, 262–266.

Seelig, J.D., and Jayaraman, V. (2015). Neural dynamics for landmark orientation and angular path integration. Nature *521*, 186–191.

Shiozaki, H.M., and Kazama, H. (2017). Parallel encoding of recent visual experience and self-motion during navigation in Drosophila. Nat. Neurosci. *20*, 1395–1403.

Smola, U., and Tscharntke, H. (1979). Twisted rhabdomeres in the dipteran eye. J. Comp. Physiol. ? A *133*, 291–297.

Song, B.-M., and Lee, C.-H. (2018). Toward a Mechanistic Understanding of Color Vision in Insects. Front. Neural Circuits *12*.

Stone, T., Webb, B., Adden, A., Weddig, N. Ben, Honkanen, A., Templin, R., Wcislo, W., Scimeca, L., Warrant, E., and Heinze, S. (2017). An Anatomically Constrained Model for Path Integration in the Bee Brain. Curr. Biol. *27*, 3069-

3085.e11.

Sun, Y., Nern, A., Franconville, R., Dana, H., Schreiter, E.R., Looger, L.L., Svoboda, K., Kim, D.S., Hermundstad, A.M., and Jayaraman, V. (2017). Neural signatures of dynamic stimulus selection in Drosophila. Nat. Neurosci. *20*, 1104–1113.

Takemura, S., Lu, Z., and Meinertzhagen, I.A.N.A. (2008). Synaptic Circuits of the Drosophila Optic Lobe : The Input Terminals to the. *513*, 493–513.

Takemura, S., Xu, C.S., Lu, Z., Rivlin, P.K., Parag, T., Olbris, D.J., Plaza, S., Zhao, T., Katz, W.T., Umayam, L., et al. (2015). Synaptic circuits and their variations within different columns in the visual system of Drosophila. Proc. Natl. Acad. Sci. *112*, 13711–13716.

Temizer, I., Donovan, J., Baier, H., and Semmelhack, J. (2015). A Visual Pathway for Looming-Evoked Escape in Larval Zebrafish. Curr. Biol. *25*, 1823–1834.

Tomlinson, A. (2003). Patterning the peripheral retina of the fly: Decoding a gradient. Dev. Cell *5*, 799–809.

Turner-Evans, D.B., and Jayaraman, V. (2016). The insect central complex. Curr. Biol. *26*, R453--R457.

Uhlhorn, J., and Wernet, M.F. (2020). Colour Vision: Self-Centered Fly Photoreceptors Communicate over Distances. Curr. Biol. *30*, R78–R81.

Wada, S. (1974). Spezielle randzonale ommatidien der fliegen (diptera : brachycera): architektur und verteilung in den komplexauaen. Zeitschrift Für Morphol. Der Tiere *77*, 87–125.

Wakakuwa, M., Kurasawa, M., Giurfa, M., and Arikawa, K. (2005). Spectral heterogeneity of honeybee ommatidia. Naturwissenschaften *92*, 464–467.

Warren, T.L., Weir, P.T., and Dickinson, M.H. (2018). Flying Drosophila melanogaster maintain arbitrary but stable headings relative to the angle of polarized light. J. Exp. Biol. *221*.

Wehner, R., and Labhart, T. (2006). Invertebrate vision.

Weir, P.T., and Dickinson, M.H. (2012). Flying drosophila orient to sky polarization. Curr. Biol. *22*, 21–27.

Weir, P.T., and Dickinson, M.H. (2015). Functional divisions for visual processing in the central brain of flying Drosophila. Proc. Natl. Acad. Sci. U. S. A. *112*, E5523-32.

Weir, P.T., Henze, M.J., Bleul, C., Baumann-Klausener, F., Labhart, T., and

Dickinson, M.H. (2016). Anatomical Reconstruction and Functional Imaging Reveal an Ordered Array of Skylight Polarization Detectors in Drosophila. J. Neurosci. *36*, 5397–5404.

Wernet, M.F., Labhart, T., Baumann, F., Mazzoni, E.O., Pichaud, F., and Desplan, C. (2003). Homothorax Switches Function of Drosophila Photoreceptors from Color to Polarized Light Sensors. Cell *115*, 267–279.

Wernet, M.F., Velez, M.M., Clark, D.A., Baumann-Klausener, F., Brown, J.R., Klovstad, M., Labhart, T., and Clandinin, T.R. (2012). Genetic dissection reveals two separate retinal substrates for polarization vision in drosophila. Curr. Biol. *22*, 12–20.

Wernet, M.F., Meier, K.M., Baumann-Klausener, F., Dorfman, R., Weihe, U., Labhart, T., and Desplan, C. (2014). Genetic Dissection of Photoreceptor Subtype Specification by the Drosophila melanogaster Zinc Finger Proteins Elbow and No ocelli. {PLoS} Genet. *10*, e1004210.

Wernet, M.F., Perry, M.W., and Desplan, C. (2015). The evolutionary diversity of insect retinal mosaics: Common design principles and emerging molecular logic. Trends Genet. *31*, 316–328.

Wolff, T., and Ready, D. (1993). Pattern formation in the Drosophila retina. In The Development of Drosophila Melanogaster, (Cold Spring Harbor Press), pp. 1277–1325.

Wu, M., Nern, A., Williamson, W.R., Morimoto, M.M., Reiser, M.B., Card, G.M., and Rubin, G.M. (2016). Visual projection neurons in the *Drosophila*lobula link feature detection to distinct behavioral programs. Elife *5*, e21022.

Wunderer, H., and Smola, U. (1982). Fine structure of ommatidia at the dorsal eye margin of Calliphora erythrocephala meigen (Diptera: Calliphoridae): An eye region specialised for the detection of polarized light. Int. J. Insect Morphol. Embryol. *11*, 25–38.

Yamaguchi, S., Desplan, C., and Heisenberg, M. (2010). Contribution of photoreceptor subtypes to spectral wavelength preference in Drosophila. Proc. Natl. Acad. Sci. *107*, 5634–5639.

Zhu, Y. (2013). The Drosophila visual system. Cell Adh. Migr. *7*, 333–344.